The US/UK

World Magnetic Model

for 2010-2015

Stefan Maus
Susan McLean
Manoj Nair
Craig Rollins (NGA)

NOAA National Geophysical Data Center
325 Broadway
NOAA E/GC3
Boulder, CO 80305-3328
USA

Susan Macmillan
Brian Hamilton
Alan Thomson

British Geological Survey
Geomagnetism Team
Murchison House
West Mains Road
Edinburgh EH9 3LA
UK

Bibliographic Reference:

Maus, S., S. Macmillan, S. McLean, B. Hamilton, A. Thomson, M. Nair, and C. Rollins, 2010, *The US/UK World Magnetic Model for 2010-2015,* NOAA Technical Report NESDIS/NGDC.

ABSTRACT

This report contains a complete description of the World Magnetic Model (WMM) 2010. Section 1 contains information that users of WMM2010 require in order to implement the model and software in navigation and heading systems, and to understand magnetic charts, poles and geomagnetic coordinate systems. Section 2 contains a detailed summary of the data used and the modeling techniques employed. Section 3 contains an assessment of model accuracy and applicability. Section 4 contains charts of all the magnetic elements at 2010.0 and their expected annual rates of change between 2010.0 and 2015.0.

Sponsored by the U.S. National Geospatial-Intelligence Agency (NGA) and the U.K. Defence Geographic Centre (DGC), the World Magnetic Model (WMM) is produced by the U.S. National Oceanographic and Atmospheric Administration's National Geophysical Data Center (NOAA/NGDC) and the British Geological Survey (BGS). It is the standard model used by the U.S. Department of Defense (DoD), the U.K. Ministry of Defence, the North Atlantic Treaty Organization (NATO) and the International Hydrographic Organization (IHO), for navigation, attitude and heading referencing systems using the geomagnetic field. It is also used widely in civilian navigation and heading systems.

CONTACTS

The model, associated software, digital charts, and documentation are available via the Web at http://www.ngdc.noaa.gov/geomag/WMM/ or by contacting NGDC, BGS, or NGA.

MODEL AND SOFTWARE SUPPORT

National Geophysical Data Center
NOAA E/GC 3
325 Broadway
Boulder, CO 80305-3328
USA
Attention: Manoj Nair or Stefan Maus
Phone: + (303) 497-4642 or -6522
Email: Manoj.C.Nair@noaa.gov or Stefan.Maus@noaa.gov
Web: http://www.ngdc.noaa.gov/geomag/WMM/

British Geological Survey
Murchison House
West Mains Road
Edinburgh, EH9 3LA
UK
Attention: Susan Macmillan or Alan Thomson
Phone: + 44 131 667 1000
Email: smac@bgs.ac.uk or awpt@bgs.ac.uk
Web: http://www.geomag.bgs.ac.uk/navigation.html

APPLICABILITY WITHIN THE U.S. DEPARTMENT OF DEFENSE

National Geospatial-Intelligence Agency

Craig Rollins
NGA-SN, Mail Stop L-41
3838 Vogel Road
Arnold, MO 63010-6238
U.S.A.

Email: Craig.M.Rollins@nga.mil

James Friederich
NGA-SN, Mail Stop L-41
3838 Vogel Road
Arnold, MO 63010-6238
U.S.A.

Email: James.E.Friederich@nga.mil

APPLICABILITY WITHIN THE U.K. MINISTRY OF DEFENCE

Defence Geographic Centre

MacLeod Building, Elmwood Avenue
Feltham, Middlesex
TW13 7AH
UK
Attention: Matthew Shimell
Email: ICGDGC-IPGeodesyC2a@mod.uk

MacLeod Building, Elmwood Avenue
Feltham, Middlesex
TW13 7AH
UK
Attention: Giles André
Email: ICGDGC-CCRegColC1@mod.uk

The NATO and military specifications for magnetic models are STANAG 7172 (draft) and MIL-W-89500 (Defense Mapping Agency, 1993). Magnetic model requirements that are more stringent than those set forth in these specifications should be addressed to NGDC and BGS (e.g., those that must include magnetic effects of the Earth's crust, ionosphere, or magnetosphere and/or require greater spatial or temporal resolution on a regional or local basis).

ACKNOWLEDGEMENTS

This work was carried out under the sponsorship of the U.S. National Geospatial-Intelligence Agency (NGA) and the UK Ministry of Defence through the Defence Geographic Centre (DGC). Heather McCullough (NOAA/NGDC) edited and proofread this report. The maps of the geomagnetic elements were designed by Jesse Varner (NOAA/NGDC and Cooperative Institute for Research in the Environmental Sciences). Hong Guo of Google helped to make the new WMM software library compatible with industry standards. Magnetic satellite data were provided by the CHAMP mission and data center (operated by GeoForschungsZentrum Helmholtz Zentrum in Potsdam, Germany, and supported by the German Aerospace Center (DLR) and by the Federal Ministry of Education and Research (BMBF)), and the Ørsted satellite mission and data center (operated by the Danish Space Center and the Ministries of Trade, Research and Transport). Many institutes and agencies are involved in the operation of geomagnetic observatories around the world. In particular we would like to thank: Centre de Recherche en Astronomie Astrophysique et Geophysique, ALGERIA; Servicio Meteorologico Nacional, ARGENTINA; Universidad Nacional de la Plata, ARGENTINA; Geoscience Australia, AUSTRALIA; Zentralanstalt für Meteorologie und Geodynamik, AUSTRIA; Institut Royal Météorologique de Belgique, BELGIUM; CNPq-Observatório Nacional, BRAZIL; Academy of Sciences, BULGARIA; Geological Survey of Canada, CANADA; Academy of Sciences, CHINA; Seismological Bureau, CHINA; Directorate General of Telecommunications, CHINA (Taiwan); Instituto Geográfico Agustín Codazzi, COLOMBIA; Academy of Sciences, CZECH REPUBLIC; Danish Meteorological Institute; DENMARK; Addis Ababa University, ETHIOPIA; Finnish Meteorological Institute, FINLAND; Sodankylä Geophysical

Observatory, FINLAND; Institut de Physique du Globe de Paris, FRANCE; Ecole et Observatoire des Sciences de la Terre, FRANCE; Institut Français de Recherche Scientifique pour le Développement, FRANCE; Academy of Sciences, GEORGIA; Ludwig Maximilians University Munich, GERMANY; Alfred-Wegener-Institute for Polar & Marine Research, GERMANY; GeoForschungsZentrum Helmholtz Zentrum in Potsdam, GERMANY; Universities of Karlsruhe and Stuttgart, GERMANY; Institute of Geology and Mineral Exploration, GREECE; Academy of Sciences, HUNGARY; Eötvös Loránd Geophysical Institute of Hungary, HUNGARY; University of Iceland, ICELAND; Indian Institute of Geomagnetism, INDIA; Meteorological and Geophysical Agency, INDONESIA; The Irish Meteorological Service, IRELAND; Survey of Israel, ISRAEL; Instituto Nazionale di Geofisica e Vulcanologia, ITALY; Japan Coast Guard, JAPAN; Japan Meteorological Agency, JAPAN; Geographical Survey Institute, JAPAN; Institute of the Ionosphere, KAZAKHSTAN; National Centre for Geophysical Research, LEBANON; Université d'Antananarivo, MADAGASCAR; Universidad Nacional Autonoma de México, MEXICO; Institute of Geological and Nuclear Sciences, NEW ZEALAND; University of Tromsø, NORWAY; Instituto Geofísico del Perú, PERU; Academy of Sciences, POLAND; Instituto Nacional de Geologia, REPÚBLICA DE MOÇAMBIQUE; Geological Survey of Romania, ROMANIA; Academy of Sciences, RUSSIA; Institute of Solar-Terrestrial Physics, RUSSIA; Dept. of Agriculture, Forestry, Fisheries & Meteorology, SAMOA; Geomagnetic College Grocka, SERBIA & MONTENEGRO; Slovenska Akademia Vied, SLOVAKIA; National Research Foundation, SOUTH AFRICA; Observatori de l'Ebre, SPAIN; Real Instituto y Observatorio de la Armada, SPAIN; Instituto Geográfico Nacional, SPAIN; Sveriges Geologiska Undersökning, SWEDEN; Swedish Institute of Space Physics, SWEDEN; Earthquake Research Institute, TURKEY; US Geological Survey, UNITED STATES OF AMERICA; British Geological Survey, UNITED KINGDOM; Academy of Sciences, UKRAINE; Ukrainian Antarctic Center, UKRAINE and National Centre for Science and Technology, VIETNAM. The INTERMAGNET program and the World Data Centers for Geomagnetism at Edinburgh and Boulder assist in the quality control and dissemination of observatory data. The magnetic activity indices Kp and Dst were computed and provided by GeoForschungsZentrum Helmholtz Zentrum and World Data Center for Geomagnetism in Kyoto, respectively. Solar wind data are measured by the Advanced Composition Explorer (ACE) satellite and made available by NASA. This model could not have been produced without the efforts of all of these institutes.

TABLE OF CONTENTS

1. THE MODEL

1.1 INTRODUCTION

The Earth is like a giant magnet. At every location on or above the Earth, its magnetic field has a more or less well-known direction, which can be used as a reference frame to orient ships, aircraft, satellites, antennas, drilling equipment and handheld devices. At some places on the globe the horizontal direction of the magnetic field coincides with the direction of geographic north (“true” north), but in general this is not the case. The angular amount by which the horizontal direction of the magnetic field differs from true north is called the magnetic declination, or simply declination (D, see Fig.1). This is the correction required to convert between a magnetic bearing and a true bearing. The main utility of the World Magnetic Model (WMM) is to provide magnetic declination for any desired location on the globe. In addition to the magnetic declination, the WMM also provides the complete geometry of the field from 1 km below the Earth’s surface to 850 km above the surface. The magnetic field extends deep into the Earth and far out into space, but the WMM is not valid there.

The Earth’s magnetism has several sources. All the sources will affect a scientific or navigational instrument but only some of them are represented in the WMM. The strongest contribution, by far, is the magnetic field produced by the Earth’s liquid-iron outer core, called the “core field”. Magnetic minerals in the crust and upper mantle make a further contribution that can be significant locally. Electric currents induced by the flow of conducting sea water through the ambient magnetic field make a further, albeit weak, contribution to the observed magnetic field. All of these are of “internal” origin. Deliberately excluded from the WMM by the data selection process and by other means are so-called “disturbance fields”. These are contributions arising from electric currents in the upper atmosphere and near-Earth space. Because the “external” magnetic fields so produced are time-varying, there is a further effect. They induce electric currents in the Earth and oceans, producing secondary internal magnetic fields, which are considered part of the disturbance field and are therefore not represented in the WMM.

The mathematical method of the WMM is an expansion of the magnetic potential into spherical harmonic functions to degree and order 12. The minimum wavelength resolved is 360° / $\sqrt{12\ x\ 13}$ = 28.8° in arc-length, corresponding to 3200 km at the Earth's surface (see Sec. 3.6.3 of Backus et al, 1996). The WMM is a model of those internal magnetic fields that are not part of the disturbance field and have spatial wavelengths exceeding 30° in arc-length. This works out to be almost the entire core field and the long-wavelength portion of the crustal and oceanic fields. In this report, the term "main field" refers to the portion of the Earth's magnetic field at epoch 2010.0 that is modeled by the WMM.

The core field changes perceptibly from year to year. This effect, called secular variation (SV), is accounted for in the WMM by a linear SV model. (Specifically, a straight line is used as the model of the time-dependence of each coefficient of the spherical harmonic representation of the magnetic potential. See Sec. 1.2). Due to unpredictable non-linear changes in the core field, the values of the WMM coefficients have to be updated every five years. The revision described in this report, WMM2010, is valid from 2010.0 to 2015.0.

1.1.1 MAGNETIC ELEMENTS

The geomagnetic field vector, $\mathbf{B}_m$, is described by 7 elements. These are the northerly intensity *X*, the easterly intensity *Y*, the vertical intensity *Z* (positive downwards) and the following quantities derived from *X*, *Y*, and *Z*: The horizontal intensity *H*, the total intensity *F*, the inclination angle *I*, (also called the dip angle and measured from the horizontal plane to the field vector, positive downwards), and the declination angle *D* (also called the magnetic variation and measured clockwise from true north to the horizontal component of the field vector). In the descriptions of *X, Y, Z, H, F, I* and *D* above, the vertical direction is perpendicular to the WGS 84 ellipsoid model of the Earth, the horizontal plane is perpendicular to the vertical direction, and the rotational directions clockwise and counter-clockwise are determined by a view from above (see Fig. 1).

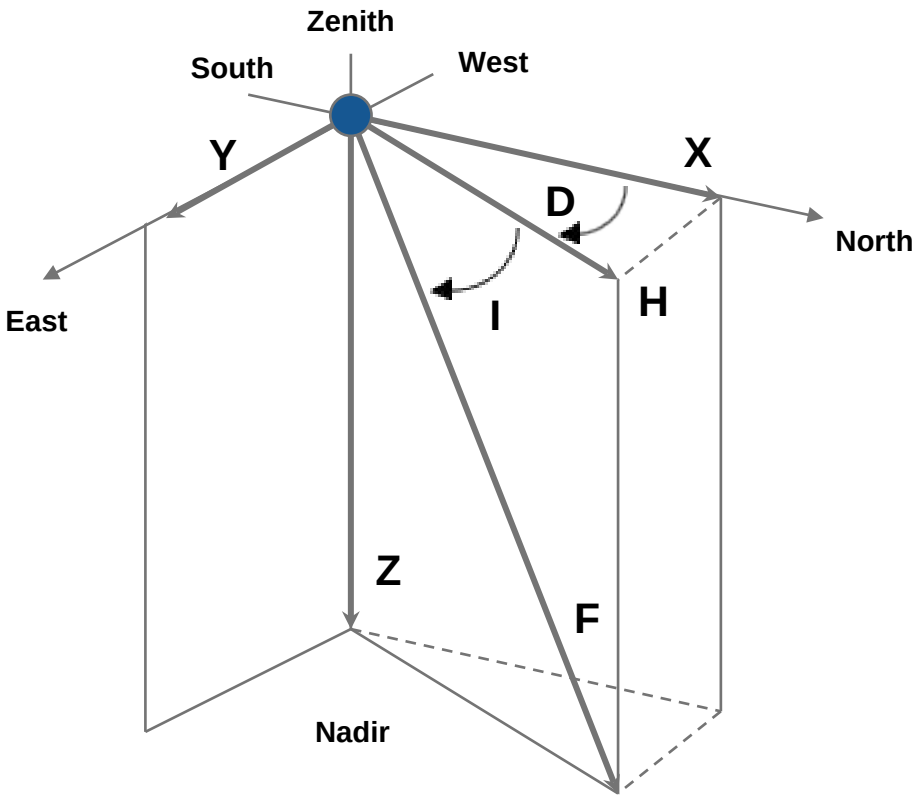

Figure 1: The 7 elements of the geomagnetic field vector B_m associated with an arbitrary point in space

The quantities *X, Y,* and *Z* are the sizes of perpendicular vectors that add vectorially to $\mathbf{B}_m$. Conversely, *X*, *Y*, and *Z* can be determined from the quantities *F*, *I*, and *D* (i.e., the quantities that specify the size and direction of $\mathbf{B}_m$).

1.1.2 GRID VARIATION

In the polar regions, or near the rotation axis of the Earth, the angle *D* changes strongly with a change in the longitude of the observer, and is therefore a poor measure of the direction of $\mathbf{B}_m$. For this reason, the WMM technical report and software have defined an auxiliary angle, *GV*, for the direction of $\mathbf{B}_m$ in the horizontal plane. Its definition is:

$$\begin{aligned} GV &= D - \lambda \quad \text{for} \quad \varphi > 55^o, \\ GV &= D + \lambda \quad \text{for} \quad \varphi < -55^o \\ GV &\text{ is undefined otherwise} \end{aligned} \tag{1}$$

where λ is the longitude and φ is the geodetic latitude. The angle *GV* should also be understood as the angle on the plane of the Universal Polar Stereographic (UPS) grid for the appropriate hemisphere at the observer's location measured clockwise from the direction parallel to the UPS Northing axis (*y*-axis) to the horizontal component of $\mathbf{B}_m$. To emphasize this, the designation GV_{UPS} may be used for the above.

The quantity GV_{UPS} defined above is an example of a more general concept, namely grid variation or grivation. Grivation is the angle on the plane of a chosen grid coordinate system at the observer's location measured clockwise from the direction parallel to the grid's Northings' axis to the horizontal component of $\mathbf{B}_m$. It is useful for local surveys, where location is given by grid coordinates rather than by longitude and latitude. It is dependent on the map projection used to define the grid coordinates. In general it is

$$GV_{grid} = D - C \tag{2}$$

where *D* is the magnetic declination and *C* is the "convergence-of-meridians" defined as the clockwise angle from the northward meridional arc to the grid Northing direction. Large scale military topographic mapping routinely employs the Universal Transverse Mercator (UTM) grid coordinates for the map projection of the sheet, for the definition of a grid to overprint, and for a grivation calculation as defined above. The latter could be notated GV_{UTM}.

In the new WMM subroutine library, both GV_{UPS} and GV_{UTM} are provided within certain restrictions. See the software user's guide.

1.1.3 RANGE OF THE MAGNETIC ELEMENTS AT THE EARTH'S SURFACE

Table 1 shows the expected range of the magnetic field elements and GV at the Earth's surface.

Table 1: Ranges of magnetic elements and *GV* at the Earth's surface

Element	Name	Alternative Name	Range at Earth's Surface			Positive Sense
			Min	Max	Unit	
X	North component	Northerly intensity	-17000	42000	nT	North
Y	East component	Easterly intensity	-18000	17000	nT	East
Z	Down component	Vertical intensity	-67000	61000	nT	Down
H	Horizontal intensity		0	42000	nT	
F	Total intensity	Total field	22000	67000	nT	
I	Inclination	Dip	-90	90	Degree	Down
D	Declination	Magnetic variation	-180	180	Degree	East / Clockwise
GV	Grid variation	Grivation	-180	180	Degree	East / Clockwise

1.2 RELEVANT MODEL EQUATIONS

This section describes the representation of the magnetic field in the WMM and lists the equations needed to obtain the magnetic field elements for the desired location and time from the WMM coefficients. All variables in this section adhere to the following measurement conventions: angles are in radians, lengths are in meters, magnetic intensities are in nano-Teslas (nT) and times are in years. The software may display these quantities in other units, which it will identify.

The main magnetic field $\mathbf{B_m}$ is a potential field and therefore can be written in geocentric spherical coordinates (longitude λ, latitude φ', radius r) as the negative spatial gradient of a scalar potential

$$\mathbf{B}_m(\lambda, \varphi', r, t) = -\nabla V(\lambda, \varphi', r, t) \tag{3}$$

This potential can be expanded in terms of spherical harmonics:

$$V(\lambda, \varphi', r, t) = a \sum_{n=1}^{N} \sum_{m=0}^{n} \left(g_n^m(t) \cos(m\lambda) + h_n^m(t) \sin(m\lambda) \right) \left(\frac{a}{r} \right)^{n+1} \mathrm{P}_n^m(\sin \varphi') \tag{4}$$

where N=12 is the degree of the expansion of the WMM, a (6371200 m) is the geomagnetic reference radius, (λ, φ', r) are the longitude, latitude and radius in a spherical geocentric reference frame, and $g_n^m(t)$ and $h_n^m(t)$ are the time-dependent Gauss coefficients of degree n and order m describing the Earth's main magnetic field. $\breve{P}_n^m(\mu)$ are the Schmidt semi-normalized associated Legendre functions defined as:

$$\begin{aligned} \breve{P}_n^m(\mu) &= \sqrt{2 \frac{(n-m)!}{(n+m)!}} P_{n,m}(\mu) \quad if \quad m > 0 \\ \breve{P}_n^m(\mu) &= \qquad\qquad P_{n,m}(\mu) \quad if \quad m = 0 \end{aligned} \tag{5}$$

Here, we use the definition of $P_{n,m}(\mu)$ commonly used in geodesy and geomagnetism (e.g., Heiskanen and Moritz, 1967; Langel, 1987). Sample functions, for geocentric latitude φ', are:

$$
\begin{aligned}
P_{3,0}(\sin\varphi') &= \frac{1}{2}(\sin\varphi')(5\sin^2\varphi'-3) \\
P_{3,1}(\sin\varphi') &= -\frac{3}{2}(\cos\varphi')(1-5\sin^2\varphi') \\
P_{3,2}(\sin\varphi') &= 15(\sin\varphi')(1-\sin^2\varphi') \\
P_{3,3}(\sin\varphi') &= 15\cos^3\varphi'
\end{aligned}
\qquad (6)
$$

These $P_{n,m}(\mu)$ are related to the $P_n^m(\mu)$ defined in Abramowitz and Stegun (1972, Chapter 8) or Gradshteyn and Ryzhik (1994, Chapter 8.7) by $P_{n,m}(\mu) = (-1)^m P_n^m(\mu)$.

WMM2010 comprises two sets of Gauss coefficients to degree and order *N=12*. One set provides a spherical-harmonic main field model for 2010.0 in units of nT, the other set provides a predictive secular variation model for the period 2010.0 to 2015.0 in units of nT/year.

A step by step procedure is provided below for computing the magnetic field elements at a given location and time ($\lambda, \varphi, h_{MSL}, t$), where λ and φ are the geodetic longitude and latitude, h_{MSL} is Mean Sea Level (MSL) height, and *t* is the time given in decimal years.

In the first step, the user is requested to provide the time, location and MSL height at which the magnetic elements are to be calculated. The MSL height is then converted to height *h* above the WGS 84 ellipsoid by using the geopotential model EGM96 (Lemoine et al, 1998). This is done by interpolating a grid of the geoid height file with a spatial resolution of 15 arc-minutes.

The geodetic coordinates (*λ, φ, h)* are then transformed into spherical geocentric coordinates (λ , φ′, *r*) by recognizing that λ is the same in both coordinate systems, and that (φ′, *r*) is computed from (φ, *h*) according to the equations:

$$
\begin{aligned}
p &= (R_c + h)\cos\varphi \\
z &= (R_c(1-e^2) + h)\sin\varphi \\
r &= \sqrt{p^2 + z^2} \\
\varphi' &= \arcsin\frac{z}{r}
\end{aligned}
\tag{7}
$$

Here, $p = \sqrt{x^2 + y^2}$, where *x*, *y* and *z* are the coordinates of a geocentric Cartesian coordinate system in which the positive x and z axes point in the directions of the prime meridian (*λ=0*) and the Earth's rotation axis, respectively. The semi-major axis *A,* reciprocal flattening *1/f,* eccentricity squared e^2 and radius of curvature of the prime vertical (also called normal section), R_c at the given latitude φ are given for the WGS 84 ellipsoid as

$$
\begin{aligned}
A &= 6378137\ m \\
\frac{1}{f} &= 298.257223563 \\
e^2 &= f(2-f) \\
R_c &= \frac{A}{\sqrt{1-e^2\sin^2\varphi}}
\end{aligned}
\tag{8}
$$

In the second step, the Gauss coefficients $g_n^m(t)$ and $h_n^m(t)$ are determined for the desired time *t* from the model coefficients $g_n^m(t_0)$, $h_n^m(t_0)$, $\dot{g}_n^m(t_0)$ and $\dot{h}_n^m(t_0)$ as

$$
\begin{aligned}
g_n^m(t) &= g_n^m(t_0) + (t - t_0)\,\dot{g}_n^m(t_0) \\
h_n^m(t) &= h_n^m(t_0) + (t - t_0)\,\dot{h}_n^m(t_0)
\end{aligned}
\tag{9}
$$

where the time is given in decimal years and $t_0 = 2010.0$ is the base date of the model. The quantities $g_n^m(t_0)$ and $h_n^m(t_0)$ are called the main field coefficients and the quantities $\dot{g}_n^m(t_0)$ and $\dot{h}_n^m(t_0)$ are called the secular variation coefficients.

In the third step, the field vector components *X'*, *Y'* and *Z'* in geocentric coordinates are computed as

$$
\begin{aligned}
X'(\lambda, \varphi', r) &= -\frac{1}{r}\frac{\partial V}{\partial \varphi'} \\
&= -\sum_{n=1}^{12}\left(\frac{a}{r}\right)^{n+2}\sum_{m=0}^{n}\left(g_n^m(t)\cos m\lambda + h_n^m(t)\sin m\lambda\right)\frac{d\,\breve{\mathrm{P}}_n^m(\sin\varphi')}{d\varphi'}
\end{aligned}
\tag{10}
$$

$$
\begin{aligned}
Y'(\lambda, \varphi', r) &= -\frac{1}{r\cos\varphi'}\frac{\partial V}{\partial \lambda} \\
&= \frac{1}{\cos\varphi'}\sum_{n=1}^{12}\left(\frac{a}{r}\right)^{n+2}\sum_{m=0}^{n} m\left(g_n^m(t)\sin m\lambda - h_n^m(t)\cos m\lambda\right)\breve{\mathrm{P}}_n^m(\sin\varphi')
\end{aligned}
\tag{11}
$$

$$
\begin{aligned}
Z'(\lambda, \varphi', r) &= \frac{\partial V}{\partial r} \\
&= -\sum_{n=1}^{12}(n+1)\left(\frac{a}{r}\right)^{n+2}\sum_{m=0}^{n}\left(g_n^m(t)\cos m\lambda + h_n^m(t)\sin m\lambda\right)\breve{\mathrm{P}}_n^m(\sin\varphi')
\end{aligned}
\tag{12}
$$

At this point, one can also compute the secular variation of the field components as

$$\begin{aligned}\dot{X}'(\lambda,\varphi',r) &= -\frac{1}{r}\frac{\partial \dot{V}}{\partial \varphi'} \\ &= -\sum_{n=1}^{12}\left(\frac{a}{r}\right)^{n+2}\sum_{m=0}^{n}(\dot{g}_n^m\cos m\lambda + \dot{h}_n^m \sin m\lambda)\,\frac{d\,\breve{\mathrm{P}}_n^m(\sin\varphi')}{d\varphi'}\end{aligned} \tag{13}$$

$$\begin{aligned}\dot{Y}'(\lambda,\varphi',r) &= -\frac{1}{r\cos\varphi'}\frac{\partial \dot{V}}{\partial \lambda} \\ &= \frac{1}{\cos\varphi'}\sum_{n=1}^{12}\left(\frac{a}{r}\right)^{n+2}\sum_{m=0}^{n} m(\dot{g}_n^m \sin m\lambda - \dot{h}_n^m \cos m\lambda)\,\breve{\mathrm{P}}_n^m(\sin\varphi')\end{aligned} \tag{14}$$

$$\begin{aligned}\dot{Z}'(\lambda,\varphi',r) &= \frac{\partial \dot{V}}{\partial r} \\ &= -\sum_{n=1}^{12}(n+1)\left(\frac{a}{r}\right)^{n+2}\sum_{m=0}^{n}(\dot{g}_n^m\cos m\lambda + \dot{h}_n^m \sin m\lambda)\,\breve{\mathrm{P}}_n^m(\sin\varphi')\end{aligned} \tag{15}$$

$$\frac{d\,\breve{\mathrm{P}}_n^m(\sin\varphi')}{d\varphi'} = (n+1)(\tan\varphi')\,\breve{\mathrm{P}}_n^m(\sin\varphi') - \sqrt{(n+1)^2 - m^2}\,(\sec\varphi')\,\breve{\mathrm{P}}_{n+1}^m(\sin\varphi') \tag{16}$$

In the fourth step, the geocentric magnetic field vector components X', Y' and Z', are rotated into the ellipsoidal reference frame, using

$$\begin{aligned}X &= X'\cos(\varphi' - \varphi) - Z'\sin(\varphi' - \varphi) \\ Y &= Y' \\ Z &= X'\sin(\varphi' - \varphi) + Z'\cos(\varphi' - \varphi)\end{aligned} \tag{17}$$

Similarly, the time derivatives of the vector components, $\dot{X}'$, $\dot{Y}'$ and $\dot{Z}'$ are rotated using

$$\begin{aligned}\dot{X} &= \dot{X}'\cos(\varphi' - \varphi) - \dot{Z}'\sin(\varphi' - \varphi)\\ \dot{Y} &= \dot{Y}'\\ \dot{Z} &= \dot{X}'\sin(\varphi' - \varphi) + \dot{Z}'\cos(\varphi' - \varphi)\end{aligned} \tag{18}$$

In the last step, the magnetic elements *H, F, I,* and *D* are computed from the orthogonal components:

$$H = \sqrt{X^2 + Y^2}, \quad F = \sqrt{H^2 + Z^2}, \quad I = \arctan(Z, H), \quad D = \arctan(Y, X) \tag{19}$$

where $\arctan(a,b)$ is $\tan^{-1}(a/b)$, taking into account the angular quadrant, avoiding a division by zero, and resulting in a declination in the range of -π to π and an inclination in the range of - π /2 to π /2. These angles in radians are then output by the WMM software in degrees.

The secular variation of these elements is computed using

$$\begin{aligned}\dot{H} &= \frac{X \cdot \dot{X} + Y \cdot \dot{Y}}{H}\\ \dot{F} &= \frac{X \cdot \dot{X} + Y \cdot \dot{Y} + Z \cdot \dot{Z}}{F}\\ \dot{I} &= \frac{H \cdot \dot{Z} - Z \cdot \dot{H}}{F^2}\\ \dot{D} &= \frac{X \cdot \dot{Y} - Y \cdot \dot{X}}{H^2}\\ G\dot{V} &= \dot{D}\end{aligned} \tag{20}$$

where $\dot{I}$, $\dot{D}$ and $G\dot{V}$ are given in radians per year. The WMM software then outputs these angles in arc-minutes per year.

1.3 THE WMM2010 COEFFICIENTS

The model coefficients, also referred to as Gauss coefficients, are listed in Table 2. These coefficients can be used to compute values for the field elements and their annual rates of change at any location near the surface of the Earth and at any date between 2010.0 and 2015.0.

Table 2: Final coefficients for WMM2010. Units are nT for the main field, and nT per year for the secular variation. The index *n* is the degree and *m* is the order. Since $h_n^m(t_0)$ and $\dot{h}_n^m(t_0)$ are not defined for *m*=0, the corresponding fields are left blank

n	*m*	$g_n^m(t_0)$	$h_n^m(t_0)$	$\dot{g}_n^m(t_0)$	$\dot{h}_n^m(t_0)$
1	0	-29496.6		11.6	
1	1	-1586.3	4944.4	16.5	-25.9
2	0	-2396.6		-12.1	
2	1	3026.1	-2707.7	-4.4	-22.5
2	2	1668.6	-576.1	1.9	-11.8
3	0	1340.1		0.4	
3	1	-2326.2	-160.2	-4.1	7.3
3	2	1231.9	251.9	-2.9	-3.9
3	3	634.0	-536.6	-7.7	-2.6
4	0	912.6		-1.8	
4	1	808.9	286.4	2.3	1.1
4	2	166.7	-211.2	-8.7	2.7
4	3	-357.1	164.3	4.6	3.9
4	4	89.4	-309.1	-2.1	-0.8
5	0	-230.9		-1.0	
5	1	357.2	44.6	0.6	0.4
5	2	200.3	188.9	-1.8	1.8
5	3	-141.1	-118.2	-1.0	1.2
5	4	-163.0	0.0	0.9	4.0
5	5	-7.8	100.9	1.0	-0.6
6	0	72.8	0.0	-0.2	0.0
6	1	68.6	-20.8	-0.2	-0.2
6	2	76.0	44.1	-0.1	-2.1
6	3	-141.4	61.5	2.0	-0.4
6	4	-22.8	-66.3	-1.7	-0.6
6	5	13.2	3.1	-0.3	0.5
6	6	-77.9	55.0	1.7	0.9
7	0	80.5		0.1	
7	1	-75.1	-57.9	-0.1	0.7
7	2	-4.7	-21.1	-0.6	0.3
7	3	45.3	6.5	1.3	-0.1
7	4	13.9	24.9	0.4	-0.1
7	5	10.4	7.0	0.3	-0.8
7	6	1.7	-27.7	-0.7	-0.3
7	7	4.9	-3.3	0.6	0.3
8	0	24.4		-0.1	
8	1	8.1	11.0	0.1	-0.1
8	2	-14.5	-20.0	-0.6	0.2
8	3	-5.6	11.9	0.2	0.4
8	4	-19.3	-17.4	-0.2	0.4
8	5	11.5	16.7	0.3	0.1
8	6	10.9	7.0	0.3	-0.1
8	7	-14.1	-10.8	-0.6	0.4
8	8	-3.7	1.7	0.2	0.3
9	0	5.4		0.0	
9	1	9.4	-20.5	-0.1	0.0
9	2	3.4	11.5	0.0	-0.2
9	3	-5.2	12.8	0.3	0.0
9	4	3.1	-7.2	-0.4	-0.1
9	5	-12.4	-7.4	-0.3	0.1
9	6	-0.7	8.0	0.1	0.0
9	7	8.4	2.1	-0.1	-0.2
9	8	-8.5	-6.1	-0.4	0.3
9	9	-10.1	7.0	-0.2	0.2
10	0	-2.0		0.0	
10	1	-6.3	2.8	0.0	0.1
10	2	0.9	-0.1	-0.1	-0.1
10	3	-1.1	4.7	0.2	0.0
10	4	-0.2	4.4	0.0	-0.1
10	5	2.5	-7.2	-0.1	-0.1
10	6	-0.3	-1.0	-0.2	0.0
10	7	2.2	-3.9	0.0	-0.1
10	8	3.1	-2.0	-0.1	-0.2
10	9	-1.0	-2.0	-0.2	0.0
10	10	-2.8	-8.3	-0.2	-0.1
11	0	3.0		0.0	
11	1	-1.5	0.2	0.0	0.0
11	2	-2.1	1.7	0.0	0.1
11	3	1.7	-0.6	0.1	0.0
11	4	-0.5	-1.8	0.0	0.1
11	5	0.5	0.9	0.0	0.0
11	6	-0.8	-0.4	0.0	0.1
11	7	0.4	-2.5	0.0	0.0
11	8	1.8	-1.3	0.0	-0.1
11	9	0.1	-2.1	0.0	-0.1
11	10	0.7	-1.9	-0.1	0.0
11	11	3.8	-1.8	0.0	-0.1
12	0	-2.2		0.0	
12	1	-0.2	-0.9	0.0	0.0
12	2	0.3	0.3	0.1	0.0
12	3	1.0	2.1	0.1	0.0
12	4	-0.6	-2.5	-0.1	0.0
12	5	0.9	0.5	0.0	0.0
12	6	-0.1	0.6	0.0	0.1
12	7	0.5	0.0	0.0	0.0
12	8	-0.4	0.1	0.0	0.0
12	9	-0.4	0.3	0.0	0.0
12	10	0.2	-0.9	0.0	0.0
12	11	-0.8	-0.2	-0.1	0.0
12	12	0.0	0.9	0.1	0.0

1.4 SINGULARITIES AT THE GEOGRAPHIC POLES

The World Magnetic Model has singularities at the North and South geographic poles. This is a mathematical issue, not a geophysical phenomenon, stemming from the ambiguity of longitude at a Pole and at any altitude over a Pole. Related to this, the North-East-Down (NED) frame of unit vectors to which the X′, Y′, Z′ quantities are referred is defined everywhere except at a Pole or over a Pole. This section extends these concepts. In the following, the North Pole is the case that is discussed, with implications for the South Pole.

To appreciate the model equations most comprehensively, let the arbitrariness of the North Pole's longitude disambiguate the North Pole's NED frame. In other words, if the Pole is assigned a longitude of λ, then the NED frame at the Pole is to be oriented so that the unit vector "N" of NED is directed opposite to the λ-meridian, the unit vector "D" is directed downward, and the unit vector "E" is directed so that NED is right-handed. This is equivalent to requiring the NED frame at longitude λ and latitude 90° to be the limit of NED frames as the latitude approaches 90° and the longitude and altitude remain fixed.

On January 1, 2010, directly above the North Pole at 6371200 meters from the Earth's center, the magnetic field vector lies in the half-plane of the 165.53°W meridian. If the Pole is assigned $\lambda = 0°$, the components X′, Y′, Z′ (also the components X, Y, Z) are 1866.4 nT, -481.8 nT, and 56232.4 nT respectively. A change in the longitude assigned to the Pole is equivalent to a rotation of the NED frame about the polar axis.

The model equations of Section 1.2 support the above pole calculation and others like it provided the equation for Y′ is extended by continuity as follows to ameliorate the factor $\cos(\varphi')$ in the denominator. As φ' approaches 90°, the function $(\breve{\mathrm{P}}_n^m(\sin\varphi'))/\cos\varphi'$ approaches zero if m > 1 and approaches certain non-zero finite limits if m = 1, and multiplies zero (constant) and can be ignored if m = 0. For m = 1 and 1 ≤ n ≤ 12 respectively, the limits are:

1	2	3	4	5	6	7	8	9	10	11	12
1	$\sqrt{3}$	$\sqrt{6}$	$\sqrt{10}$	$\sqrt{15}$	$\sqrt{21}$	$2\sqrt{7}$	6	$3\sqrt{5}$	$\sqrt{55}$	$\sqrt{66}$	$\sqrt{78}$

Alternately, for $m > 0$, the functions $(\breve{\mathrm{P}}_n^m(\sin\varphi'))/\cos\varphi'$ can be expanded as polynomials in $\sin\varphi'$ and $\cos\varphi'$.

1.5 MODEL EQUATIONS NUMERICAL EXAMPLE

A software implementation of the relevant model equations is provided with this report. Most software developers should find the C programs and/or C subroutines provided to be sufficient for their purposes, after adaptations are made to their own software structures.

To aid software developers who need to re-implement the model equations for special requirements, Tables 3a to 3c provide a numerical example showing the intermediate calculations of Section 1.2. For the purpose of verifying the correct implementation of the equations, the tables display many more digits than are warranted by the accuracy of the WMM.

The output in Table 3c includes grivation calculations for four grid systems, whether or not the grid system is commonly used in that part of the world. This is helpful for the purposes of verifying that the mathematics is correctly implemented in the software, and if not used the unwanted grid systems may be ignored.

Table 3a: High-precision numerical example, given values for time, altitude, latitude, and longitude

Time	2012.5000 0000	yr
Height-above-Ellipsoid	100.0000 0000	km
Latitude	-80.0000 0000	deg
Longitude	240.0000 0000	deg

Table 3b: High-precision numerical example, computations of the magnetic field elements

1	lambda	4.18879 02048	rad
2	phi	-1.39626 34016	rad
3	h	1 00000.00000 00000	m
4	t	2012.50000 00000	yr
5	phi-prime	-1.39512 89589	rad
6	r	64 57402.34844 73705	m
7	g(1,0,t)	-29467.60000 00000	nT
8	g(1,1,t)	-1545.05000 00000	nT
9	g(2,0,t)	-2426.85000 00000	nT
10	g(2,1,t)	3015.10000 00000	nT
11	g(2,2,t)	1673.35000 00000	nT
12	h(1,0,t)	0.00000 00000	nT
13	h(1,1,t)	4879.65000 00000	nT
14	h(2,0,t)	0.00000 00000	nT
15	h(2,1,t)	-2763.95000 00000	nT
16	h(2,2,t)	-605.60000 00000	nT
17	Xprime	5478.08914 74225	nT
18	Yprime	14765.37032 43050	nT
19	Zprime	-50632.17770 56324	nT
20	Xprime-dot	20.58517 51801	nT/yr
21	Yprime-dot	1.02725 92716	nT/yr
22	Zprime-dot	83.50809 72670	nT/yr
23	X	5535.52491 48687	nT
24	Y	14765.37032 43050	nT
25	Z	-50625.93054 78794	nT
26	Xdot	20.49042 68023	nT/yr
27	Ydot	1.02725 92716	nT/yr
28	Zdot	83.53139 62281	nT/yr
29	F	53024.92848 40226	nT
30	H	15768.89967 29956	nT
31	D	1.21211 40681	rad
32	I	-1.26884 21543	rad
33	Fdot	-77.32705 44552	nT/yr
34	Hdot	8.15485 76192	nT/yr
35	Ddot	-0.00119 38570	rad/yr
36	Idot	0.00061 53148	rad/yr

Table 3c: High-precision numerical example, Grivation calculations. Angles are in degrees.

Grid System	UPS	UPS	UTM	UTM
Grid zone	**North**	**South**	**10**	**11**
TrueN-to-GridN	240.00000 00000	-240.0000000000	-2.9545046801	2.9545046801
GridN-to-MagN	-170.5509796081	309.4490203919	72.4035250720	66.4945157119
TrueN-to-MagN	69.4490203919	69.4490203919	69.4490203919	69.4490203919

1.6 SUPERSESSION OF THE MODELS

WMM2010 supersedes WMM2005 (McLean et al, 2004) and should replace it in navigation and other systems. Also included with the model is software for computing the magnetic field components *X, Y, Z, H, F, I, D* and auxiliary angle GV as defined above. WMM2010 is to be used from January 1, 2010 to December 31, 2014. In late December of 2014, barring unforeseen circumstances, the U.S. and U.K. agencies will replace WMM2010 with a new degree and order 12 main field model, and a new degree and order 12 predictive secular-variation model.

1.7 POLICY ON ALTERNATE SOFTWARE FOR THE U.S. DEPARTMENT OF DEFENSE

The WMM2010 product release includes several items of software by which the WMM2010 model may be computed and/or its subroutines incorporated into larger DoD systems. It is hoped that the software provided is useful for most occasions of DoD systems procurement and development.

If there are special requirements, and the model equations must be implemented anew or a separate interpolation algorithm invented, the software developer may use the label WMM2010 for the resulting product provided the resulting software agrees with the relevant model equations within the following tolerances:

Between latitudes 89.992°S and 89.992°N,

Quantities in nanoTeslas shall be correct to within 0.1 nT

Quantities in nanoTeslas/year shall be correct to within 0.1 nT/year

(see Sec. 1.4 for the computation problems exactly at the Poles).

This policy is designed to promote interoperability and to track departures from consistency when necessary. This policy permits systems developers to display as many digits as needed and not display unneeded digits. This policy allows that the computations be taken to less than full double precision accuracy and the software retain the WMM2010 label. This policy refers to the allowed computational error in the software, not to the accuracy or limitations of the science or the geomagnetic model.

If there are special requirements, and the model equations are implemented anew or separate interpolation algorithm invented, and it is required to sacrifice accuracy for speed of computation so that the above tolerances are not met, the label WMM2010 may not be applied to the resulting product. In this situation, the DoD entity or contractor is urged to apply to NGA or NGDC acting on behalf of NGA for the label to adopt to indicate that this is a modification of WMM2010.

1.8 MAGNETIC POLES AND GEOMAGNETIC COORDINATE SYSTEMS

There are different ways of defining magnetic poles. The most common understanding is that they are the positions on the Earth's surface where the geomagnetic field is vertical, that is, perpendicular to the ellipsoid. These positions are called **dip poles**, and the north and south dip poles do not have to be (and are not now) antipodal. In principle the dip poles can be found by experiment, conducting a magnetic survey to determine where the field is vertical. In practice the geomagnetic field is vertical on oval-shaped loci traced on a daily basis, with very considerable variation from one day to another.

Other definitions originate from models of the geomagnetic field. The WMM representation of the field includes a magnetic dipole at the center of the Earth. This dipole defines an axis that intersects the Earth's surface at two antipodal points. These points are called **geomagnetic poles**. The geomagnetic poles, otherwise known as the dipole poles, can be computed from the

first three Gauss coefficients of the WMM. Based on the WMM2010 coefficients for 2010.0 the geomagnetic north pole is at 72.21°W longitude and 80.02°N geocentric latitude (80.08°N geodetic latitude), and the geomagnetic south pole is at 107.79°E longitude and 80.02°S geocentric latitude (80.08°S geodetic latitude). The axis of the dipole is currently inclined at 9.98° to the Earth's rotation axis. The same dipole is the basis for the simple geomagnetic coordinate system of geomagnetic latitude and longitude (see Sec. 4, Geomagnetic longitude and latitude in Mercator projection). The geomagnetic equator is at geomagnetic latitude 0°.

The WMM can also be used to calculate dip pole positions. These **model dip poles** are computed from all the Gauss coefficients using an iterative method. In 2010.0 the north dip pole computed from WMM2010 is located at longitude 132.35°W and geodetic latitude 84.97°N and the south dip pole at longitude 137.34°E and geodetic latitude 64.42°S.

Scientists, map makers and polar explorers have an interest in the locations of the dip and geomagnetic poles. Although one cannot make any observations in the region of the geomagnetic poles that might indicate their positions, these poles are arguably of greater significance than the dip poles. This is because the auroral ovals, which are approximately 5° latitude bands where the spectacular aurora are likely to be seen, are approximately centered on the geomagnetic poles. They are usually displaced slightly to the night-side of the geomagnetic poles and greatly vary in size: bands of greatest activity occur between 15° and 25° from the geomagnetic poles.

A further concept is that of **eccentric dipole**, or off-centered dipole. The location of the center of the eccentric dipole (sometimes known as magnetic center), computed using the first eight Gauss coefficients for 2010.0, is at (r, φ', λ) = (563 kilometers, 22.49°N, 140.22°E). The axis of the eccentric dipole is parallel to the axis of the (centered) dipole field.

Table 4: Computed pole positions based on the WMM2010

	Date	North	South
Geomagnetic Poles	2010.0	72.21°W 80.02° N (geocentric) 80.08° S (geodetic)	107.79° E 80.02° S (geocentric) 80.08° S (geodetic)
Model Dip Poles	2010.0	132.35° W 84.97° N	137.34° E 64.42° S
Eccentric Dipole	2010.0	r = 563 km; φ' = 22.49°N; λ = 140.22°E	

1.9 DESCRIPTION OF CHARTS

All charts of the magnetic elements and their annual rates of change, and of grid variation, are available in digital PDF format on CD-ROM or from the WMM web site (http://www.ngdc.noaa.gov/geomag/WMM). They are replicated in Section 4.

The following charts are available:

- Main field magnetic elements *X, Y, Z, H, F, I* and *D* on the Mercator projection between latitudes 70°S and 70°N.
- Main field magnetic elements *X, Y, Z, H, F, I* and *D* on the north and south polar stereographic projection for latitudes northward of 55°N and southward of 55°S.
- Secular variation of *X, Y, Z, H, F, I* and *D* on the Mercator projection between latitudes 70°S and 70°N.
- Secular variation of *X, Y, Z, H, F, I* and *D* on the north and south polar stereographic projection for northward of 55°N and southward of 55°S.
- Grid variation (GV) and its annual change on the north and south polar stereographic projection for northward of 55°N and southward of 55°S.
- Geomagnetic latitude and longitude on the Mercator projection between latitudes 70°S and 70°N.

1.10 TEST VALUES

To verify the correctness of a coefficient update or new software installation, Table 5 provides test values to validate software output. The WMM coefficient file, software that executes the WMM, and several derived products are distributed by NOAA/NGDC and BGS both online and offline on behalf of NGA and DGC.

Table 5: WMM2010 test values. The computation was carried out with double precision arithmetic. Single precision arithmetic can cause differences of up to 0.1 nT. Heights are with respect to the WGS 84 Ellipsoid. Grid Variation is with respect to the Grid North of the Universal Polar Stereographic Projection

Date	Alt (km)	Lat (deg)	Lon (deg)	X (nT)	Y (nT)	Z (nT)	H (nT)	F (nT)	I (deg)	D (deg)	GV (deg)
2010.0	0	80	0	6649.5	-714.6	54346.2	6687.8	54756.2	82.98	-6.13	-6.13
2010.0	0	0	120	39428.8	664.9	-11683.8	39434.5	41128.9	-16.50	0.97	
2010.0	0	-80	240	5657.7	15727.3	-53407.5	16714.0	55961.8	-72.62	70.21	310.21
2010.0	100	80	0	6332.2	-729.1	52194.9	6374.0	52582.6	83.04	-6.57	-6.57
2010.0	100	0	120	37452.0	611.9	-11180.8	37457.0	39090.1	-16.62	0.94	
2010.0	100	-80	240	5484.3	14762.8	-50834.8	15748.6	53218.3	-72.79	69.62	309.62
2012.5	0	80	0	6658.0	-606.7	54420.4	6685.5	54829.5	83.00	-5.21	-5.21
2012.5	0	0	120	39423.9	608.1	-11540.5	39428.6	41082.8	-16.31	0.88	
2012.5	0	-80	240	5713.6	15731.8	-53184.3	16737.2	55755.7	-72.53	70.04	310.04
2012.5	100	80	0	6340.9	-625.1	52261.9	6371.6	52648.9	83.05	-5.63	-5.63
2012.5	100	0	120	37448.1	559.7	-11044.2	37452.2	39046.7	-16.43	0.86	
2012.5	100	-80	240	5535.5	14765.4	-50625.9	15768.9	53024.9	-72.70	69.45	309.45
Date	**Alt (km)**	**Lat (deg)**	**Lon (deg)**	**Xdot (nT/yr)**	**Ydot (nT/yr)**	**Zdot (nT/yr)**	**Hdot (nT/yr)**	**Fdot (nT/yr)**	**Idot (min/yr)**	**Ddot (min/yr)**	
2010.0	0	80	0	3.4	43.2	29.7	-1.3	29.3	0.31	22.25	
2010.0	0	0	120	-2.0	-22.7	57.3	-2.3	-18.5	4.54	-1.98	
2010.0	0	-80	240	22.4	1.8	89.3	9.3	-82.5	2.18	-4.20	
2010.0	100	80	0	3.5	41.6	26.8	-1.3	26.5	0.30	22.48	
2010.0	100	0	120	-1.6	-20.9	54.6	-1.9	-17.5	4.56	-1.91	
2010.0	100	-80	240	20.5	1.0	83.5	8.1	-77.4	2.10	-4.11	
2012.5	0	80	0	3.4	43.2	29.7	-0.6	29.4	0.26	22.26	
2012.5	0	0	120	-2.0	-22.7	57.3	-2.3	-18.3	4.55	-1.98	
2012.5	0	-80	240	22.4	1.8	89.3	9.3	-82.4	2.20	-4.19	
2012.5	100	80	0	3.5	41.6	26.8	-0.6	26.5	0.25	22.50	
2012.5	100	0	120	-1.6	-20.9	54.6	-1.9	-17.3	4.57	-1.91	
2012.5	100	-80	240	20.5	1.0	83.5	8.2	-77.3	2.12	-4.10	

2. CONSTRUCTION OF THE MODEL

2.1 BACKGROUND ON THE GEOMAGNETIC FIELD

The Earth's magnetic field (**B**) is a vector quantity varying in space (***r***) and time (*t*). The field, as measured by a magnetic sensor on or above the Earth's surface, is actually a composite of several magnetic field contributions, generated by a variety of sources. These fields are superimposed and the sources and fields interact through inductive processes with each other. The most important of these geomagnetic sources are:

a. the core field, ($\mathbf{B}_{core}$), generated in Earth's conducting, fluid outer core;

b. the crustal field, ($\mathbf{B}_{crust}$), from Earth's crust/upper mantle;

c. the combined disturbance field, ($\mathbf{B}_{disturbance}$), from electrical currents flowing in the upper atmosphere and magnetosphere, which also induce electrical currents in the sea and the ground

Thus, the observed magnetic field is a sum of contributions:

$$\mathbf{B}(\boldsymbol{r}, t) = \mathbf{B}_{core}(\boldsymbol{r}, t) + \mathbf{B}_{crust}(\boldsymbol{r}) + \mathbf{B}_{disturbance}(\boldsymbol{r}, t) \quad (21)$$

$\mathbf{B}_{core}$ is the dominating part of the field, accounting for over 95% of the field strength at the Earth's surface. *Secular variation* is the slow change in time of $\mathbf{B}_{core}$. The field arising from magnetized crustal rocks, $\mathbf{B}_{crust}$, varies spatially, but is nearly constant in time for the time-scales considered here. In most locations $\mathbf{B}_{crust}$ is much smaller in magnitude than $\mathbf{B}_{core}$ but can have significant local impact on the use of magnetic compass devices. The field arising from currents flowing in the ionosphere and magnetosphere and their resultant induced currents in the Earth's mantle and crust, $\mathbf{B}_{disturbance}$, varies both with location and time.

$\mathbf{B}_{crust}$ has spatial variations on the order of meters to thousands of kilometers and cannot be fully modeled with low degree spherical harmonic models. Therefore, the WMM does not include contributions from the crust except for those of very long wavelength. $\mathbf{B}_{crust}$ is usually smaller at sea than on land, and decreases with increasing altitude. The rock magnetization resulting in B_{crust} may be either induced (by the core field) or remnant or a combination of both.

The field arising from currents flowing in the ionosphere and magnetosphere and their associated induced currents in the Earth, $B_{disturbance}$ varies both with location and time. Figure 2 shows the various current systems. The disturbance field can vary both regularly, with fundamental periods of one day and one year, as well as irregularly on time scales of seconds to days. The regular variations are both diurnal and annual, and they are essentially generated by the daylit atmosphere at altitudes of 100-130 kilometers, ionized by the Sun's radiation, being moved in the Earth's magnetic field by winds and tides, thus producing the necessary conditions (motion of a conductor in a magnetic field) for a dynamo to operate. Further daily and annual variations are caused by the rotation of the Earth in the magnetospheric field, which is approximately fixed in orientation relative to the Sun. The irregular variations are due to magnetic storms and sub-storms. Magnetic storms generally have three phases: an initial phase, often with a sudden commencement and increased horizontal field at mid-latitudes; a main phase; and a recovery phase. The main phase involves an intensification of the ring current (Fig. 2) from the plasma sheet.

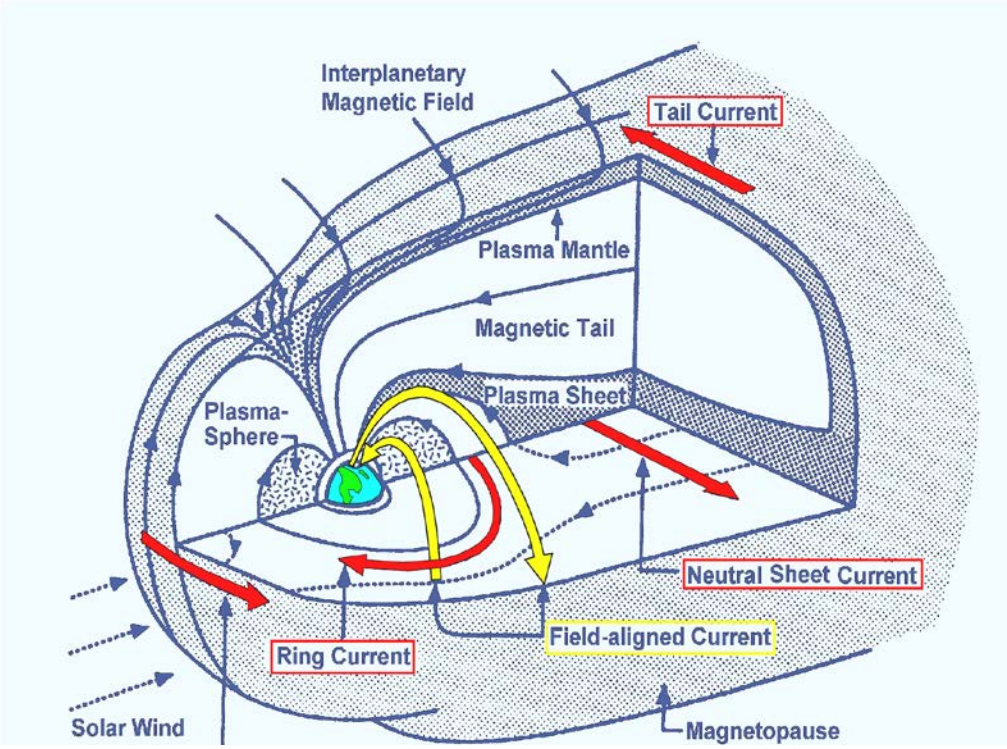

Figure 2: Current systems of the magnetosphere

During the recovery phase the ring current returns to normal over a number of days and associated sub-storms subside. Magnetic storm and sub-storm effects are generally more severe at high geomagnetic latitudes where the ionized region of the upper atmosphere (the ionosphere) is coupled to the magnetosphere by field-aligned currents. They are therefore strongly influenced by the interplanetary magnetic field and current systems in the magnetotail. Both the regular and irregular disturbance field variations are modulated by season and the solar magnetic activity cycle. The primary disturbance field is often known as the external field, as its main sources, the ionosphere and magnetosphere, are external to the surface of the Earth where geomagnetic measurements have been traditionally made. However, this term can be confusing when using satellite data, as the ionospheric dynamo region (90-120 kilometers) is below satellite altitude and therefore effectively internal to the orbital region. For further information about the crustal and disturbance fields (and general information about geomagnetism) see Merrill et al (1996) and Parkinson (1983).

2.2 DATA ACQUISITION AND QUALITY CONTROL

To create an accurate magnetic field model, it is necessary to have vector component measurements with good global coverage and low noise levels. The German CHAMP satellite is presently the most suitable global magnetic observing system. Measurements of the total intensity of the magnetic field are further available from the Danish Ørsted satellite. This latter satellite ceased providing vector component measurements around 2005. Also available are ground observatory hourly mean data. Although with poorer spatial coverage, the observatory data can provide valuable constraints on the time variations of the geomagnetic field.

2.2.1 SATELLITE DATA

The principal characteristic of satellite data is their global coverage using consistent instrumentation collected within a relatively short time span. The inclination of the orbit (the angle between the plane containing the satellite's path and the earth's equatorial plane) determines the latitudinal extent of the data coverage; an inclination of 90° provides 100% coverage, an inclination of slightly less or slightly more than 90° results in gaps with no data for small regions around the geographic poles. Another important characteristic of satellite data is that localized, small-scale crustal magnetization and electromagnetic induction effects close to the Earth surface are strongly attenuated at satellite altitude, resulting in a cleaner magnetic environment for measuring the main field.

The Ørsted and CHAMP satellites slowly drift in local time (details below) with the Earth rotating beneath them. Thus, they provide a crude picture of the entire Earth within 24 hours. During this time each satellite completes about 15 orbits, with a longitudinal spacing of around 24 degrees. Both CHAMP and Ørsted data were used in the production of WMM2010.

2.2.1.1 CHAMP

CHAllenging Minisatellite Payload (CHAMP; http://op.gfz-potsdam.de/champ) is a German satellite mission dedicated to improving gravity and magnetic field models of the Earth. CHAMP was proposed in 1994 by GeoForschungsZentrum Potsdam in response to an initiative of the German Space Agency (DLR) to support the space industry in the "New States" of the united Germany by financing a small satellite mission. CHAMP was launched with a Russian COSMOS vehicle on 15 July 2000 into a low Earth orbit. Initially designed to last 5 years, the mission is now projected to complete a full decade before re-entry in mid-2010.

SATELLITE AND ORBIT

A limiting factor for low-altitude Earth satellite missions is the considerable drag of the atmospheric neutral gas below 600 kilometers. Satellite drag was the primary factor in the short lifespan (7 months) of Magsat (1979/1980) and the reason a higher altitude orbit was chosen for Ørsted. To achieve long mission duration on a low orbit, CHAMP was given a large weight (522 kilograms), a small cross section, and a stable attitude. It was launched into an almost circular, near polar (inclination = 87.3°) orbit with an initial altitude of 454 kilometers. While Magsat was on a strictly sun-synchronous dawn/dusk orbit, CHAMP advances one hour in local time within eleven days. It takes approximately 90 minutes to complete one revolution at a speed of about 8 kilometers/second. The decay of CHAMP's orbital altitude depends on the neutral gas density, which is enhanced by solar activity. CHAMP's orbit has been raised 4 times to prolong the mission (Fig. 3).

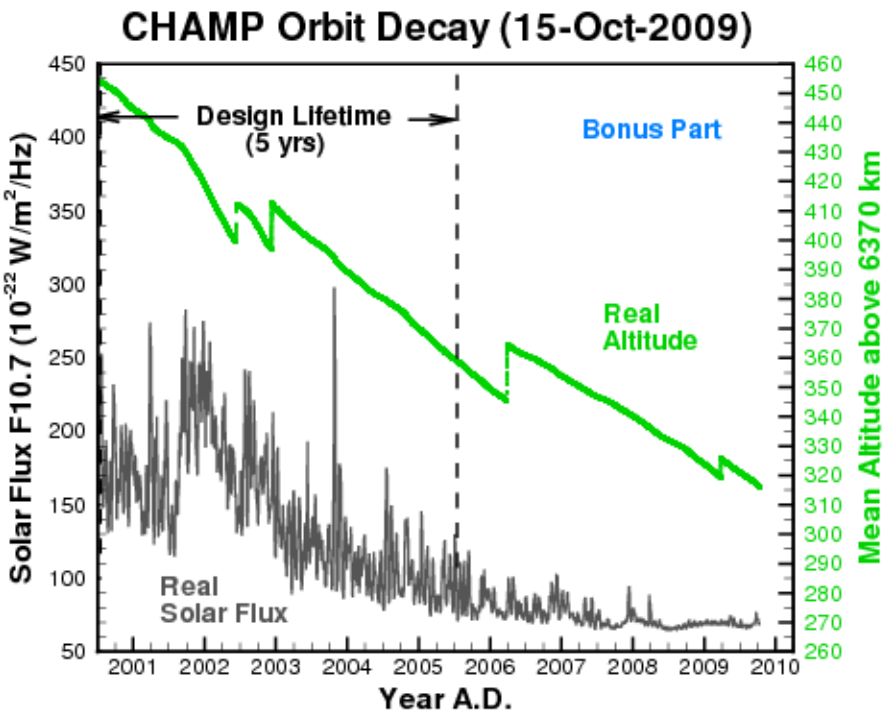

Figure 3: The decay of CHAMP's orbital altitude (http://adsc.gfz-potsdam.de)

MAGNETIC MISSION INSTRUMENTATION

The magnetic instruments of CHAMP are very similar to those of Ørsted (see Sec. 2.2.1.2). CHAMP carries the same scalar and vector magnetometers. The star imager is built by the same laboratory, but is equipped with a dual head (Fig. 4).

MAGNETOMETERS

At the tip of the 4-meter long boom, a proton precession Overhauser magnetometer measures the total intensity of the magnetic field, once per second. This instrument, which was developed by LETI, Grenoble, has an absolute accuracy of 0.5 nT. Its measurements are used in the absolute calibration of two redundant vector magnetometers, located mid-boom on an optical bench. These fluxgate magnetometers were developed and supplied by DTU Lyngby, Denmark. They sample the field at 50 hertz with a resolution < 0.1 nT.

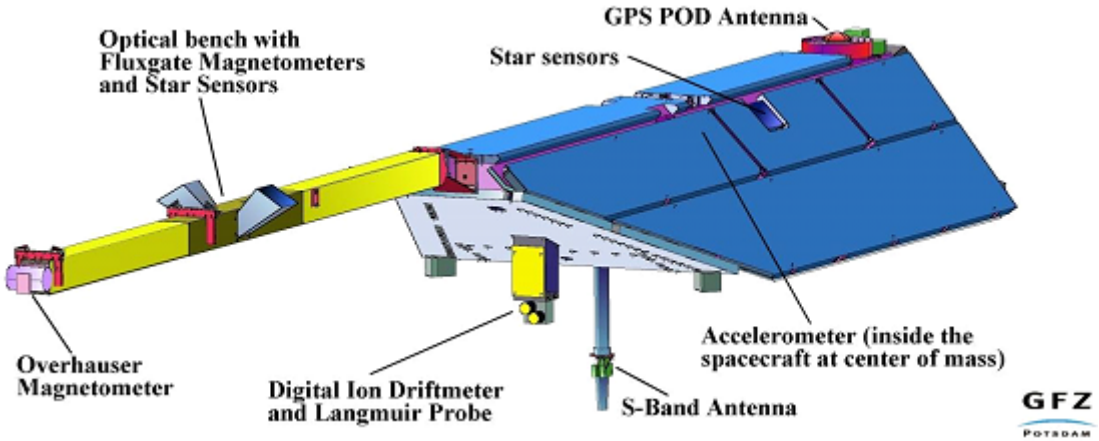

Figure 4: Front view of the CHAMP satellite

STAR IMAGERS

A star imager, developed and supplied by DTU Lyngby, Denmark, gives the orientation of the optical bench in space. Attitude uncertainty is the largest source of error in satellite vector magnetic data. Star imagers are often blinded by the sun or moon and provide unreliable attitude with regard to rotations about their direction of vision (bore sight). For this reason, CHAMP was equipped with a dual-head star imager, improving relative attitude by an order of magnitude to about 3 arc-seconds accuracy for rotations about all axes, corresponding to around 0.5 nT accuracy for the vector components. Since this high accuracy is only achieved in dual-head mode (62% of CHAMP data), future magnetic field missions (e.g., the European Space Agency mission *Swarm*, scheduled for launch in 2011) will have triple-head star imagers. A further, redundant dual-head star imager on the body of CHAMP is of limited utility for the magnetic field measurements, due to the flexibility of the boom.

ELECTRIC FIELD, ELECTRON DENSITY AND TEMPERATURE

The Air Force Research Laboratory, USA provided a Digital Ion Drift Meter (DIDM) and a Planar Langmuir Probe (PLP). The DIDM, designed to measure the electric field from ion velocities, partly failed due to frictional overheating during the launch phase of CHAMP. The PLP, which was not damaged, provides the spacecraft electric potential, electron temperature and electron density, once in 15 seconds. These quantities are used to correct magnetic field measurements for the diamagnetic effect of the plasma surrounding the satellite. The PLP measurements have thus turned out to be very useful for accurate geomagnetic field modeling.

GPS RECEIVER

Apart from providing the accurate position of CHAMP, the Black Jack GPS receiver (supplied by NASA) has the important task of providing an absolute time frame. A pulse delivered every second is used to synchronize all of the instruments on board. Furthermore, it provides a stable reference frequency for the proton precession magnetometer readings, giving them absolute accuracy.

DATA PRODUCTS

CHAMP's standard science products are labeled from level-0 to level-4, according to the amount of pre-processing applied to the original data. Scientific utility starts with level-2 products, which are calibrated, flagged and merged with accurate orbits and are supplied as daily files in Common Data Format (CDF). Level-3 products comprise the final processed, edited, and calibrated data that were used in the WMM. Derived products such as the initial CHAMP main field model CO2 (Holme et al, 2003) are classified as level-4. The level-2 to level-4 products are archived and distributed by the Information System and Data Centre (ISDC) at GFZ Potsdam (http://isdc.gfz-potsdam.de/champ).

2.2.1.2 ØRSTED

The Danish satellite Ørsted (http://web.dmi.dk/projects/oersted) is a dedicated satellite for geomagnetic field modeling. It was successfully launched on 23 February 1999 from Vandenburg Air Force Base in California on a Delta II rocket, along with the American ARGOS (Advanced Research Global Observation Satellite) and the South African micro-satellite SUNSAT. Initially planned for a minimum of 14 months, Ørsted is still delivering high quality data, as of November 2009, more than 10 years following its launch.

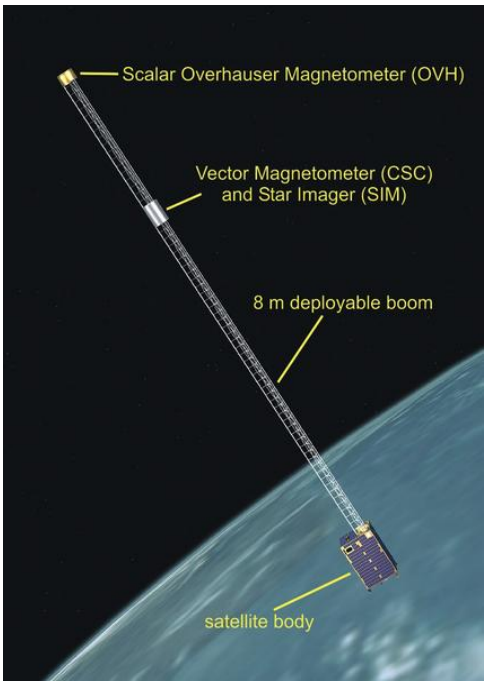

Figure 5: Ørsted satellite

SATELLITE AND ORBIT

The Ørsted satellite (Fig. 5) has a mass of 62 kilograms and measures 34 by 45 by 72 centimeters when the 8-meter boom is stowed. The main receiving station is at the Danish Meteorological Institute in Copenhagen. The satellite was

launched into a retrograde orbit with the ascending node at start of mission being 14:11 local time, apogee ~850 kilometers, perigee ~640 kilometers, inclination 96.5°, nodal period 99.6 minutes, longitude increment -24.9°/orbit and local time increment -0.88 minutes/day, corresponding to a drift of the orbital plane by 128.5°/year. The satellite velocity is approximately 7.5 kilometers/second.

MAGNETOMETERS

At the quietest location, the tip of the 8-meter boom, an Overhauser magnetometer (OVH) measures the strength of the magnetic field. It is accurate to 0.5 nT. The main purpose of this instrument is the absolute calibration of the measurements of the vector magnetometer. The OVH was built at LETI in Grenoble and was provided by the French Space Board, CNES. At some distance from the OVH (to avoid mutual disturbances of the magnetometers), a Compact Spherical Coil (CSC) fluxgate magnetometer measures the magnetic vector field (strength and direction). This instrument is stable to within 0.5 nT over time spans of several days. It was built at the Danish Technical University.

STAR IMAGER

A single-head star imager is co-located with the CSC-magnetometer to determine its orientation. The star imager is accurate to about 30 arc-seconds for rotations around its axis of vision (bore sight) and to about 5 arc-seconds for rotations about any axis perpendicular to the bore sight. This instrument was built at the Danish Technical University.

PARTICLE DETECTORS

Particle detectors were placed on the main body of the satellite to measure the flux of fast electrons (0.03-1 MeV), protons (0.2-30 MeV), and alpha-particles (1-100 MeV) around the satellite. This instrument was built at the Danish Meteorological Institute.

GLOBAL POSITIONING SYSTEM (GPS) RECEIVERS

Ørsted has a Turbo-Rogue GPS Receiver to accurately determine the position of the satellite and provide time synchronization for the instruments. The GPS Receiver was supplied by NASA, built at their Jet Propulsion Laboratory.

The calibrated data products relevant to main field modeling are the MAG-F product for the strength of the field (scalar data) and the 'MAG-L' product for the vector field. The data are available through the Danish National Space Institute (http://www.space.dtu.dk).

2.2.1.3 IN-ORBIT CALIBRATION OF SATELLITE MAGNETOMETERS

Experience with several satellite missions shows that calibration parameters can change significantly during deployment into space. Furthermore, calibration parameters exhibit gradual changes over the life of the mission. Regular in-flight calibration and updates of the respective parameters is therefore essential. To enable a successful calibration in orbit, it is of critical importance that the instruments are built in such a way that they can be described by a linear model with constant (over one day) calibration parameters. While these parameters may change slowly over the mission lifetime, they must be independent of strength or direction of the ambient magnetic field. In particular, past satellite magnetic missions have shown that it is not possible to perform an in-orbit scalar calibration of a vector magnetometer when the component readings suffer from a ‘transverse field effect’.

The linear instrument model used for successfully calibrating both Ørsted and CHAMP satellite magnetic data is described in detail by Olsen et al (2003). It can be formulated as a linear transform from the desired quantity **B**, the magnetic field vector in the reference frame of the star tracker, to the instrument output vector **E** as

$$\mathbf{E} = \underline{\mathbf{S}}\ \underline{\mathbf{P}}\ \underline{\mathbf{R}}\ \mathbf{B} + \mathbf{b} \qquad (22)$$

where $\underline{\mathbf{S}}$ is a diagonal matrix of scale factors, $\underline{\mathbf{P}}$ corrects for non-orthogonalities of the sensor elements, $\underline{\mathbf{R}}$ rotates from the star tracker reference frame into the vector magnetometer frame, and **b** is the offset vector. Each of these corrections has three parameters which have to be determined in the calibration.

The scalar in-orbit calibration is based on a comparison between the readings of the scalar and vector magnetometer. In a least-squares estimation procedure, the nine calibration parameters of a fluxgate can be determined. Here, the synthetic laboratory test field is replaced by the natural ambient field recorded over a day. This allows for regular verification of the offset vector **b**, non-orthogonalities $\underline{\mathbf{P}}$, and scale factors $\underline{\mathbf{S}}$.

The calibration parameters of the matrix **R**, namely the three rotation angles between the magnetometer and star tracker reference systems, are determined in a final, independent step. To determine these angles, one makes use of the fact that div**(B)** is zero, and chooses measurements outside of the auroral current regions, where curl**(B)** is also zero. Under these circumstances, the effect of misalignments of the star tracker and vector magnetometer reference system can be separated cleanly from genuine magnetic fields, and the three calibration parameters of the matrix **R** can be determined by a least-squares inversion. Obviously, this calibration can only succeed if the vector magnetometer and the star tracker are co-mounted onto an optical bench with sufficient rigidity and temperature stability.

2.2.2 OBSERVATORY DATA

One of the principal characteristics of observatory data is the long-term continuous coverage in time, in the region where the WMM is most used. The spatial distribution of observatories is largely determined by the location of habitable land and by the availability of local expertise, funds, and energy supply. While the distribution is uneven and sparse compared to that of satellite data, it has been reasonably constant in time (Fig. 6).

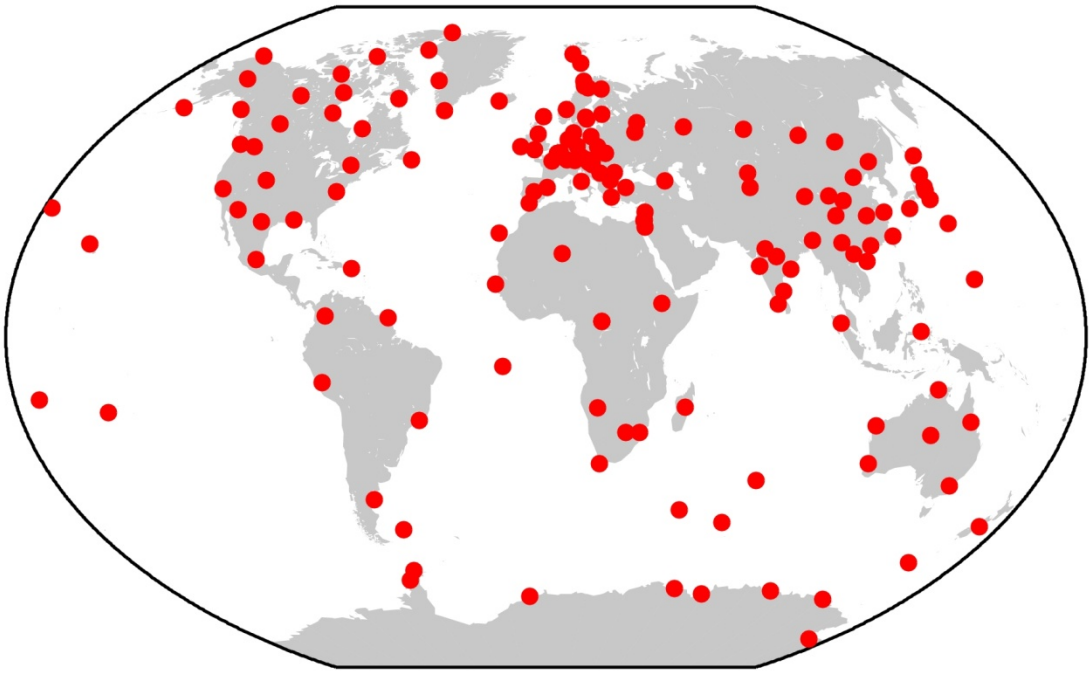

Figure 6: Locations of observatory data used in WMM2010

INSTRUMENTATION

There are three categories of instruments at an observatory. The first category comprises variometers, which make continuous measurements of elements of the geomagnetic field vector. Both analog and digital variometers require temperature-controlled environments, extremely stable platforms, and can generally operate without manual intervention. Today, the most common type of variometer is the tri-axial fluxgate magnetometer.

The second category comprises absolute instruments that can make measurements of the magnetic field in terms of absolute physical basic units or universal physical constants. The most common types of absolute instrument are the fluxgate theodolite, for measuring *D* and *I,* and the proton precession magnetometer for measuring *F*. In the former instrument the basic unit of measurement is an angle. To determine these angles, the fluxgate sensor mounted on the telescope of a non-magnetic theodolite is used to detect when it is perpendicular to the magnetic field vector. With the fluxgate sensor operating in this null-field mode, the stability of the sensor and its electronics is maximized. To complete the determination of *D* and *I*, true north is found by reference to a fixed mark of known azimuth, usually by astronomical observations. In a proton precession absolute magnetometer, the universal physical constant is the gyromagnetic ratio of the proton. Measurements with a fluxgate theodolite can only be made manually while a proton magnetometer can operate automatically.

The third category comprises semi-absolute instruments. These are instruments that measure deviations from a field, which is determined on a regular basis using an absolute instrument. One example is a proton vector magnetometer where artificial orthogonal bias fields are applied to a proton precession magnetometer sensor, located at the center of a set of coils through which currents can be passed, to obtain the components of the field vector. Like variometers, these instruments are temperature-sensitive and require stable platforms. For more information on magnetic instrumentation and operation of magnetic observatories, see Macmillan (2007) and Jankowski and Sucksdorff (1996).

DATA COLLATION AND QUALITY CONTROL

BGS and NGDC actively collect observatory data through their involvement in the World Data Center (WDC) system. They maintain databases suitable for magnetic field modeling, maintain contacts with organizations operating magnetic observatories, and collaborate with other WDCs. Each year BGS sends requests to all organizations with operating observatories for the latest data and other relevant information. The WDCs for geomagnetism benefit greatly from the efforts of INTERMAGNET whose objectives are to establish a global network of cooperating digital magnetic observatories, to adopt modern standard specifications for measuring and recording equipment, and to facilitate data exchange and the production of geomagnetic products in close to real time. In addition to operating five of the observatories shown in Figure 6, BGS operates one of six INTERMAGNET GINs (Geomagnetic Information Node), and plays a leading role in the INTERMAGNET organization (http://www.intermagnet.org). The hourly means used in the WMM were attained from http://www.wdc.bgs.ac.uk and selected preliminary INTERMAGNET data for 2009.

The quality of the data an observatory produces is the responsibility of the operator. The most important aspect of the quality for global modeling is the stability of the baseline. A baseline is the difference between the calibrated variometer data and the absolute observations. A baseline with many points, low scatter, few drifts and offsets is an indicator of good quality. Baseline plots for the INTERMAGNET observatories are available on the annual CDs of definitive data.

Quality assurance and control measures, other than those carried out by the observatory operators, are also accomplished by INTERMAGNET through its observatory standardization program, the WDCs, and by participation in the International Association of Geomagnetism and Aeronomy (IAGA) Observatory Workshops.

Final quality control procedures, prior to deriving the WMM, are achieved by BGS. For the hourly means, this involves plotting all data to identify typographical errors and jumps, and plotting differences between data and initial global models to identify drifts. If a problem in a particular dataset for the WMM is identified, an enquiry is sent to the observatory operator. If this problem is not resolved, the data are not used in the production of the final WMM. Observatories used in the production of WMM2010 are listed in Table 6.

Table 6: Observatories used in production of WMM2010. The number of data is the number of selected hourly mean values and * indicates an observatory record with a jump

IAGA code	Latitude	Longitude	Altitude (km)	Number of data
AAA	43.250	76.917	1.300	1096
AAE	9.033	38.767	2.441	1250
ABG *	18.633	72.867	0.007	993
ABK	68.350	18.817	0.380	855
AIA	-65.250	295.733	0.010	835
ALE	82.500	297.650	0.060	281
AMS	-37.833	77.567	0.048	1323
AMT	31.550	34.917	0.350	256
API	-13.800	188.233	0.004	936
AQU	42.383	13.317	0.682	1182
ARS	56.433	58.567	0.290	1141
ASC	-7.950	345.617	0.177	1196
ASP	-23.767	133.883	0.557	1528
BDV	49.083	14.017	0.496	1338
BEL	51.833	20.800	0.180	1472
BFE	55.633	11.667	0.080	1158
BFO	48.333	8.317	0.641	332
BGY	31.717	35.083	0.750	710
BJN	74.500	19.200	0.020	478
BLC	64.333	263.967	0.030	830
BMT	40.300	116.200	0.183	1205
BNG *	4.317	18.567	0.395	969
BOU	40.133	254.767	1.650	1380
BOX	58.033	38.967	0.000	816
BRW	71.300	203.383	0.012	788
BSL	30.350	270.367	0.008	1238
CBB	69.117	254.967	0.020	832
CBI	27.100	142.183	0.155	999
CDP	31.000	103.700	0.653	1018
CLF	48.017	2.267	0.145	1482
CMO	64.867	212.133	0.090	894
CNB	-35.317	149.367	0.859	1417
CNH	43.833	125.300	0.234	488
CSY	-66.283	110.533	0.040	548
CTA	-20.083	146.267	0.370	1531
CZT	-46.433	51.867	0.155	1347
DLR	29.483	259.083	0.355	1198
DOB	62.067	9.117	0.660	861
DOU	50.100	4.600	0.225	1353
DRV	-66.667	140.017	0.030	915
DVS	-68.583	77.967	0.000	163
EBR	40.817	0.500	0.046	1340
ELT	29.667	34.950	0.250	1000
ESA	39.233	141.350	0.396	1234
ESK	55.317	356.800	0.245	1316
EYR	-43.417	172.350	0.120	1398
FCC	58.783	265.917	0.015	1135
FRD	38.217	282.633	0.069	1444

IAGA code	Latitude	Longitude	Altitude (km)	Number of data
FRN	37.083	240.283	0.331	1388
FUQ	5.467	286.267	2.543	1415
FUR	48.167	11.283	0.572	1473
GCK	44.633	20.767	0.231	301
GDH	69.250	306.467	0.024	559
GLM	36.400	94.900	2.802	661
GNA	-31.783	115.950	0.060	1472
GUA	13.583	144.867	0.150	1371
GUI	28.317	343.567	0.868	1096
GZH	22.967	112.450	0.011	883
HAD	51.000	355.517	0.095	1473
HBK	-25.883	27.700	1.522	1263
HER	-34.417	19.233	0.026	1472
HLP	54.600	18.817	0.001	1273
HON	21.317	202.000	0.004	1339
HRB	47.867	18.183	0.120	1338
HRN	77.000	15.550	0.015	655
HTY	33.117	139.800	0.220	869
HUA	-12.050	284.667	3.312	1586
IQA *	63.750	291.483	0.100	843
IRT	52.167	104.450	0.540	1513
IZN	40.500	29.733	0.256	477
KAK	36.233	140.183	0.036	1406
KDU	-12.683	132.467	0.014	1494
KIR	67.833	20.417	0.390	450
KNY	31.417	130.883	0.107	1215
KNZ	35.250	139.950	0.342	1235
KOU	5.217	307.267	0.010	1212
KSH	39.500	76.000	1.321	371
LER	60.133	358.817	0.085	1108
LIV	-62.667	299.600	0.019	709
LMM	-25.917	32.583	0.010	168
LNP	25.000	121.167	0.100	244
LOV	59.350	17.817	0.025	495
LRM	-22.217	114.100	0.004	1358
LRV	64.183	338.300	0.005	931
LVV *	49.900	23.750	0.400	1003
LZH	36.083	103.850	1.560	1228
MAB	50.300	5.683	0.440	1347
MAW	-67.600	62.883	0.012	1037
MBO	14.400	343.050	0.007	1449
MCQ	-54.500	158.950	0.008	1520
MEA	54.617	246.650	0.700	1288
MID	28.217	182.617	0.003	209
MIZ	39.117	141.200	0.125	1235
MMB	43.917	144.183	0.042	1420
MOS	55.467	37.317	0.200	518
MZL	49.600	117.400	0.682	998
NAQ	61.167	314.567	0.004	1067
NCK	47.633	16.717	0.160	1338
NEW	48.267	242.867	0.770	1377
NGK	52.067	12.683	0.078	1473

IAGA code	Latitude	Longitude	Altitude (km)	Number of data
NGP *	21.150	79.083	0.000	688
NUR	60.500	24.650	0.105	1075
NVS	54.850	83.233	0.130	1477
OTT	45.400	284.450	0.075	1497
PAF	-49.350	70.250	0.015	1270
PAG	42.517	24.183	0.556	1131
PBQ	55.283	282.250	0.040	1017
PEG	38.083	23.933	0.380	522
PHU	21.033	105.950	0.005	1310
PND	11.917	79.917	0.000	616
PPT	-17.567	210.417	0.357	1339
PST	-51.700	302.117	0.135	960
QGZ	19.000	109.800	0.227	506
QIX	34.600	108.200	0.893	818
QSB	33.867	35.650	0.525	839
RES	74.683	265.100	0.030	779
SBA	-77.850	166.783	0.010	659
SFS	36.500	353.883	0.075	1317
SHU	55.350	199.533	0.080	517
SIL	24.933	92.817	0.000	735
SIT	57.067	224.667	0.024	1148
SJG	18.100	293.850	0.424	1278
SOD	67.367	26.633	0.178	884
SPT	39.550	355.650	0.922	1352
SSH	31.100	121.183	0.100	803
STJ	47.600	307.317	0.100	1130
SUA	44.683	26.250	0.084	866
TAM	22.800	5.533	1.373	1432
TAN	-18.917	47.550	1.375	931
TEO	19.750	260.817	2.280	721
TFS	42.100	44.700	0.980	383
THJ	24.000	102.700	1.820	1018
THL	77.483	290.833	0.057	738
THY	46.900	17.900	0.187	1335
TIR	8.667	77.817	0.000	688
TND	1.283	124.950	0.704	523
TRO	69.667	18.950	0.105	502
TRW	-43.267	294.617	0.030	1249
TSU	-19.200	17.583	0.083	1121
TUC	32.167	249.267	0.770	1397
TUN	3.517	98.567	0.000	219
UJJ	23.183	75.783	0.000	410
UPS	59.900	17.350	0.050	646
VAL	51.933	349.750	0.014	1332
VIC	48.517	236.583	0.197	1424
VNA	-70.667	351.733	0.000	719
VSK	17.667	83.317	0.000	587
VSS	-22.400	316.350	0.457	1165
WHN	30.533	114.567	0.042	864
WIK	48.267	16.317	0.400	841
WNG	53.750	9.067	0.050	1313
YKC	62.483	245.517	0.198	882

2.2.3 OTHER DATA AND DERIVED PRODUCTS

Other magnetic data and products used in the production of the WMM are various magnetic activity indices derived from observatory data, and solar wind data measured by the ACE satellite. These are used to either select the data for input to the model or to form part of the input to the model.

INDEX K_P

The planetary Kp ("Planetarische Kennziffer") index (http://www-app3.gfz-potsdam.de/kp_index/description.html) is based on the K-index, a local index of the three-hourly range in magnetic activity of the two horizontal field components (*X* and *Y*) relative to an assumed quiet-day curve for the geomagnetic observatory. Local disturbance levels are determined by measuring the range (difference between the highest and lowest values) during three-hourly time intervals for the most disturbed magnetic field component. The range is then converted into a local K-index according to a pseudo-logarithmic scale, which is station specific, in an attempt to normalize the frequency of the different disturbance sizes. The three-hourly Kp index is the average of local K values from 13 selected, subauroral stations and is expressed in a scale of thirds (28 values). The IAGA station codes (in order of geomagnetic latitude) are: LER, MEA, SIT, ESK, UPS, OTT, BFE, HAD, WNG, NGK, FRD, CNB and EYR. The Kp index is used to select measurements during magnetically undisturbed times.

INDEX A_M

The a_m index (m=mondial; http://isgi.cetp.ipsl.fr/lesdonne.htm) is derived from observatory K indices, as is the Kp index, but using data from 21 observatories that provide a more global distribution than those used for the Kp index. The a_m index is sometimes used as an alternative to the Kp index in selecting data during quiet times.

INDEX DST

Charged particles trapped by the geomagnetic field in the magnetosphere drift around the Earth at a distance of 3-8 Earth radii creating a westward electric ring current whose field opposes the main geomagnetic field. The strength of this field is on the order of tens of nT during quiet times and several hundred nT during magnetic storms. Magnetopause, tail, and partial ring currents represent additional contributions leading to asymmetries in the field which increase during storms. The symmetric part of this composite disturbance field is tracked by the Dst (disturbance storm-time) index (Sugiura, 1964; http://wdc.kugi.kyoto-u.ac.jp/dstdir). It is derived from the measurements collected at four low latitude observatories. The Dst is used both for data selection and, in terms of the Est/Ist index described below, as a quantitative correction of the disturbance field.

INDICES EST / IST

The Dst index is meant to track the strength of a uniform field in the magnetic northward direction. In practice, however, the measured field is the sum of the external and induced parts. When representing magnetospheric fields by Dst, it is important to separate the external and internal contributions to Dst due to their very different geometries. Using a global conductivity model of the Earth, the Dst index can be separated into Est and Ist indices tracking the external and internal contributions, respectively (Maus and Weidelt, 2004). The Est/Ist indices are available at http://www.ngdc.noaa.gov/geomag/est_ist.shtml. They are used to subtract contributions of the magnetic disturbance field from the data used for estimating the WMM coefficients.

POLAR CAP (PC) INDICES

The Polar Cap indices characterize geomagnetic activity over the polar caps caused by changes in the interplanetary magnetic field (IMF) and solar wind. In particular they characterize the electric field defining the polar cap convection. There are two indices: one for the north based on data from Thule (THL) observatory (derived by the Danish Meteorological Institute), and one for the south based on data from Vostok (VOS) observatory (derived by the Arctic and Antarctic Research Institute in St. Petersburg). These indices are used to select undisturbed data at high northern and southern latitudes. PC indices are available at http://www.ngdc.noaa.gov/stp/SOLAR/pcindex.html.

INDEX IE

The IE index is a 1-minute auroral zone index derived by the Finnish Meteorological Institute using data from the Image magnetometer chain (Viljanen and Hakkinen, 1997). Due to its timeliness, it is used in the WMM instead of the more widely known AE index, to select undisturbed data at high northern latitudes.

INTERPLANETARY MAGNETIC FIELD

The solar wind drives electric currents in the Earth's magnetosphere and ionosphere. An interplanetary magnetic field (IMF) is carried by the plasma of the solar wind. Relevant for the response of the magnetosphere is the speed of the solar wind and the direction and strength of the IMF. These solar wind parameters are monitored by NASA's Advanced Composition Explorer (ACE) satellite. Using magnetospheric models, the ACE solar wind measurements are projected downstream onto the magnetospheric bow shock and are made available by NASA as 1-minute readings in geocentric magnetospheric coordinates at http://omniweb.gsfc.nasa.gov/hw.html. The IMF is used both for data selection and as a quantitative parameter to correct for magnetospheric disturbance fields.

MERGING ELECTRIC FIELD E_M

The merging electric field, derived from the IMF and solar wind speed (http://omniweb.gsfc.nasa.gov/hw.html), is a parameter suitable for describing the variation of the magnetospheric tail current field. Following Kan and Lee (1979), the merging electric field, E_m, is calculated as

$$E_m = v_{SW}\left(B_y^2 + B_z^2\right)^{\frac{1}{2}} \sin^2\left(\frac{\Theta}{2}\right) \tag{23}$$

where v_{SW} is the solar wind velocity, B_y and B_z are the IMF components in the Geocentric Solar Magnetospheric (GSM) frame and Θ is the clock angle of the IMF. The merging electric

field goes into saturation for strong solar wind driving. In the parameterization of the tail current field we therefore use the effective field, E'_m, defined as

$$E'_m = \frac{E_{thresh} E_m}{\sqrt{E_{thresh}^2 + E_m^2}} \tag{24}$$

where the threshold electric field is E_{thresh} = 8 mV/m.

The merging electric field is used both for data selection and quantitative correction of disturbance fields.

SOLAR FLUX INDEX F10.7

Extreme ultraviolet (EUV) radiation from the sun ionizes the Earth's atmosphere. A moving 81-day average of the F10.7 solar flux index (available at http://www.spaceweather.gc.ca/sx-eng.php) has been shown to provide a good proxy for the intensity of the EUV radiation. The moving average, commonly referred to as F10.7a, also provides a useful proxy for the progression of the solar cycle (http://www.swpc.noaa.gov/SolarCycle). Magnetic activity is known to lag behind the solar cycle. In magnetospheric field models, the time varying bias of the Dst index can therefore be described using F10.7a with a 20 month time lag. The F10.7a index was used here to correct for solar-cycle dependent magnetospheric disturbance fields.

2.3 DERIVATION OF THE MODEL

Since the WMM only describes the long-wavelength internal part of the geomagnetic field, it is important to separate unrelated contributions to the field, which would otherwise contaminate the WMM coefficients. A successful modeling strategy relies on three elements:

1. DATA SELECTION

Measurements during daytime and during periods of strong solar activity are contaminated by external current systems, which are difficult to accurately model. Therefore, only nighttime data during magnetically quiet periods, as inferred from the above-described indices, were used in estimating the WMM coefficients.

2. *DATA CORRECTIONS*

Some contributions to the measured magnetic field, such as the diamagnetic effect of ionospheric plasma (Lühr et al, 2003) or motional induction by tidal ocean currents (Kuvshinov and Olsen, 2005; Maus, 2007), can be accurately modeled and were corrected for prior to the estimation of the WMM main field coefficients.

3. *USE OF EXTENDED PARENT MODELS*

To account for contributions that have not been removed in the previous two steps, an extended set of model parameters is co-estimated with the WMM model coefficients. These account for smaller-wavelength internal magnetic field contributions (spherical harmonic degree larger than 12), second time derivatives (secular acceleration) and contributions from currents external to the Earth. The set of WMM coefficients plus the extended model parameters is called a *parent model* of the WMM. Two different parent models were produced, reflecting different modeling strategies employed by NGDC for the main field model and BGS for the secular variation model.

2.3.1 PARENT MODEL FOR MAIN FIELD COEFFICIENTS

Only satellite measurements were used to produce the main field parent model. Of the three satellite magnetic missions of the past decade, CHAMP (Reigber et al, 2002) provides the optimal data basis, with close to 100% data retrieval rate, small polar gap and dual-head star camera for low-noise attitude determination. The following three subsections describe data selection, corrections and parent model parameterization for the main field coefficients.

DATA SELECTION

The latest three years of available CHAMP satellite measurements were used, spanning the time period 2006.5 to 2009.7. All data were sub-sampled to 20 seconds, corresponding to about 150 kilometers along-track spacing. Separate, overlapping data sets were compiled for mid-latitudes (-60° to 60° geomagnetic latitude) and high-latitudes (> 50° and <-50°). Vector data were only used at mid-latitudes. Scalar and vector data at mid-latitudes were selected from the 22:00-5:00 local time sector. Data at high-latitudes were used from all local times. No exclusion for certain solar zenith angle ranges was made. A further selection requirement was

that attitude data from dual-head star camera mode and electron density and temperature measurements were available.

Table 7: Summary of data selection criteria. Mid-latitudes refer to track segments covering -60° to 60° geomagnetic latitude and high latitudes refers to overlapping tracks at <-50° and >50° (See Sec. 2.2.3 for further information)

	Mid-latitudes	High-latitudes
$\|Dst\|$	≤ 30 nT	≤ 30 nT
$\|dDst/dt\|$	≤ 2 nT/h	≤ 5 nT/h
a_m	≤ 12	≤ 27
a_m 3 hours before	≤ 15	≤ 27
$\|By\ of\ IMF\|$		≤ 8 nT
Bz of IMF		≥ -2 nT, ≤ 6nT
E_m		≤ 0.8 mV/m
Diamagnetic effect	≤ 5 nT	
Jump in diam. eff.	≤ 2 nT	

DATA CORRECTION AND WEIGHTING

The following corrections were applied to the fully calibrated satellite data:

1. The magnetic signals of motional induction in the oceans due to the 8 major tidal constituents up to spherical harmonic degree 45 were subtracted, as predicted by Kuvshinov and Olsen (2005).

2. The signature of plasma pressure gradient currents was subtracted using the correction for the diamagnetic effect, as proposed by Lühr et al (2003), making use of *in situ* electron density and temperature measurements by CHAMP.

3. A magnetospheric field model was subtracted from the data. Due to the local-time asymmetry of magnetospheric fields, day-side data have to be included in their modeling. Since day-side data are too noisy for being included in the modeling of the main field, the magnetospheric fields are best estimated in a separate processing step. We used a revised version of the model described in Maus and Lühr (2005). This 18-parameter model quantifies the quiet-time magnetospheric fields, modulated by the Interplanetary Magnetic Field and solar activity. Details of the magnetospheric model are given in Lühr and Maus (2009).

The local data density per unit area at orbital altitude and per year was determined, and data were then weighted accordingly in order to achieve approximate uniform weight in space and time. Such a weighting scheme improves the accuracy of the resulting model.

MODEL DESCRIPTION

The parent model for the main field is comprised of:

1. The static part of the internal field to degree and order 40
2. The secular variation (SV) to degree and order 16
3. The secular acceleration (SA) to degree and order 16
4. A daily varying degree-1 external field, as proposed by Olsen et al (2006), represented by a single value of the strength of the axial dipole in the Solar-Magnetic (SM) frame for every 24-hour interval

The model coefficients were estimated in a non-iterative least-squares approach, where the information from the scalar data was linearized using POMME-5 (Maus et al, 2006) as a starting model. The SV coefficients were damped starting at degree and order 14, while the SA coefficients were damped for degrees 9 and higher.

2.3.2 PARENT MODEL FOR SECULAR VARIATION COEFFICIENTS

A combined dataset of satellite and ground observatory measurements was used to produce the parent model for estimating the secular variation coefficients. By using data from both satellites and observatories the spatial and temporal continuity is enhanced so as to better characterize the secular variation. The following three subsections describe data selection, data weighting, and parent model parameterization for the secular variation coefficients.

DATA SELECTION

CHAMP and Ørsted scalar and vector data were selected between 1999.2 and 2009.6. All satellite data were sub-sampled every 60th second, corresponding (at a velocity of 8 kilometers/second) to about 500 kilometers along-track spacing. Scalar and vector data were then selected from the 22:30-5:00 local time sector. No exclusion for certain solar zenith angle ranges was made. Additional selection criteria are given in Table 8.

Scalar and vector observatory hourly means were calculated using the 01:00 to 02:00 local time sector for 152 observatories around the world. To minimize contamination of observatory data from ionospheric sources, data were selected only when the ionosphere at 110 kilometers above the observatory was in darkness. For high geomagnetic latitudes (> 50 and <-50 degrees) observatory data were projected onto an *a priori* model vector and the resulting pseudo-scalar data were used in the inversion. For other latitudes, vector data were used. Additional selection criteria are given in Table 8. The observatories used and the final numbers of selected hourly mean values are listed in Table 6. For observatories with unreported baseline shifts, the time series were split, and separate crustal biases were introduced in the parent model for the periods preceding and following the jump.

Table 8: Summary of satellite and observatory data selection criteria (see Sec. 2.2.3 for further information)

Satellite data selection criteria	
Magnetic indices:	
K_p	≤ 2-
K_p for previous 3 hours	≤ 2-
|*dDst/dt*|	≤ 5 nT/h
IE	≤ 30 nT
PC	≤ 0.2 mV/m
Solar wind data:	
Bz of IMF	≥ 0 nT, ≤ 6 nT
By of IMF	≥ -3 nT, ≤ 3 nT
Bx of IMF	≥ -10 nT, ≤ 10 nT
Solar wind speed	≤ 450 km/s
Data consistency check:	
|observed magnetic field value - value from *a priori* model|	≤ 100 nT
|scalar F from OVH – vector F from CSC|	≤ 2 nT
Observatory data selection criteria	
Magnetic indices:	
K_p	≤ 2+
|*dDst/dt*|	≤ 5 nT/h
Solar wind data:	
Bz of IMF	≥ 0 nT

DATA CORRECTION AND WEIGHTING

Corrections were not applied to the CHAMP and Ørsted data as the magnetospheric field signals are co-estimated in the parent model. They were weighted according to a combination of the following three quantities (Thomson et al, 2009):

1. A measure of local magnetic activity using the standard deviation along short segments (60 samples) of satellite track.
2. A larger-scale noise estimator derived from activity measured at the geographically nearest magnetic observatories to the sample point.
3. The number of data per unit area of the globe relative to the mean number of data per unit area. This effectively down-weights higher latitude data.

The observatory data were first rotated from the geodetic coordinate system into the geocentric coordinate system (using equations in Sec. 1.2). They were weighted according to the following two criteria:

1. High latitude pseudo-scalar data were assigned lower weight than lower latitude vector data.
2. All data were further weighted according to the cosine of the solar zenith angle.

The final ratio of the total weights (equals the number of data/mean variance) for the different data types is CHAMP 2.1 : Ørsted 1.0 : Observatories 1.3.

MODEL DESCRIPTION

The parent model comprises:

1. The static part of the internal field to degree and order 60
2. Piecewise-linear time dependence to internal degree and order 13 with nodes 1 year apart
3. Degree and order 1 external field with time-dependence derived from the Vector Magnetic Disturbance index (Thomson and Lesur, 2007); piecewise-linear terms with nodes 1 year apart; and 24-hour, semi-annual, and annual periodicities. Induced terms are also included
4. Individual terms for the observatory crustal biases

The model coefficients were estimated using an iterative re-weighted least-squares technique; the iterations were required on two accounts (1) to deal with the scalar data that are not linear functions of the model coefficients and (2) to use a more realistic estimate of error distribution than the Gaussian or normal distribution. The Laplacian distribution of errors is assumed.

The secular variation coefficients were set equal to the average of yearly samples of the secular variation from 2005.0 to 2009.0 of the internal coefficients of the parent model.

2.3.3 VALIDATION PROCESS

The existence of two parent models permitted inter-comparison of sets of WMM2010 coefficients. The use of slightly different data sets and modeling methods allows for semi-independent validation of the resulting models, adding confidence to the resulting WMM. The final coefficients were drawn from the NGDC parent model for the main field and from the BGS parent model for the secular variation.

3. ASSESSMENT OF THE MODEL

This section discusses the accuracy and limitations of the WMM2010. In particular, it assesses possible sources of disagreement between the measurement of a magnetic field element and the prediction of the WMM2010. Apart from man-made disturbances of the measurement, which are not discussed here, there are two sources of disagreement between magnetic field observations and the WMM. The first is due to inaccuracies in the model coefficients. The second is due to the fact that the WMM does not account for all of the contributions to the observed magnetic field. The WMM accuracy and limitations are discussed in the two following sections, followed by a summary in terms of a total error budget.

3.1 ACCURACY OF THE WMM2010

Changes of the fluid flow in the Earth's outer core lead to unpredictable changes in the Earth's magnetic field. Fortunately, the system has large inertia, so these changes take place over time scales of many years. By surveying the field for several years, one can precisely map the present field and its rate of change, and then linearly extrapolate the rate out into the future for several years. Provided that suitable satellite magnetic observations are available, the prediction of the WMM is highly accurate on its release date and then subsequently deteriorates towards the end of the 5-year epoch, when it has to be updated with revised values of the model coefficients.

The accuracy requirements for the WMM are detailed in the military specification MIL-W-89500 (Defense Mapping Agency, 1993). In summary, the requirement is that the global root mean square (RMS) difference between the WMM and the observed magnetic field at sea level should be within 1° for *D* and *I*, within 140 nT for *X* and *Y*, within 200 nT for *H* and *Z* and within 280 nT for *F* for the entire 5-year lifetime of the model. In addition, at polar latitudes above 55°, the RMS difference for *GV* should be within 1°.

3.1.1 CONSISTENCY OF INDEPENDENT PARENT MODEL PREDICTIONS

Some insight into the uncertainties of the WMM2010 coefficients can be gained by comparing the predictions of different modeling approaches. The parent models of NGDC and BGS differ both in the data used (only CHAMP satellite data for the former and a combination of CHAMP, Ørsted and ground observatory data for the latter), as well as in the way different contributions to the field are represented and extrapolated into the future. Each parent model provides sets of coefficients for both the main field and the secular variation. In the final WMM, the NGDC set was used for the main field and the BGS set was used for the secular variation. The second and third rows in Table 9 list the differences between the predictions of the two sets of coefficients. As expected, differences are small at the onset of the epoch and significantly increase towards the end. Due to unpredictable changes in the magnetic field, the true errors in 2015 will likely be somewhat larger than estimated in this way. Maps of declination differences for the start (Fig. 7) and end (Fig. 8) of the model validity provide an indication of where the largest uncertainties are concentrated.

Table 9: Root mean square (RMS) differences at the Earth's surface. The last row provides the most realistic estimate of WMM2010 accuracy at its end-of-life in 2015. Values are given in nT and degrees, as applicable

Row		X	Y	Z	H	F	I	D	GV
1	MIL-W-89500 requirement threshold	140	140	200	200	280	1.0	1.0	1.0
2	NGDC Parent – BGS Parent in 2010.0	5	2	6	4	6	0.01	0.08	0.18
3	NGDC Parent – BGS Parent in 2015.0	36	32	60	36	38	0.10	0.20	0.42
4	WMM2010-WMM2005 in 2005.0	11	8	16	11	13	0.02	0.08	0.18
5	WMM2010-WMM2005 in 2010.0	61	58	101	61	79	0.12	0.25	0.50

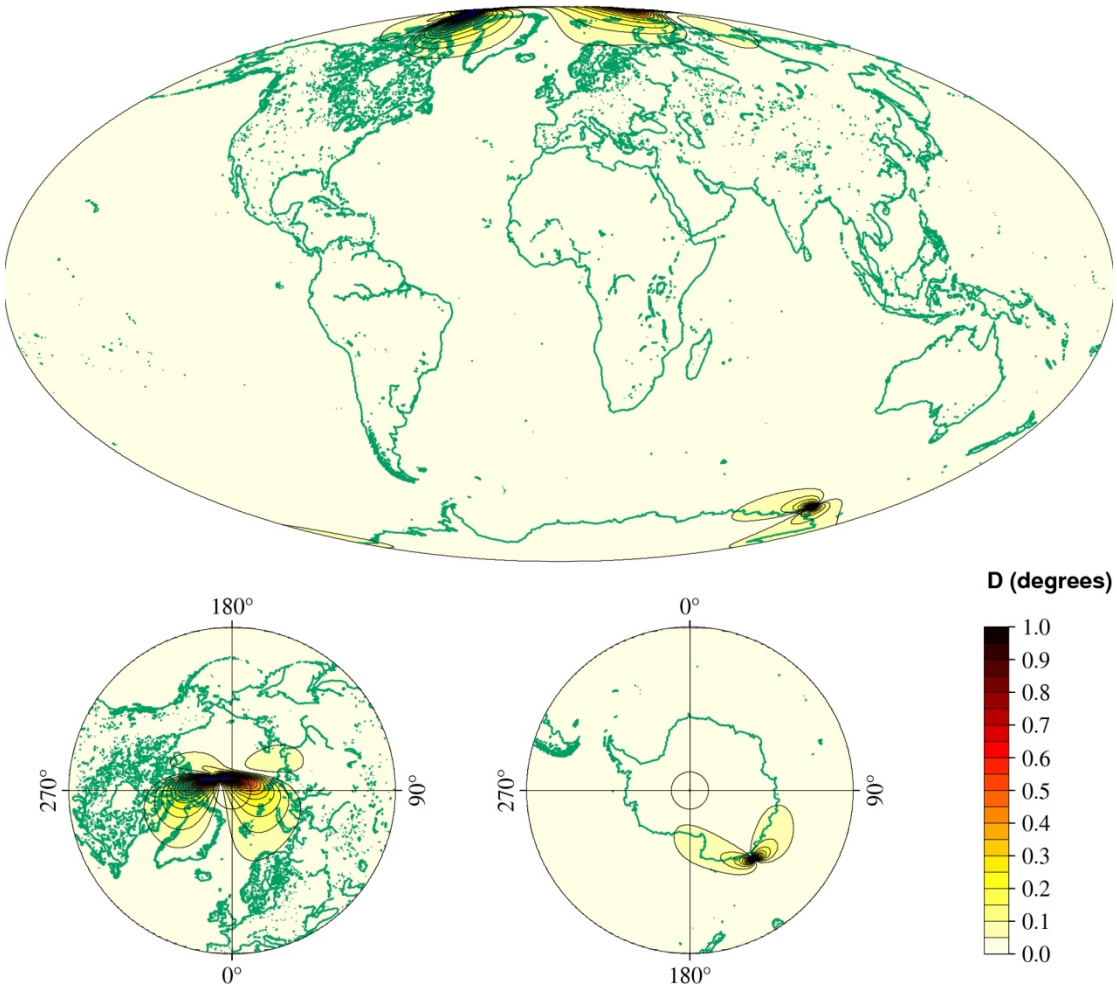

Figure 7: Absolute WMM2010 declination uncertainty for 2010.0, estimated from the difference between the independently-derived NGDC and BGS model coefficient sets

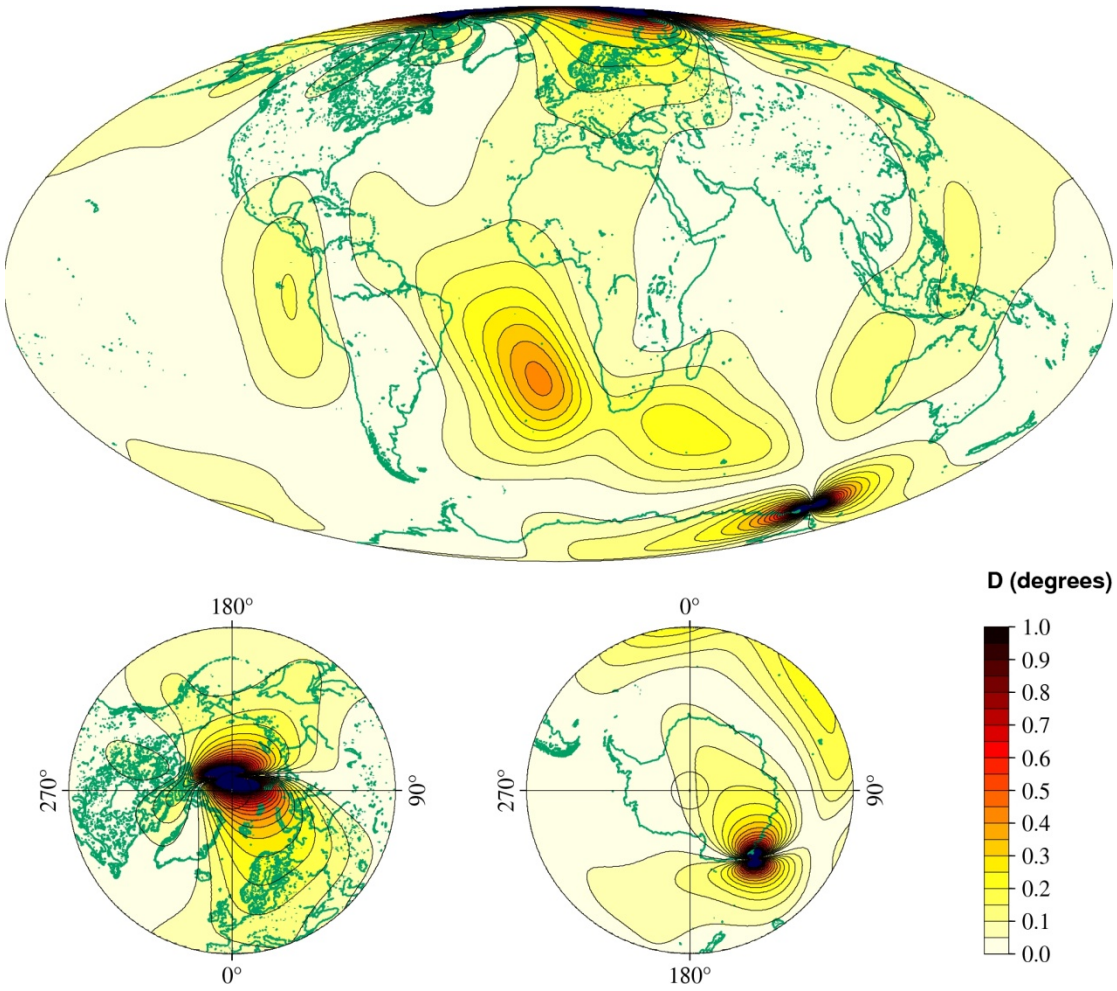

Figure 8: Absolute WMM2010 declination uncertainty at the end of the model validity in 2015.0, from the difference between the NGDC and BGS model coefficient sets

3.1.2 RETROSPECTIVE LOOK AT WMM2005

As discussed above, the WMM is accurate at the onset of the epoch and then deteriorates towards the end of the valid period. Thus, WMM2005 is most accurate in 2005.0 and deteriorates as it approaches 2010.0, while WMM2010 is most accurate in 2010.0. A comparison between WMM2005 and WMM2010 therefore offers two opportunities. The first opportunity is that the comparison in 2005 provides an internal consistency check of WMM2010. Since the secular variation coefficients were estimated from years 1999 to 2009, the hind-cast of the model for 2005.0 is expected to be better than the forecast for 2015.0. Row 4 of Table 9 indeed shows that the differences in 2005 between the two models are reasonably low. The second opportunity is to compare the WMM2005 prediction for 2010.0 with the main field of WMM2010. This comparison assesses the accuracy of the WMM2005 at the end of its lifetime. As shown in row 5 of Table 9, the accuracy of WMM2005 was well within the military specification. The magnetic field observing systems used to produce WMM2010 are very similar to the ones used for WMM2005. Taking progress in magnetic field modeling methodology into account, and the fact that the past five years were under magnetically quiet solar minimum conditions, one can expect the accuracy of the WMM2010 to reach and possibly exceed the accuracy of the WMM2005. The last row of Table 9 therefore provides a conservative estimate of WMM2010 accuracy at the end of its lifetime in 2015.0.

The differences between the WMM2005 and WMM2010 predictions for the magnetic field in 2010 are further displayed in Figure 9. The spatial distribution of discrepancies is not necessarily an indication of where the largest errors will occur in the future. However, the largest uncertainties in the declination and grid variation will again be concentrated near the magnetic poles, where the strength of the horizontal component of the field is lowest.

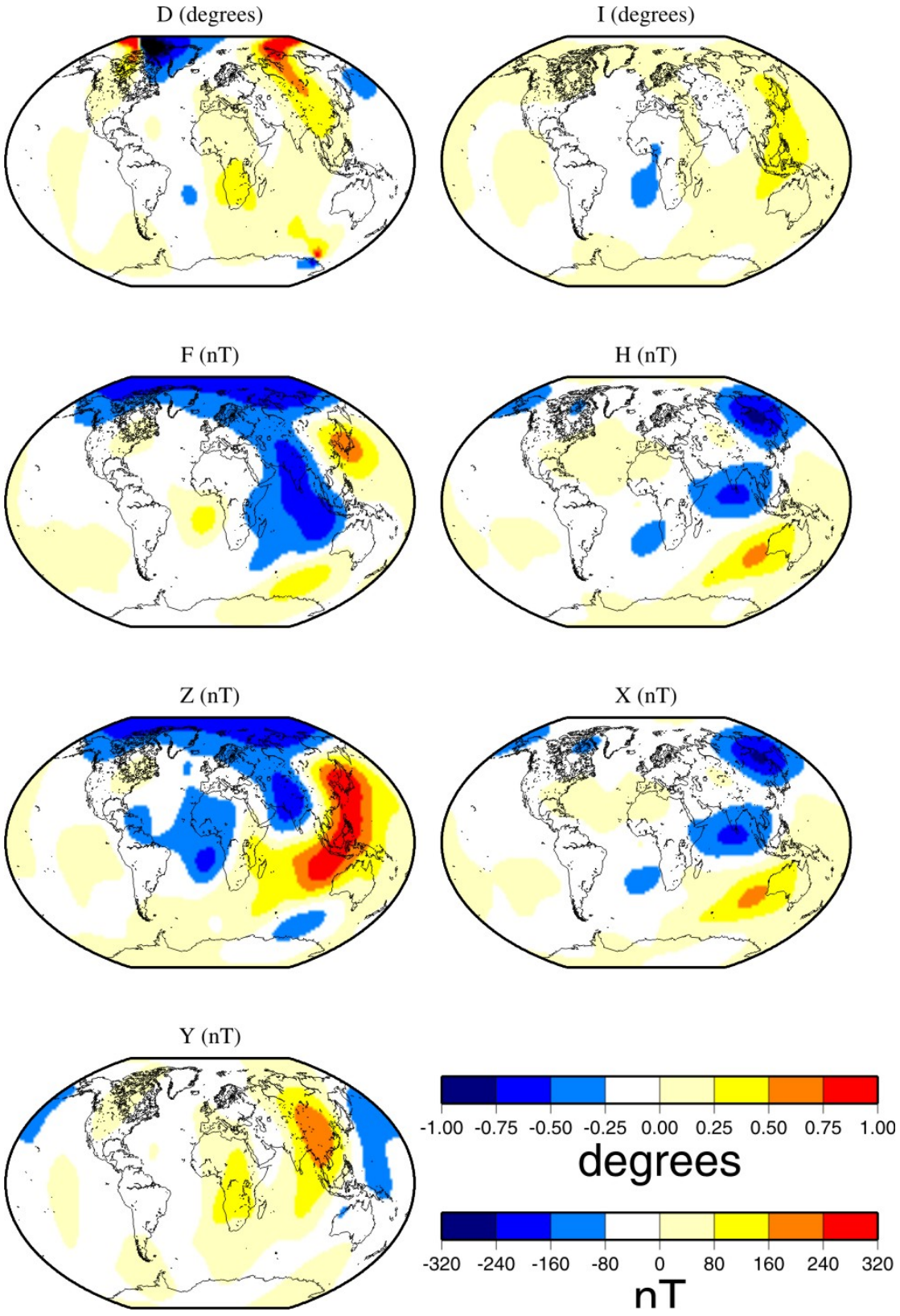

Figure 9: Differences between WMM2010 and WMM2005 in 2010.0 at the Earth's surface

3.2 LIMITATIONS OF THE WMM2010

The WMM2010 is valid for the period 1 January 2010 through 31 December 2014 between altitudes of 1 kilometer below the surface to 850 kilometers above the surface of the Earth.

It is important to recognize that the WMM and the charts produced from this model characterize only the long-wavelength portion of the Earth's internal magnetic field, which is primarily generated in the Earth's fluid outer core. The portions of the geomagnetic field generated by the Earth's crust and upper mantle, and by the ionosphere and magnetosphere, are largely unrepresented in the WMM. Consequently, a magnetic sensor such as a compass or magnetometer may observe spatial and temporal magnetic anomalies when referenced to the WMM. In particular, certain local, regional, and temporal magnetic declination anomalies can exceed 10 degrees. Anomalies of this magnitude are uncommon but they do exist. Declination anomalies on the order of 3 or 4 degrees are not uncommon but are usually of small spatial extent.

The magnetic satellite missions of the past decade have lead to a significant improvement in the accuracy with which the WMM model coefficients can be determined. Currently, the much larger source of discrepancies between model and observation is therefore due to contributions to the magnetic field which are not included in the model. The magnitude of the contribution of the crustal and disturbance fields at the Earth surface can be estimated by a comparison of the WMM with ground magnetic observatory measurements.

To assess the strength of the crustal and disturbance field contributions at the Earth's surface, the available magnetic observatory measurements for the years 1996-2006 were analyzed. The internal field was separated from the disturbance field by making use of the fact that the internal field changes slowly with time scales of years, while the disturbance field is characterized by periods shorter than a few months. The internal field was determined by fitting a spline function with a nodal distance of 1 year to the quiet-time observatory measurements, using a separate spline for each vector component at each observatory. In Section 3.2.1 it is compared to the relevant WMM. The disturbance field was then inferred as the difference between the observatory measurement and the internal field given by the spline function. The statistics of the disturbance field are given in Section 3.2.2.

3.2.1 CRUSTAL FIELD CONTRIBUTION

On land, spatial anomalies are produced by mountain ranges, ore deposits, ground struck by lightning, geological faults, and cultural features such as trains, planes, vehicles, railroad tracks, power lines, etc. The corresponding deviations are usually smaller at sea, increase with increasing latitude, and decrease with increasing altitude of an air- or spacecraft. In ocean areas these anomalies occur most frequently along continental margins, near seamounts, and near ocean ridges, trenches, and fault zones, particularly those of volcanic origin.

Subtracting the appropriate WMM from the observatory spline function gives the part of the internal field that is not represented by the WMM. Apart from inaccuracies in the WMM, which were already discussed in Section 3.1, the residuals primarily reflect the crustal field. This contribution, listed in row 3 of Table 10, was determined for the year 2000 in which good coverage by 140 observatories was available in our data set. For the year 2000, the WMM2000 is known to represent the main field very accurately. Therefore, its disagreement with the observatory spline functions provides the local crustal contribution. However, the magnetic observatories are all land-based, and some are close to large crustal magnetic anomalies. Average crustal contributions at sea are likely to be weaker than over land. The globally averaged crustal contribution could therefore be significantly lower than indicated in row 3 of Table 10.

Since the crustal field is almost constant in time, it can be inferred from all available satellite, marine and aeromagnetic measurements of the past decades. These data have been compiled into an ellipsoidal degree-720 Enhanced Magnetic Model (EMM), available at http://www.ngdc.noaa.gov/geomag/EMM. Developed as a research model for NGA, the EMM 2010 provides consistent global representation of the magnetic field, including the crustal field, down to wavelengths of approximately 56 kilometers. The new WMM subroutine library was designed in such a way that it can be used with the EMM model. Use of the EMM should be considered in applications with higher demands in pointing accuracy.

3.2.2 DISTURBANCE FIELD CONTRIBUTION

The disturbance field is the sum of the contributions of ionospheric and magnetospheric electric currents, plus the corresponding contributions from currents induced by the external time-varying magnetic fields in the Earth and oceans. The strength of the disturbance field is modulated by the 11-year solar cycle (Fig. 10). Periods of strong magnetic activity (magnetic storms) occur primarily at solar maximum, although they tend to lag behind the solar cycle by about 2 years. The epoch of WMM2010 starts in the quietest part of the solar cycle and extends into its most active part.

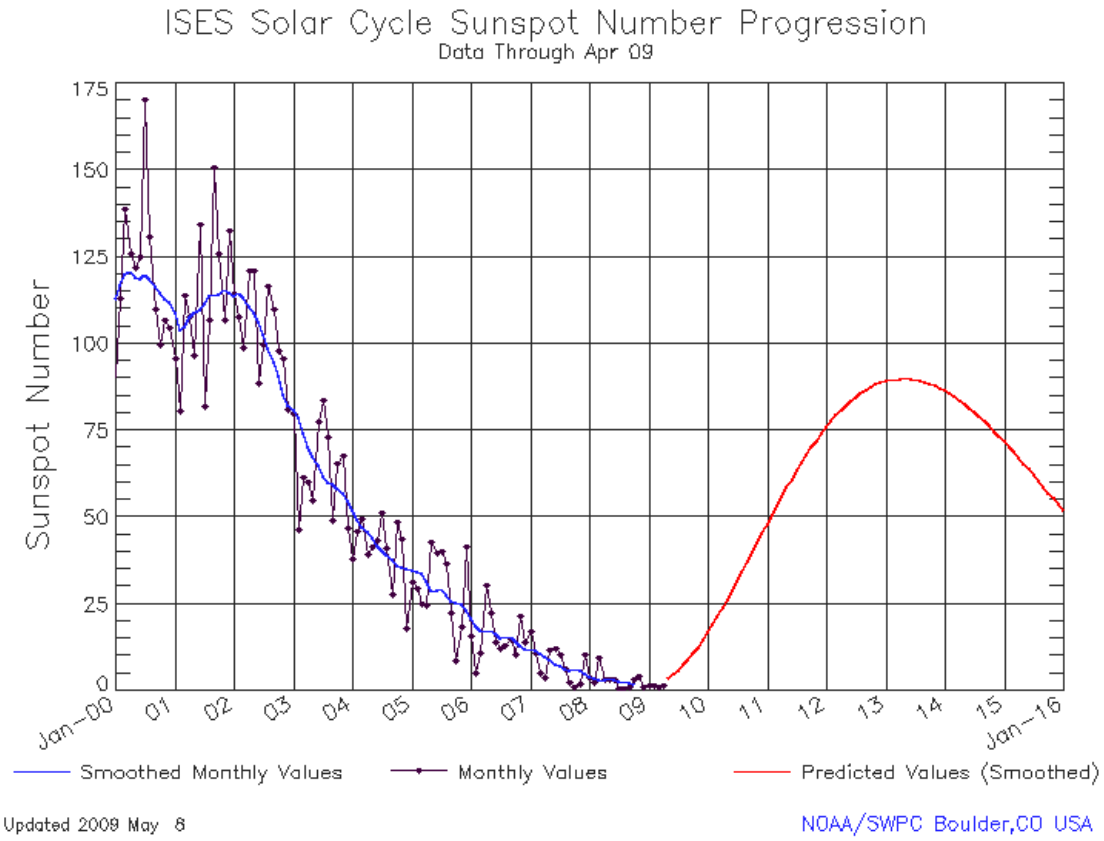

Figure 10: The progression of the solar cycle has significant influence on the strength of the disturbance field. Magnetic storms are most common around and for a few years after solar maximum

To assess the contribution of the disturbance field, the internal field represented by the spline from the observatory measurements was subtracted. The residuals then provided an estimate of the time-varying disturbance field. To account for dependence on solar activity, separate estimates for solar minimum (1997) and solar maximum (2003) conditions were derived (rows

4 and 5 of Table 10). The average was taken over the entire year and no data were excluded. One may also be interested to know how strongly the magnetic elements are affected by magnetic storms. The results for moderate storms (Kp 6, about 360 days affected per solar cycle) are listed in row 6, while the peak disturbances during extreme magnetic storms (Kp 9, about 4 days per solar cycle) are listed in row 7. See http://www.swpc.noaa.gov/NOAAscales for further information on the classification of geomagnetic storms.

3.3 TOTAL ERROR BUDGET

The results displayed in Table 10 can be interpreted in terms of an average error budget at the Earth's surface. Since these errors are statistically independent, the expected total error is calculated as the root of the sum of squares. For example, the expected difference between the observed and modeled declination in 2010 (solar minimum conditions) is

$$\sqrt{0.08^2 + 1.67^2 + 0.28^2} = 1.70° \tag{25}$$

while the worst-case scenario for the magnetic declination during an extreme magnetic storm in 2015 is given by

$$\sqrt{0.25^2 + 1.67^2 + 2.76^2} = 3.24° \tag{26}$$

Table 10: Estimated root-mean-square contributions to the observed magnetic field at the Earth's surface after subtracting the WMM2010. The WMM2010 inaccuracy in 2015.0 was taken as the WMM2005 inaccuracy 5 years earlier. The crustal contribution was estimated from land-based observatories and is likely to be lower at sea. Higher values of *GV* (compared to *D*) reflect the larger uncertainties of the declination at high latitudes, the only regions where *GV* is defined. Values are given in nT and degrees, as applicable

Row		X	Y	Z	H	F	I	D	GV
1	WMM2010 inaccuracy in 2010.0	5	2	6	4	6	0.01	0.08	0.18
2	in 2015.0	61	58	101	61	79	0.12	0.25	0.50
3	Crustal magnetization	401	241	556	367	611	0.37	1.67	3.09
4	Disturbance field, solar minimum	32	22	25	33	27	0.03	0.28	0.52
5	solar maximum	58	36	44	59	46	0.06	0.43	0.79
6	moderate magnetic storm	126	72	90	129	95	0.14	0.87	1.61
7	extreme magnetic storm	349	210	199	336	229	0.35	2.76	5.07

4. CHARTS

This section provides the WMM2010 charts in the following order:

- Main field maps for 2010.0 in Mercator projection for *X, Y, Z, H, F, I* and *D* (see pgs. 56-59)
- Main field maps in north polar stereographic projection (see pgs. 60-66)
- Main field maps in south polar stereographic projection (see pgs. 67-73)
- Secular variation maps for 2010.0 – 2015.0 in Mercator projection for *X, Y, Z, H, F, I* and *D* (see pgs. 74-77)
- Secular variation maps in north polar stereographic projection (see pgs. 78-84)
- Secular variation maps in south polar stereographic projection (see pgs. 85-91)
- Grivation maps (see pgs. 92-95)
- Geomagnetic longitude and latitude in Mercator projection (see pg. 96)

The white stars on the maps indicate the 2010.0 positions of the dip poles.

MAIN FIELD MAPS: MERCATOR PROJECTION

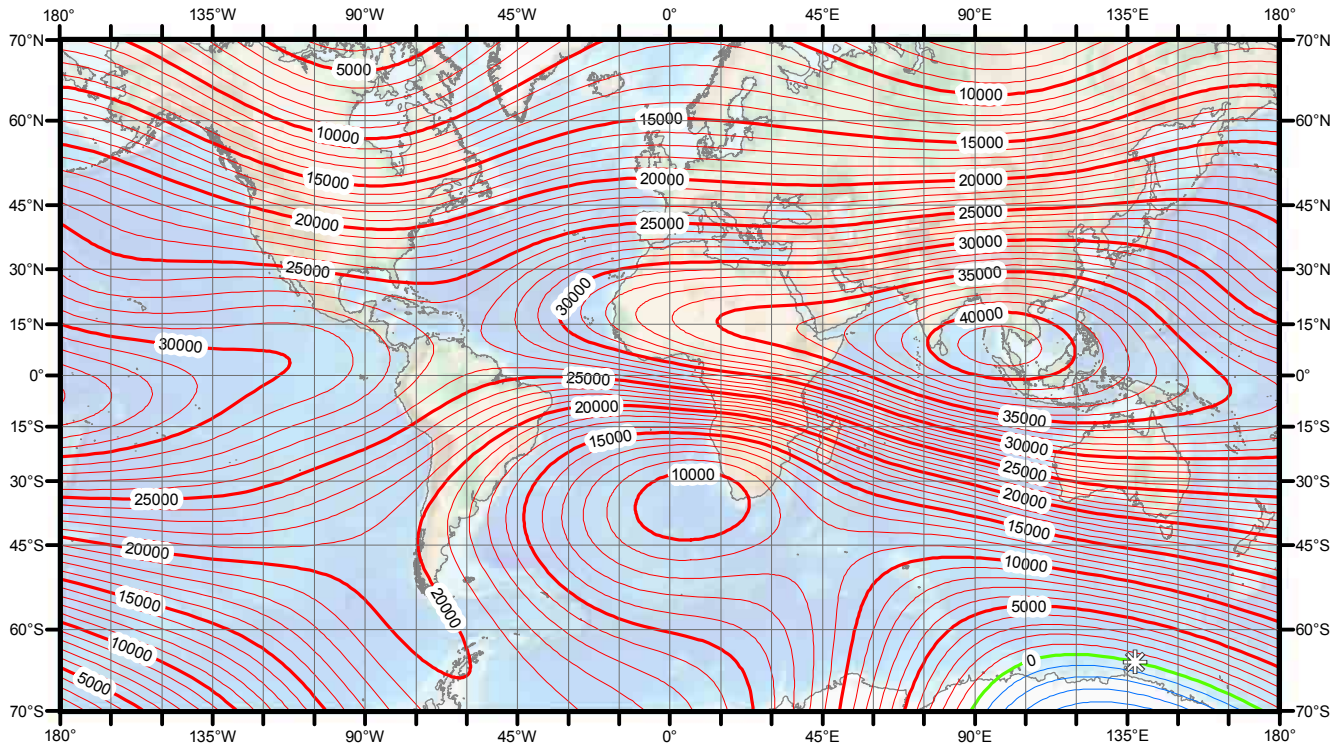

Main field north component (X). Contour interval is 1000 nT. Mercator projection.

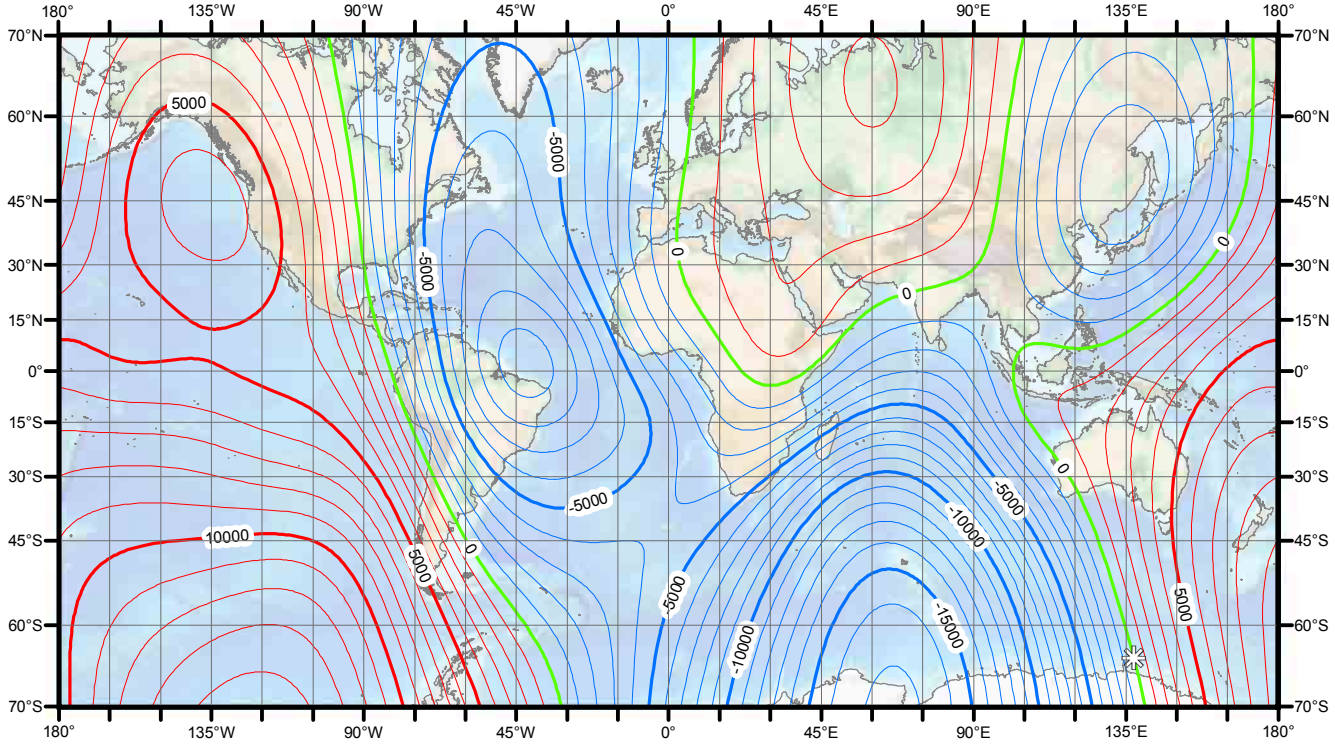

Main field east component (Y). Contour interval is 1000 nT, red contours positive (east); blue negative (west); green zero line. Mercator projection.

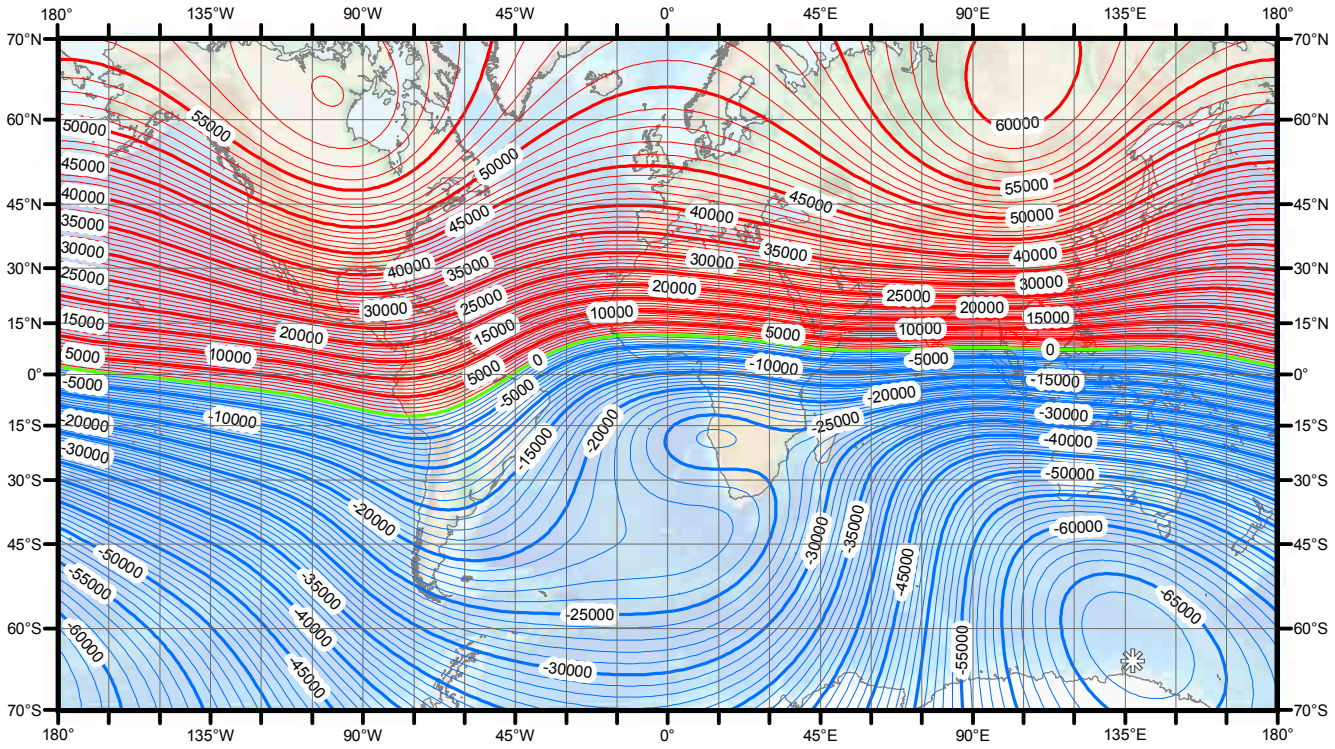

Main field down component (Z). Contour interval is 1000 nT, red contours positive (down); blue negative (up); green zero line. Mercator projection.

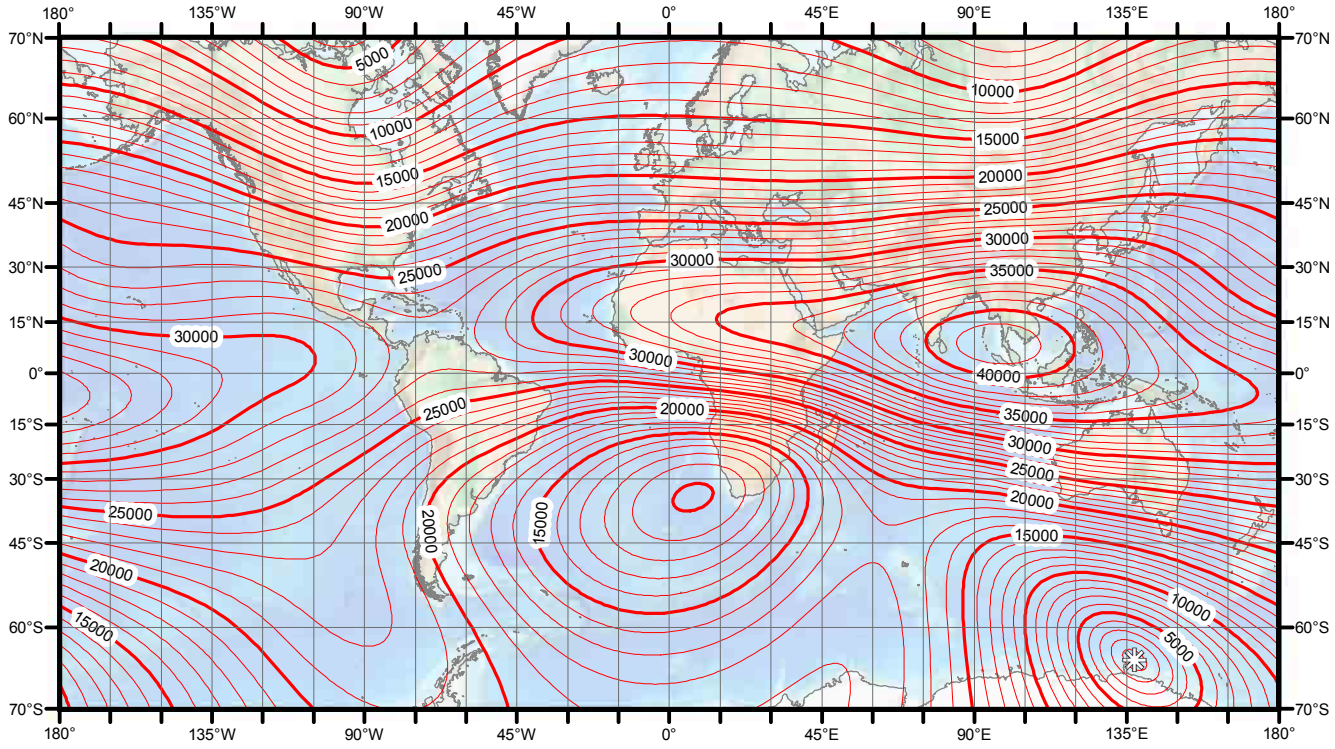

Main field horizontal intensity (H). Contour interval is 1000 nT. Mercator projection.

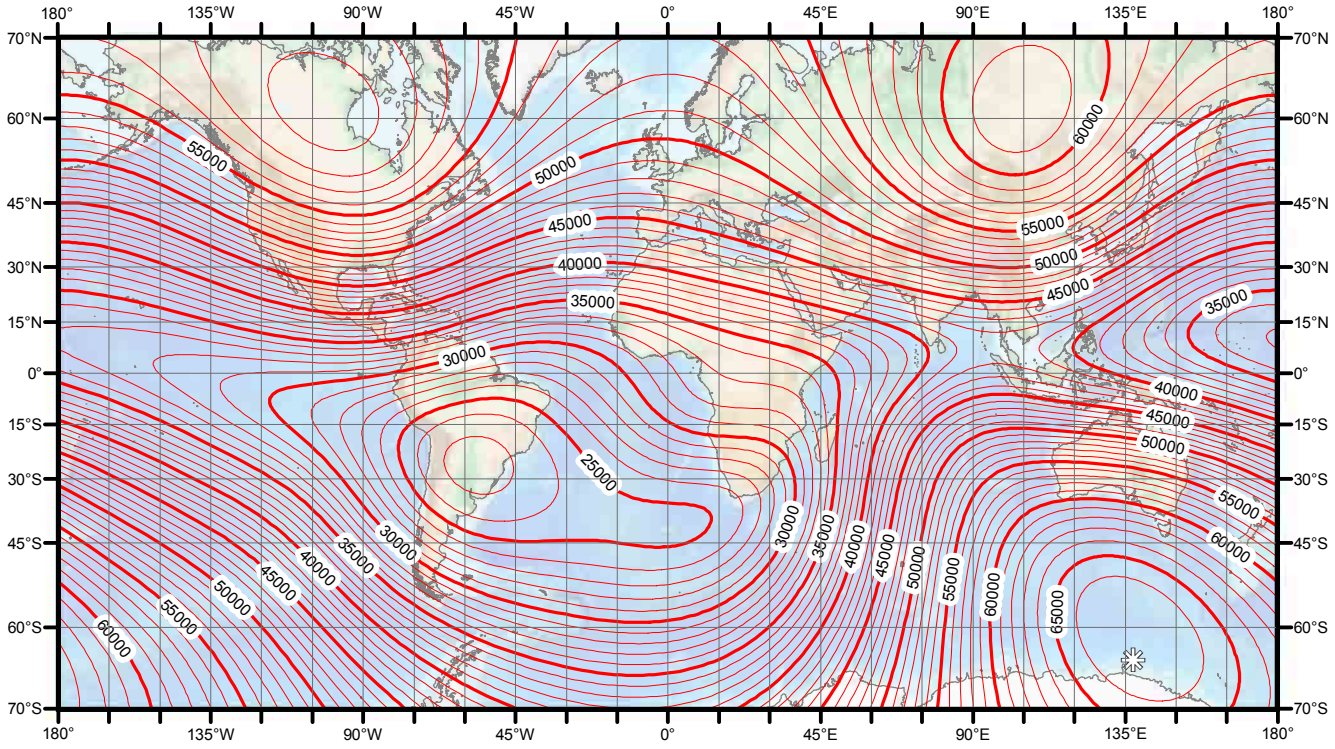

Main field total intensity (F). Contour interval is 1000 nT. Mercator projection.

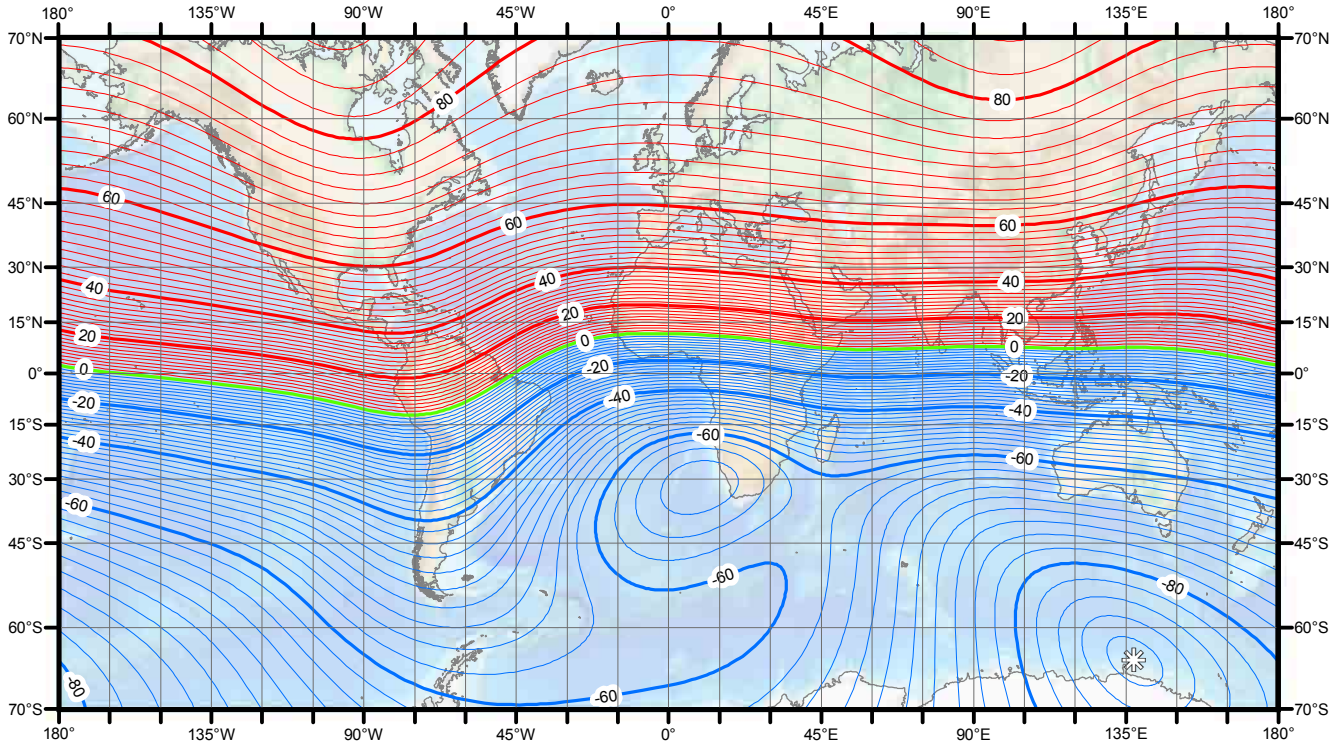

Main field inclination (I). Contour interval is 2 degrees, red contours positive (down); blue negative (up); green zero line. Mercator projection.

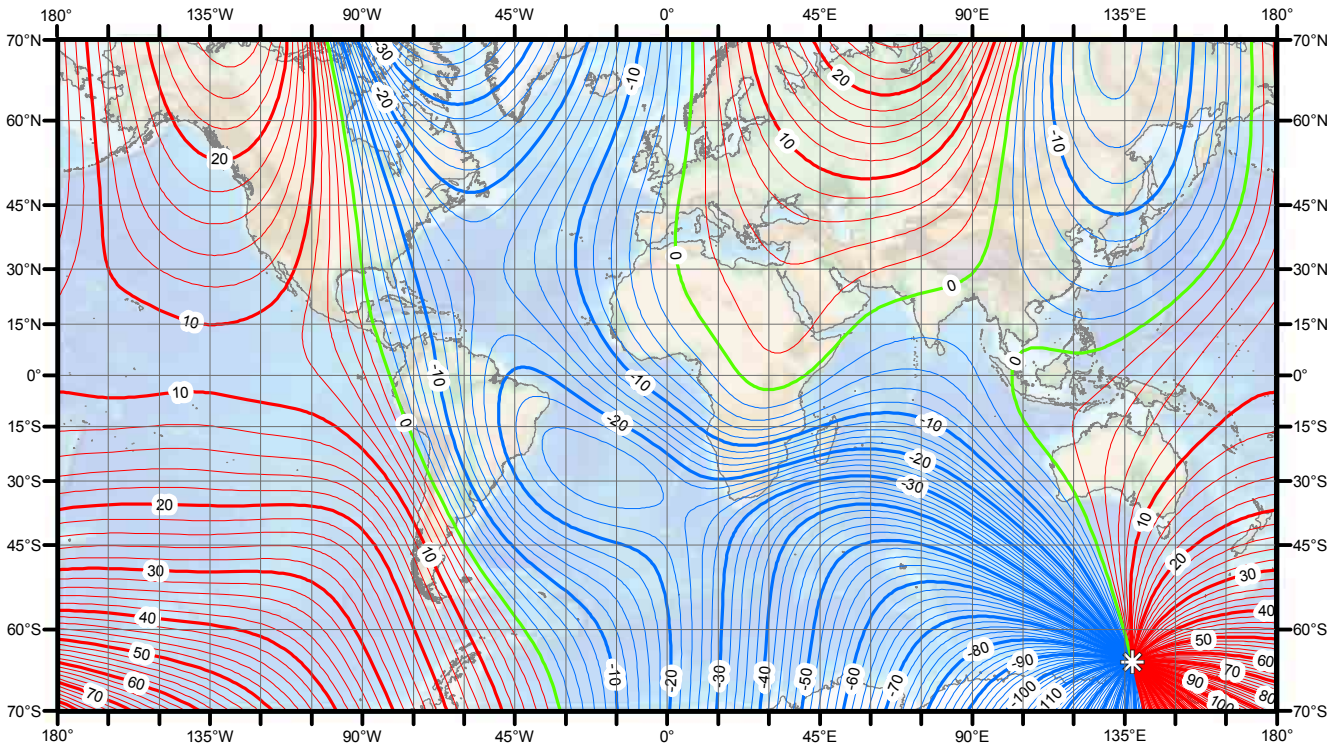

Main field declination (D). Contour interval is 2 degrees, red contours positive (east); blue negative (west); green (agonic) zero line. Mercator projection.

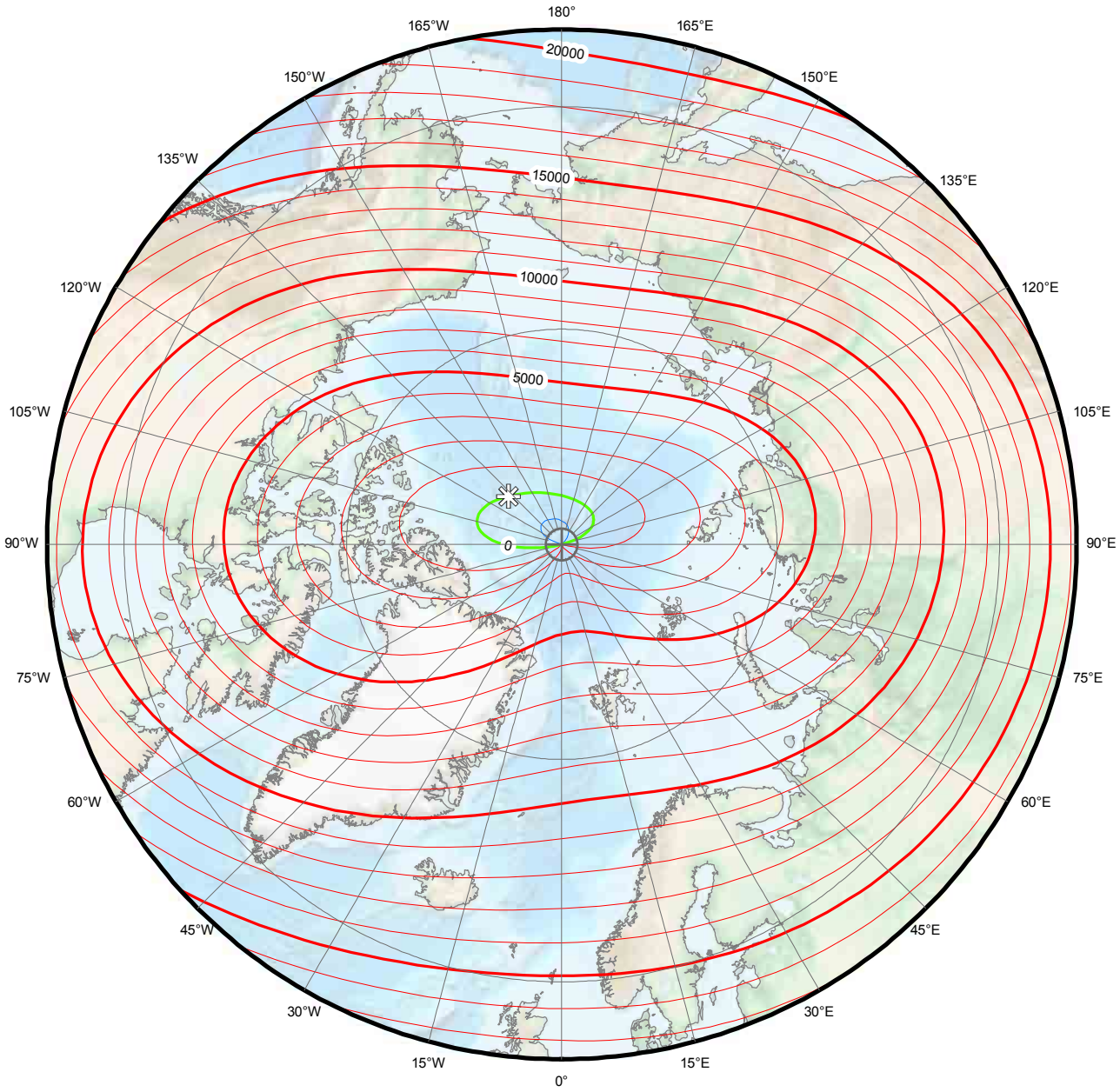

Main field north component (X). Contour interval is 1000 nT. North polar region. Polar Stereographic Projection.

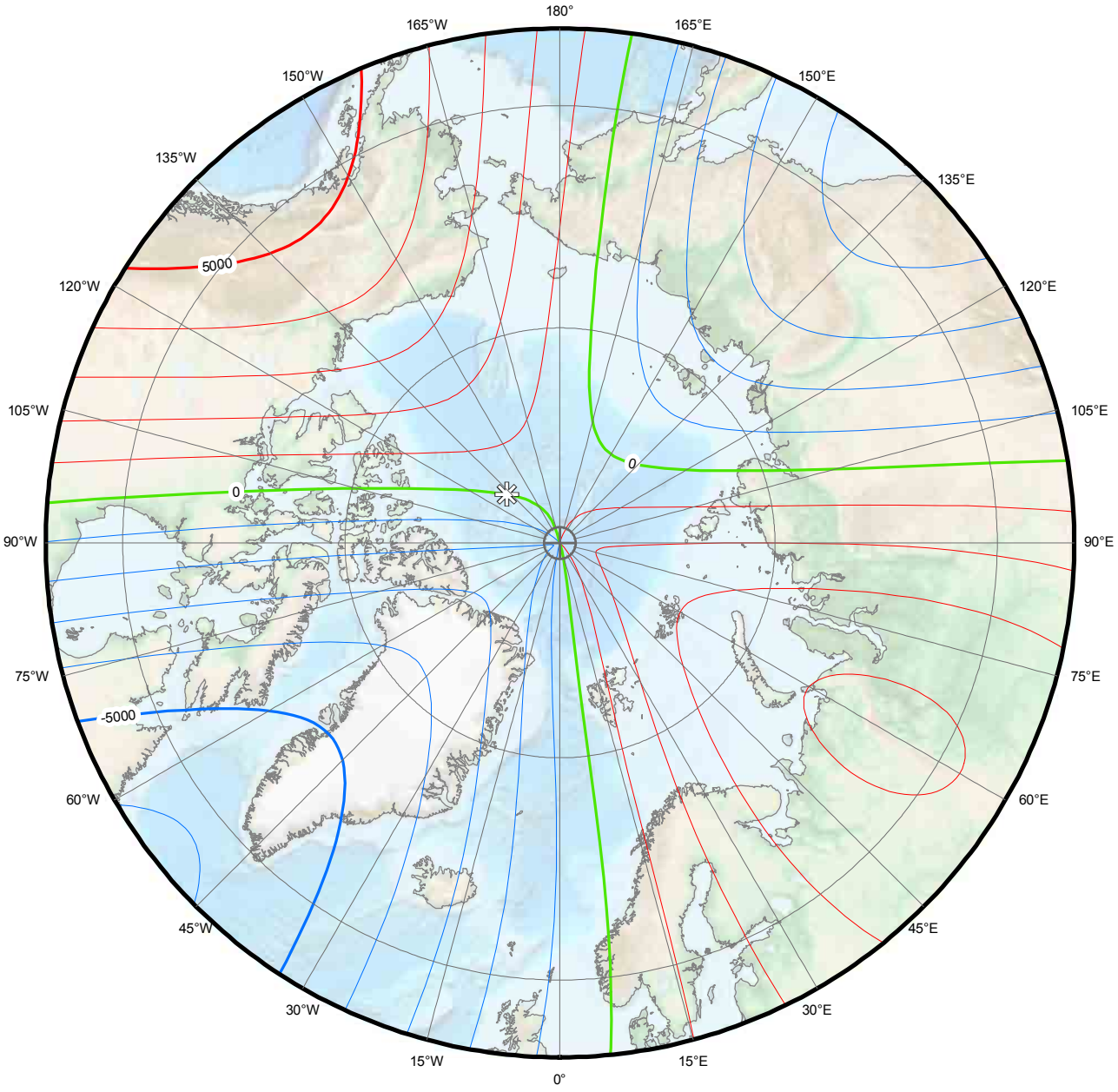

Main field east component (Y). Contour interval is 1000 nT, red contours positive (east); blue negative (west); green zero line. North polar region. Polar Stereographic Projection.

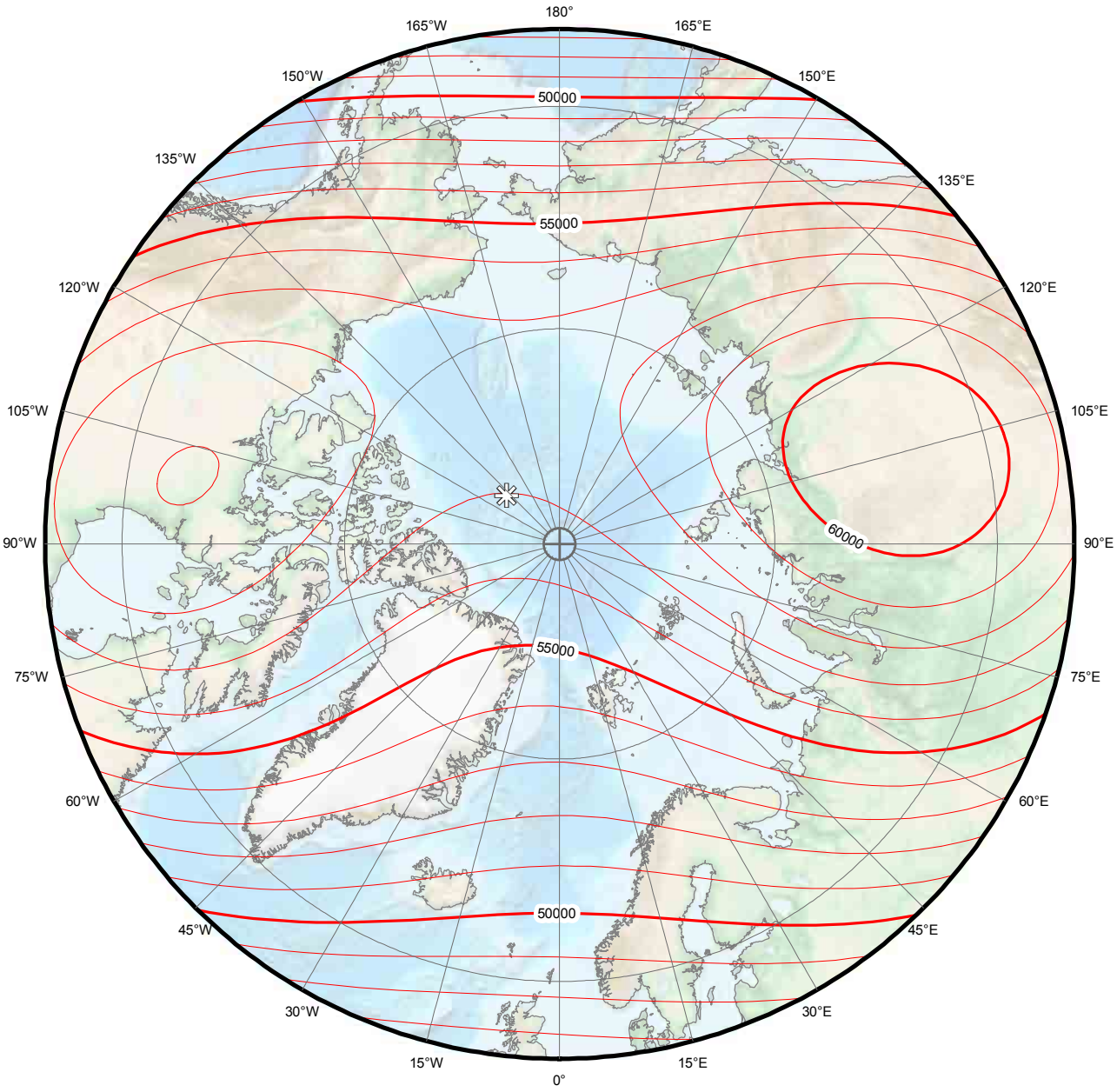

Main field down component (Z). Contour interval is 1000 nT. North polar region.
Polar Stereographic Projection.

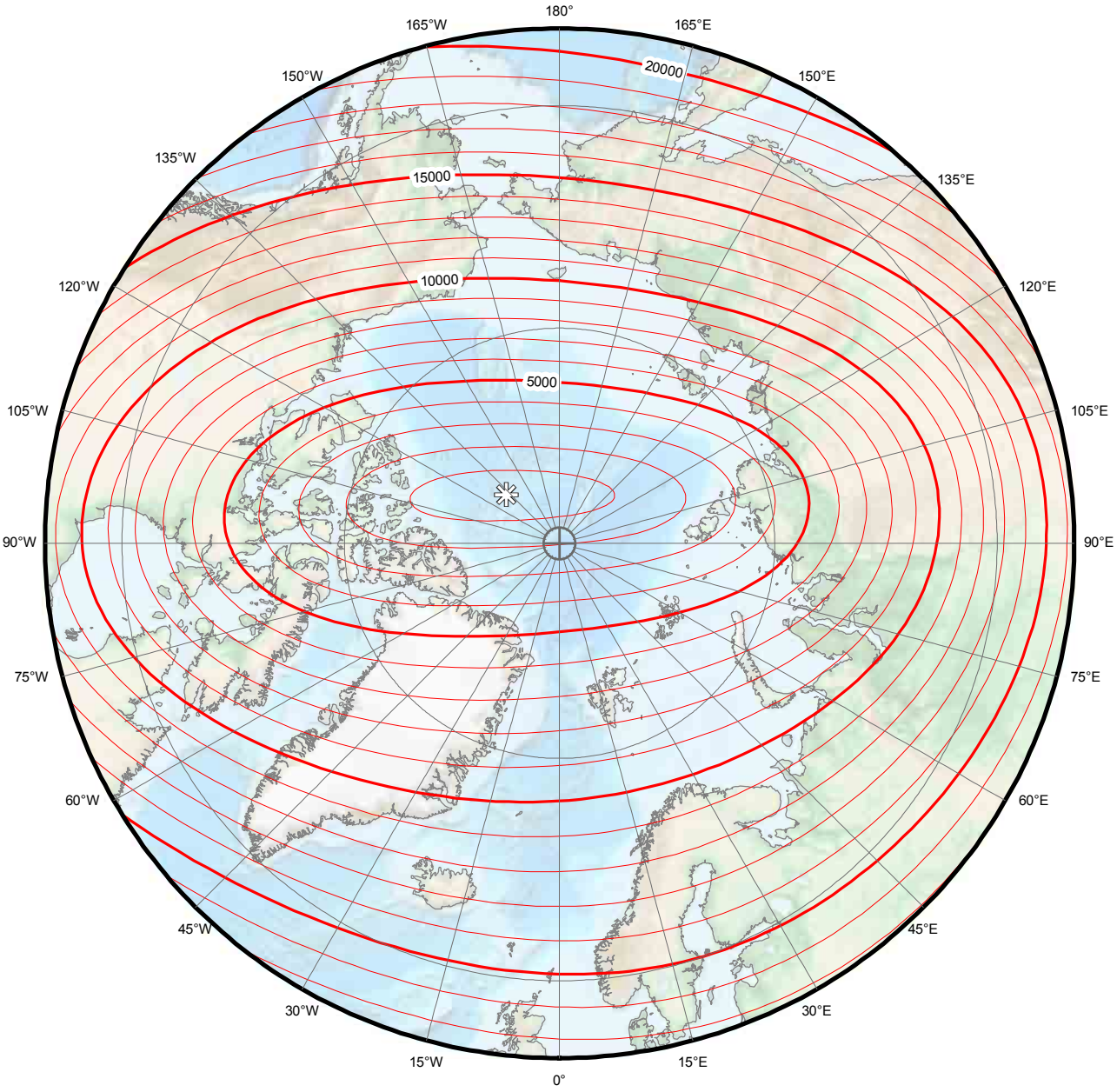

Main field horizontal intensity (H). Contour interval is 1000 nT. North polar region. Polar Stereographic Projection.

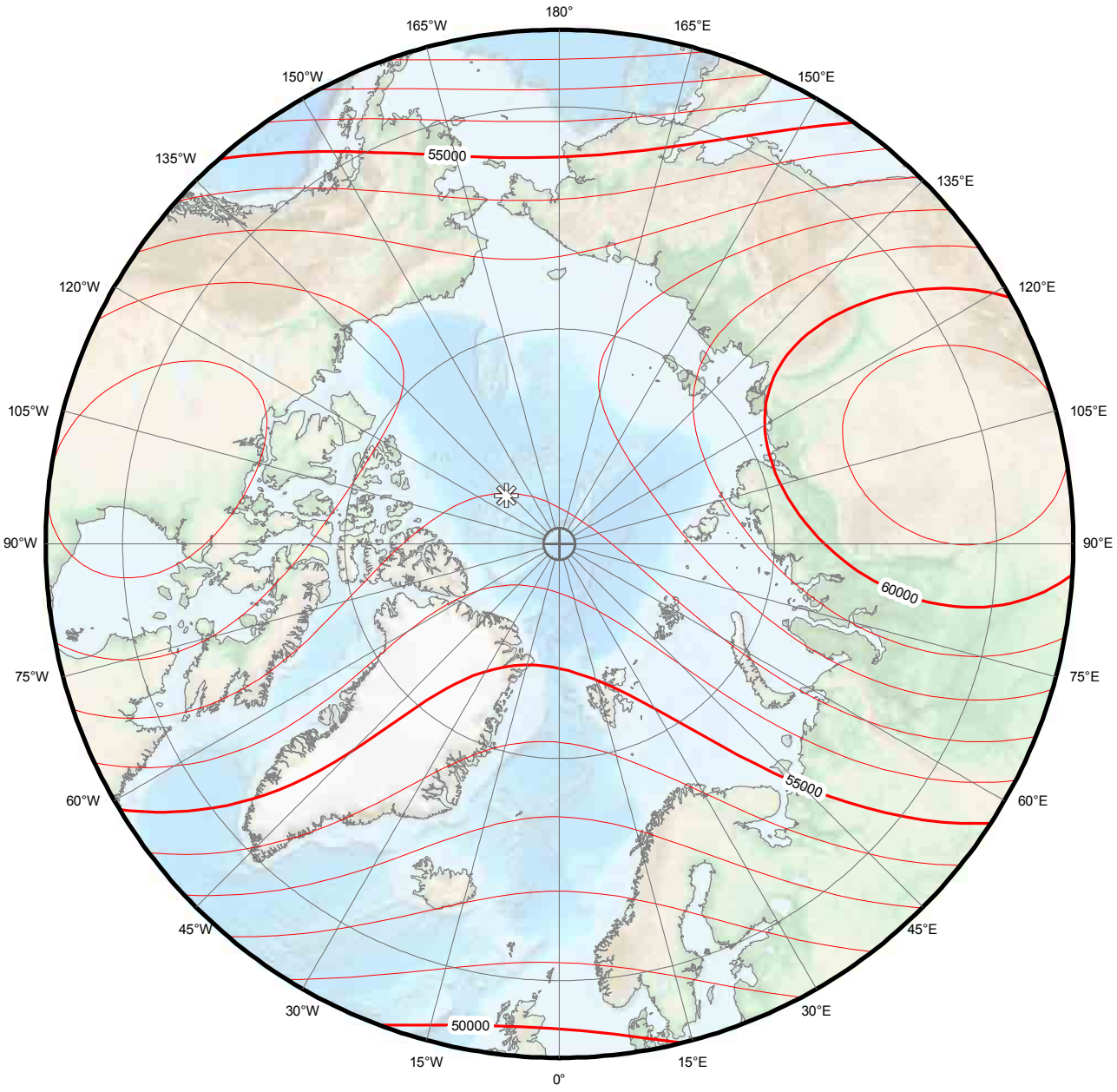

Main field total intensity (F). Contour interval is 1000 nT. North polar region.
Polar Stereographic Projection.

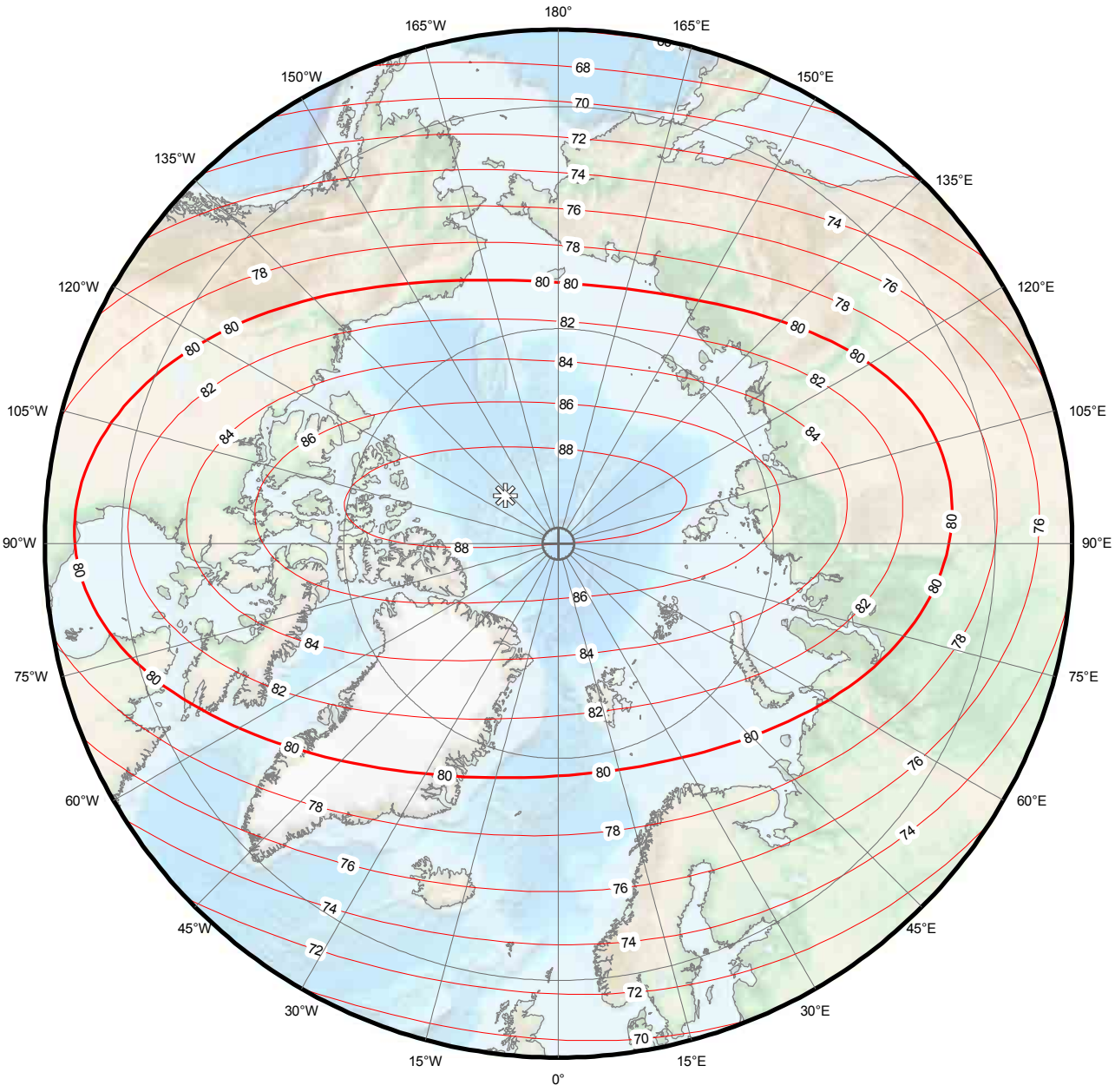

Main field inclination (I). Contour interval is 2 degrees. North polar region.
Polar Stereographic Projection.

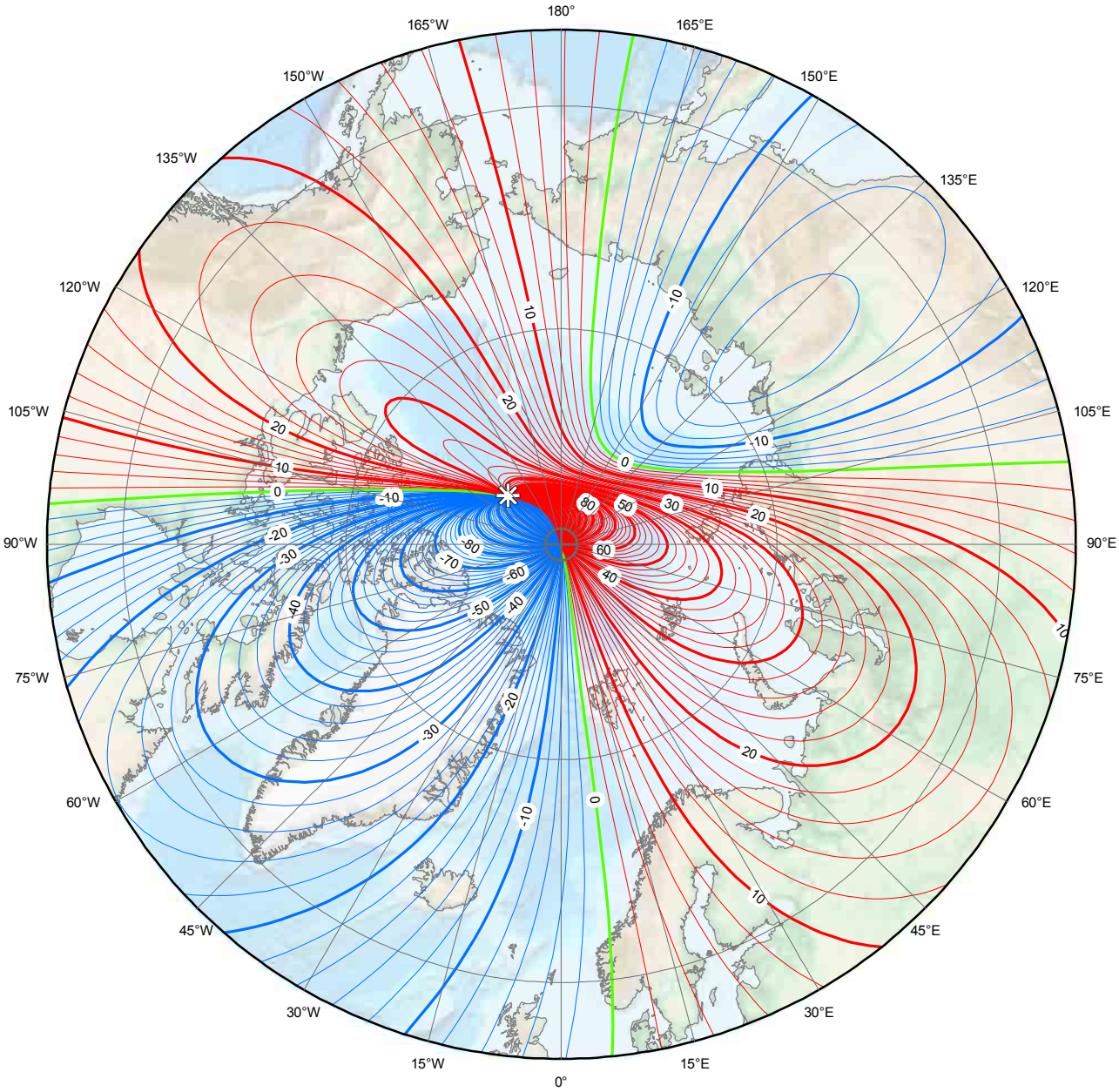

Main field declination (D). Contour interval is 2 degrees, red contours positive (east); blue negative (west); green zero (agonic) line. North polar region. Polar Stereographic Projection.

MAIN FIELD MAPS: SOUTH POLAR STEREOGRAPHIC PROJECTION

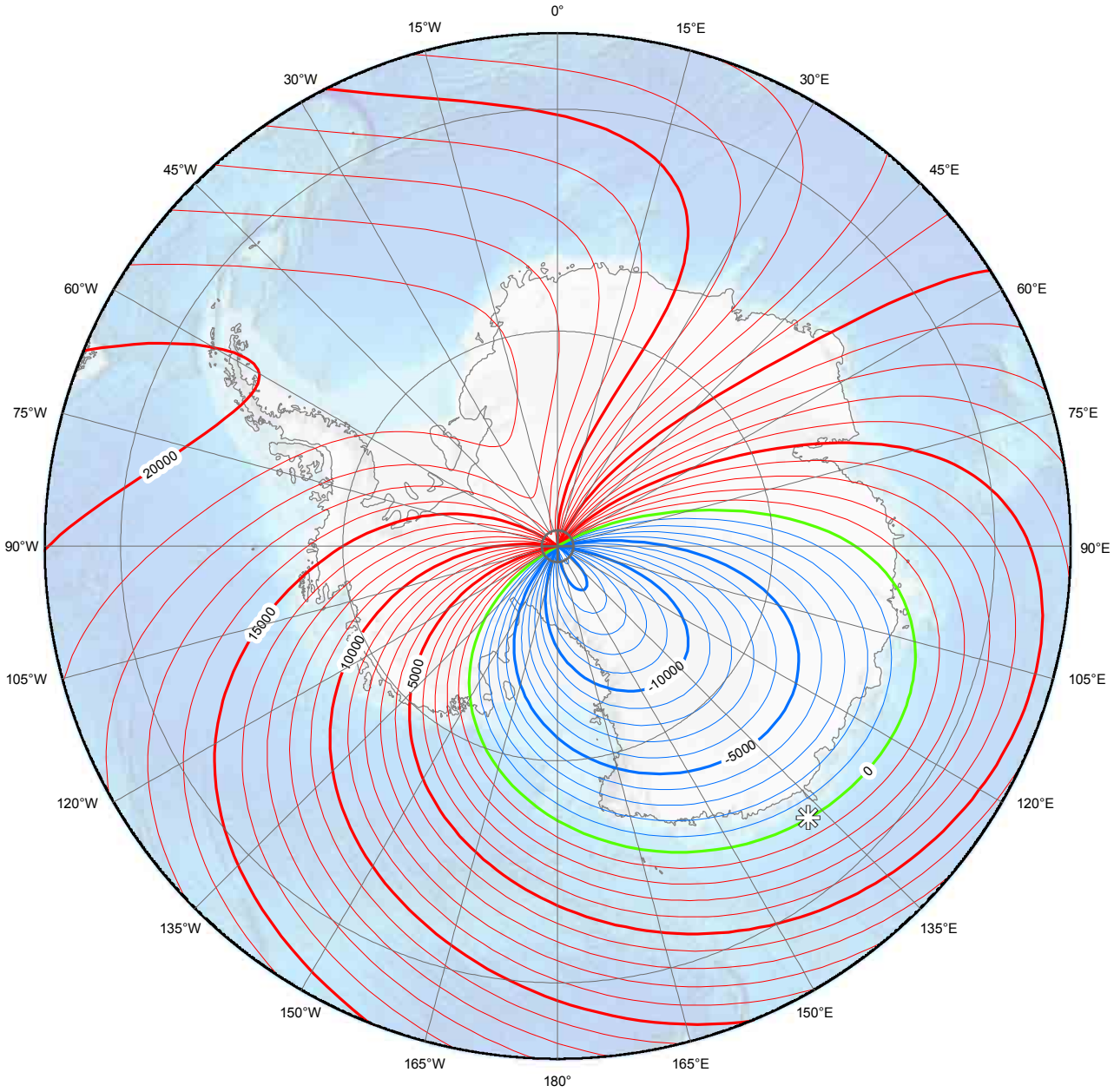

Main field north component (X). Contour interval is 1000 nT, red contours positive (north); blue negative (south); green zero line. South polar region. Polar Stereographic Projection.

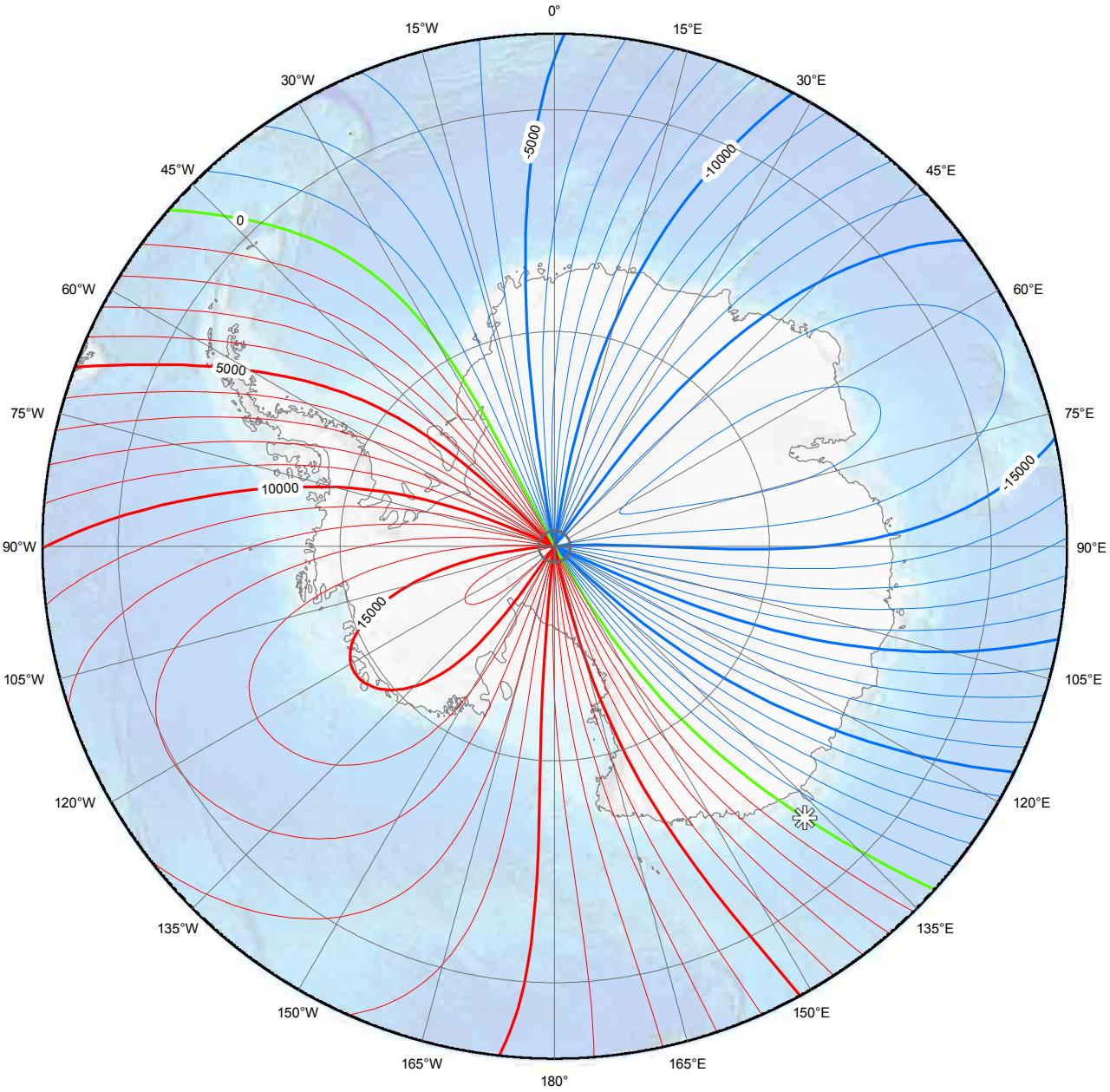

Main field east component (Y). Contour interval is 1000 nT, red contours positive (east); blue negative (west); green zero line. South polar region. Polar Stereographic Projection.

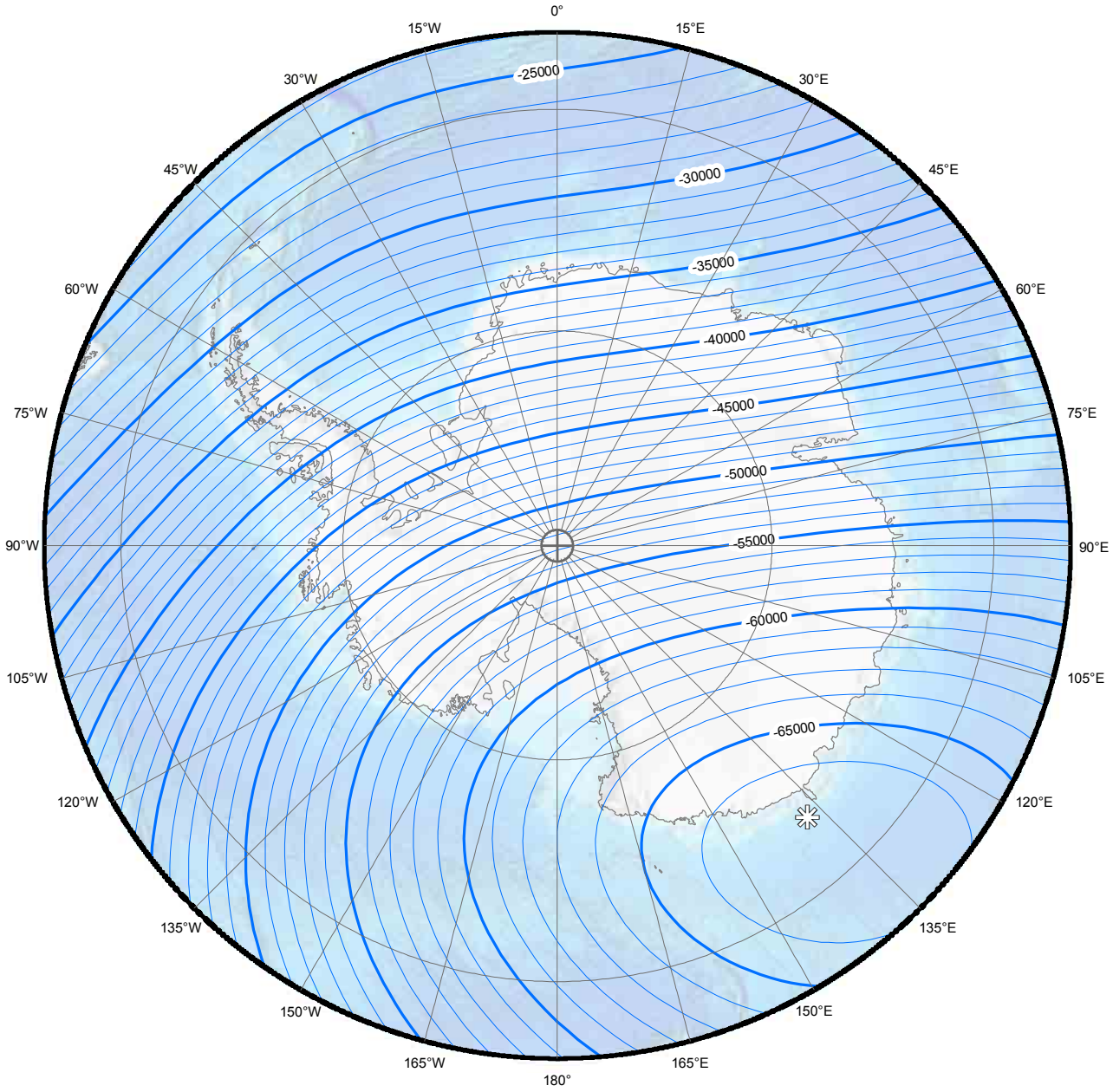

Main field down component (Z). Contour interval is 1000 nT. South polar region.
Polar Stereographic Projection.

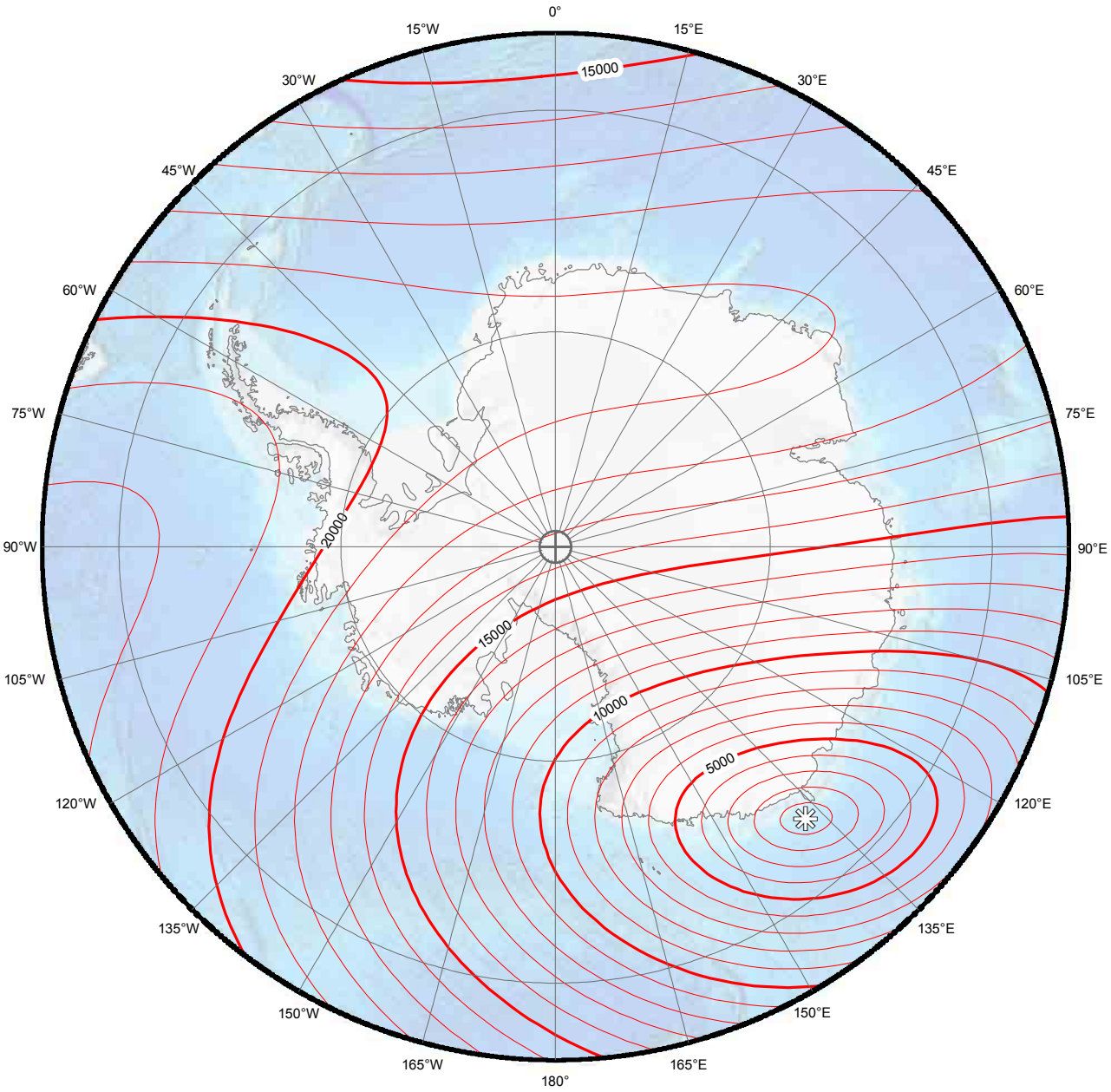

Main field horizontal intensity (H). Contour interval is 1000 nT. South polar region.
Polar Stereographic Projection.

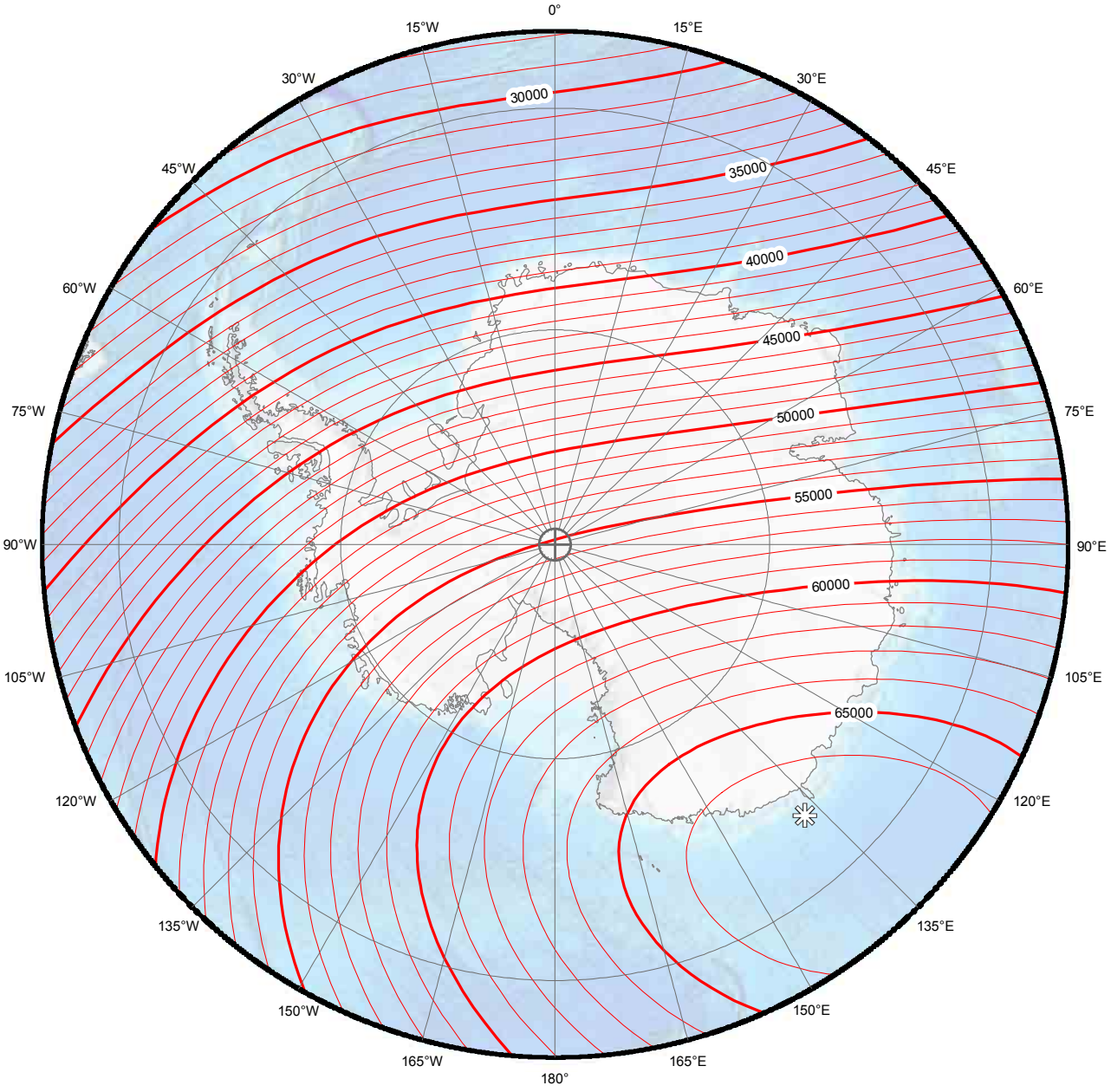

Main field total intensity (F). Contour interval is 1000 nT. South polar region. Polar Stereographic Projection.

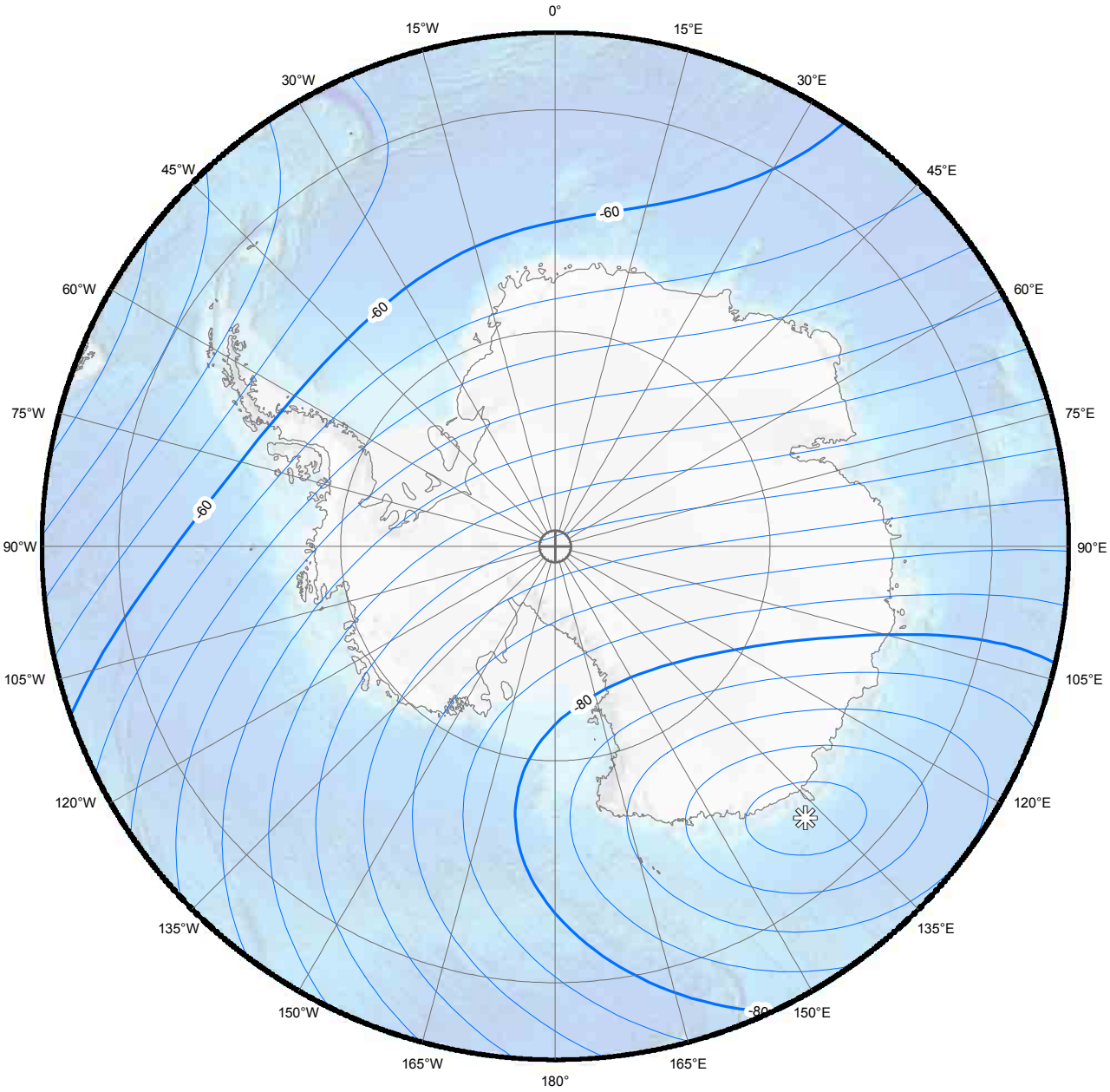

Main field inclination (I). Contour interval is 2 degrees. South polar region. Polar Stereographic Projection.

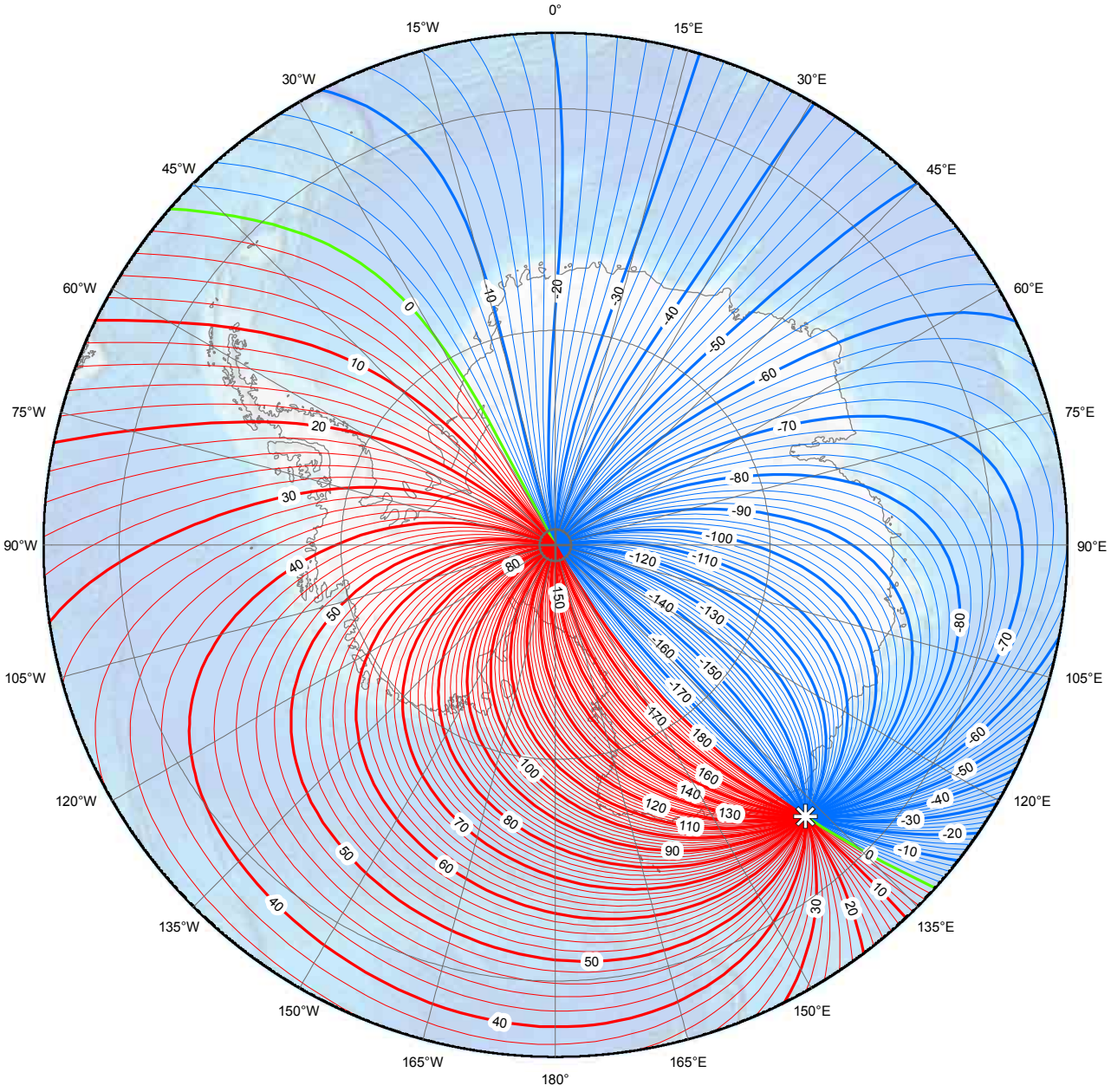

Main field declination (D). Contour interval is 2 degrees, red contours positive (east); blue negative (west); green zero (agonic) line. South polar region. Polar Stereographic Projection.

SECULAR VARIATION MAPS: MERCATOR PROJECTION

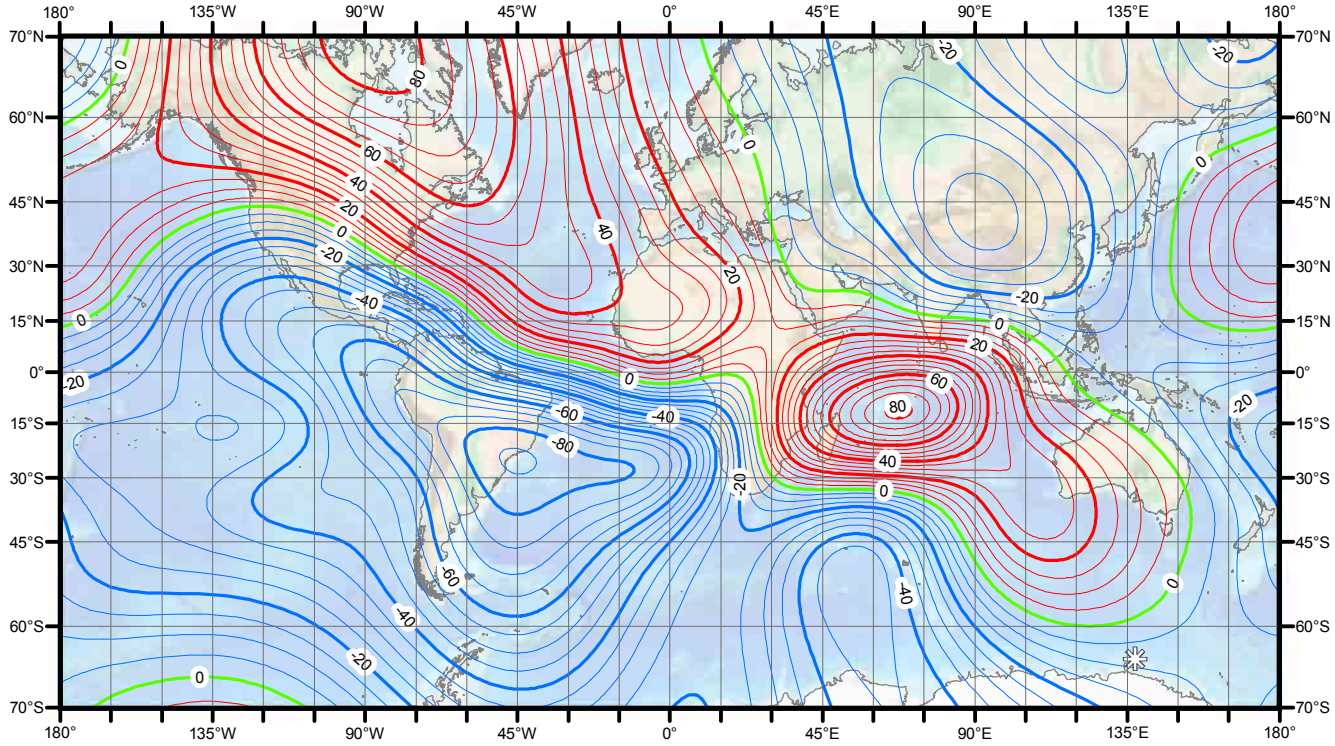

Annual change north component (X). Contour interval is 5 nT / year, red contours positive (north) change; blue negative (south) change; green zero change. Mercator Projection.

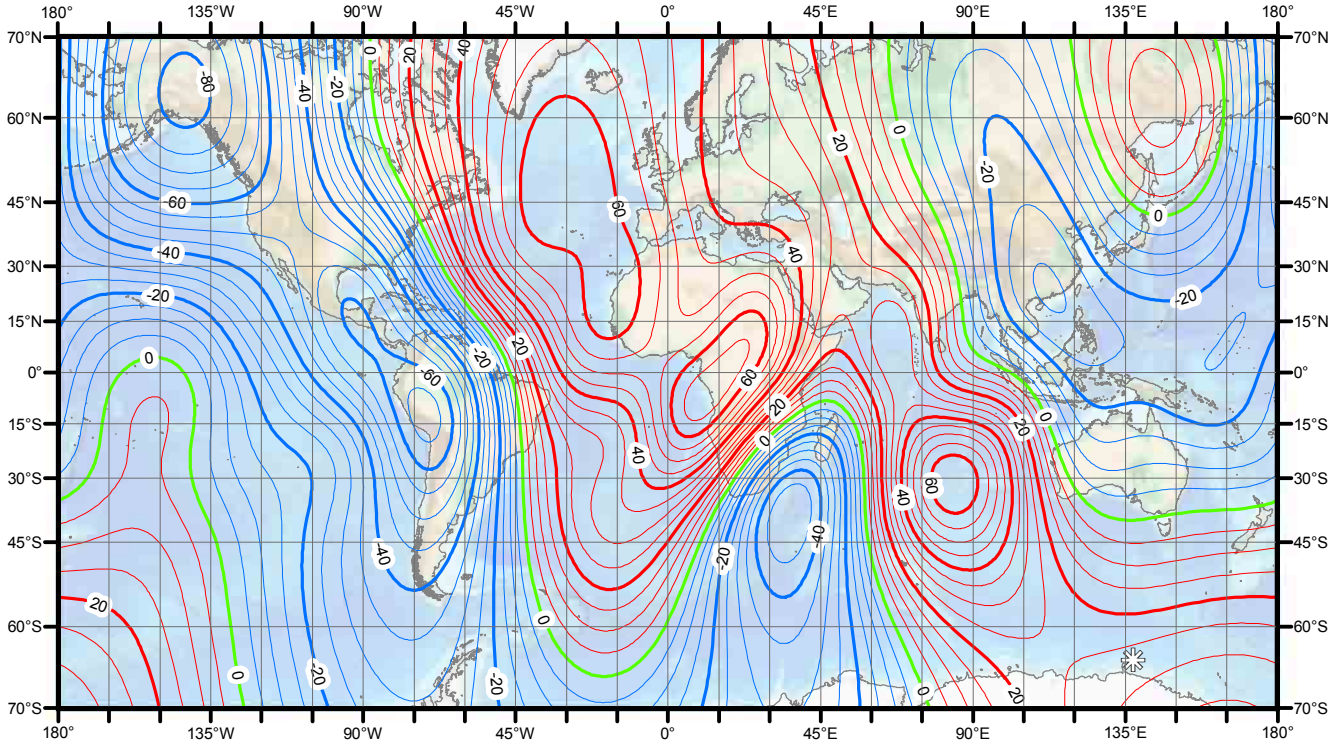

Annual change east component (Y). Contour interval is 5 nT / year, red contours positive (east) change; blue negative (west) change; green zero change. Mercator Projection.

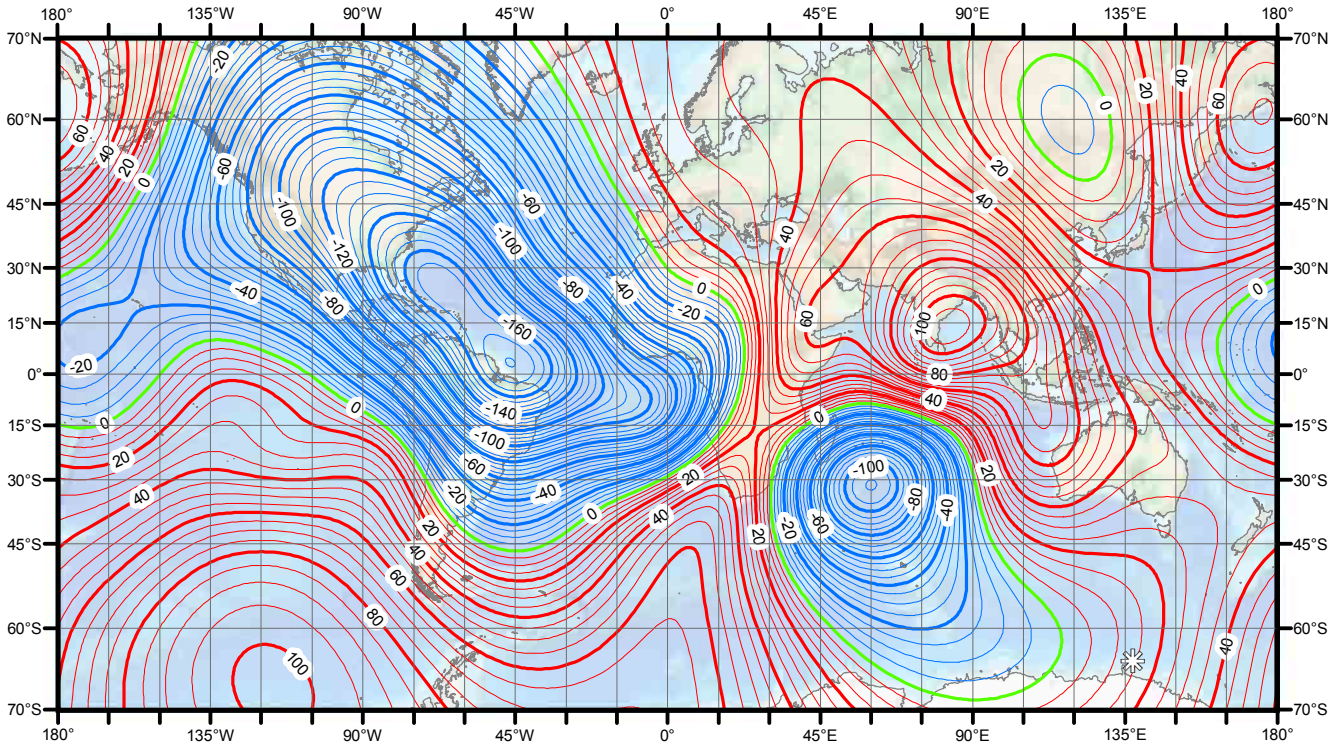

Annual change down component (Z). Contour interval is 5 nT / year, red contours positive (down) change; blue negative (up) change; green zero change. Mercator Projection.

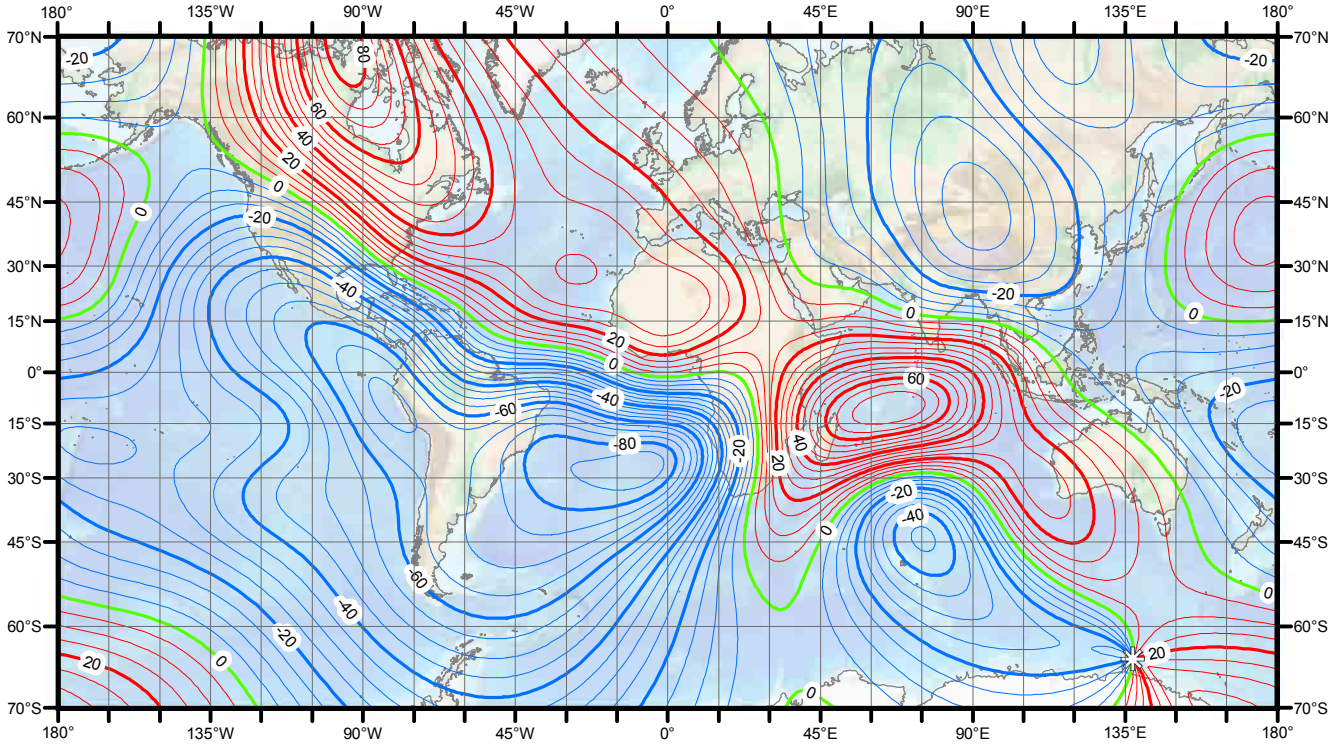

Annual change horizontal intensity (H). Contour interval is 5 nT / year, red contours positive change; blue negative change; green zero change. Mercator Projection.

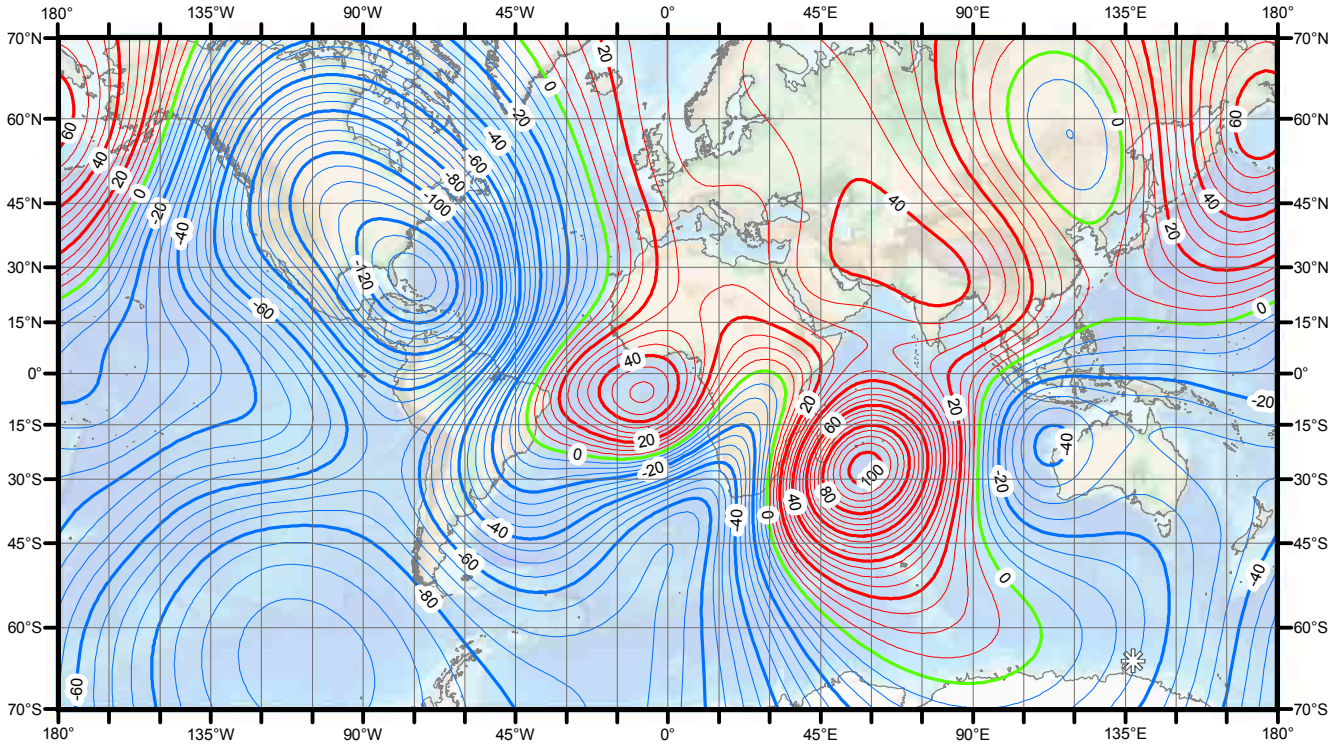

Annual change total intensity (F). Contour interval is 5 nT / year, red contours positive change; blue negative change; green zero change. Mercator Projection.

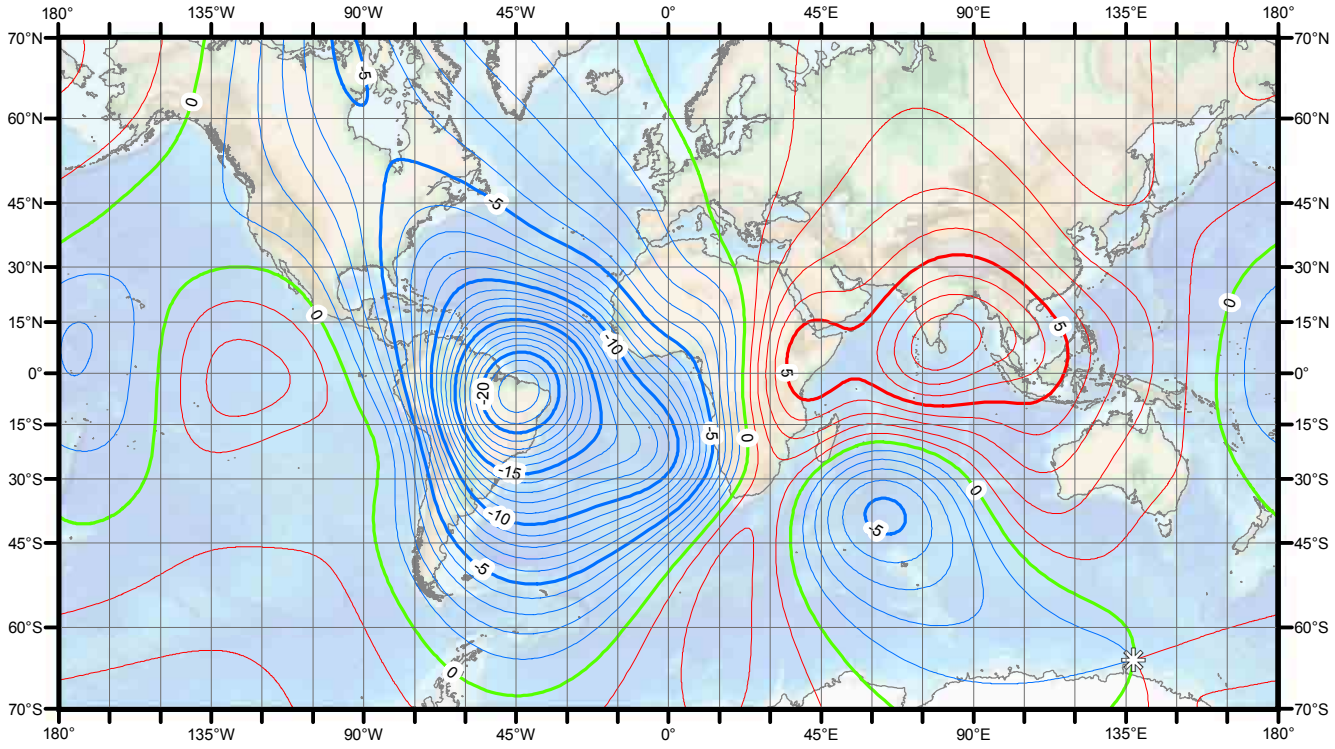

Annual change inclination (I). Contour interval is 1 arc-minute / year, red contours positive (downward) change; blue negative (upward) change; green zero change. Mercator Projection.

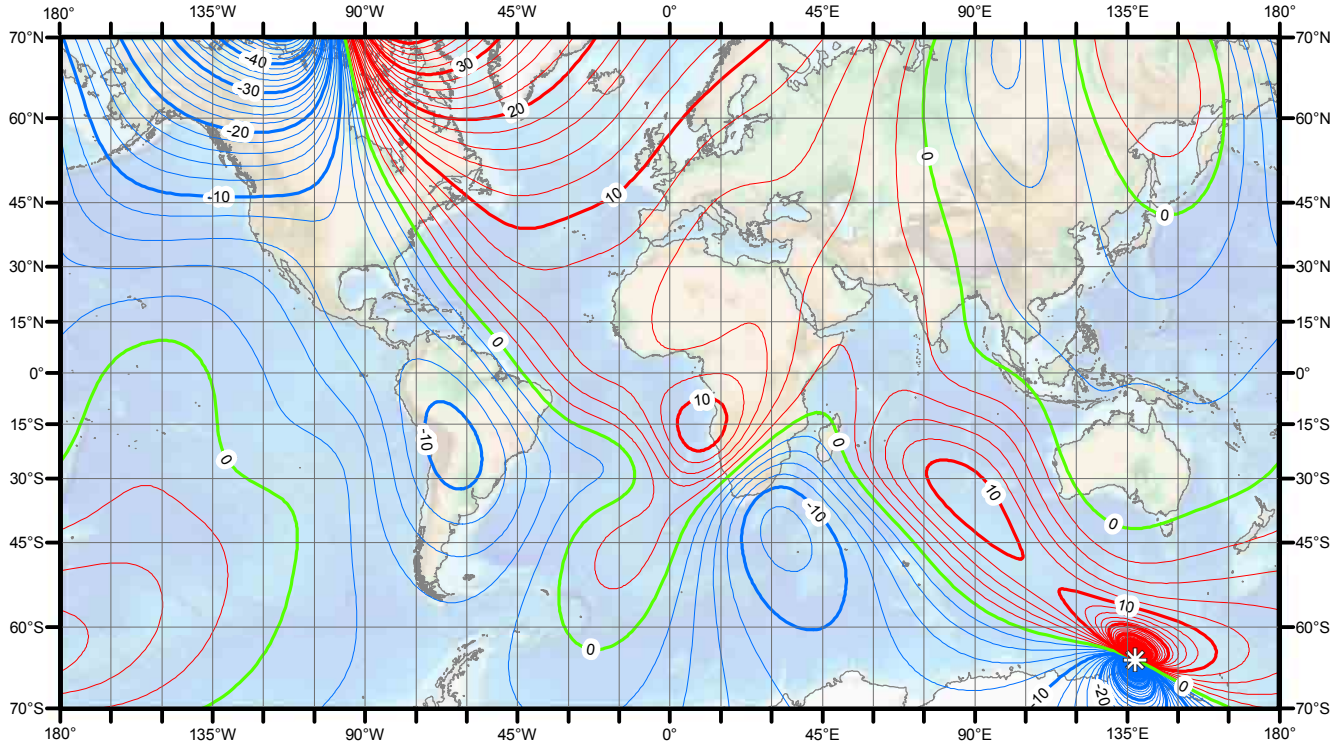

Annual change declination (D). Contour interval is 2 arc-minutes / year, red contours positive (clockwise) change; blue negative (counter-clockwise) change; green zero change. Mercator Projection.

SECULAR VARIATION MAPS: NORTH POLAR STEREOGRAPHIC PROJECTION

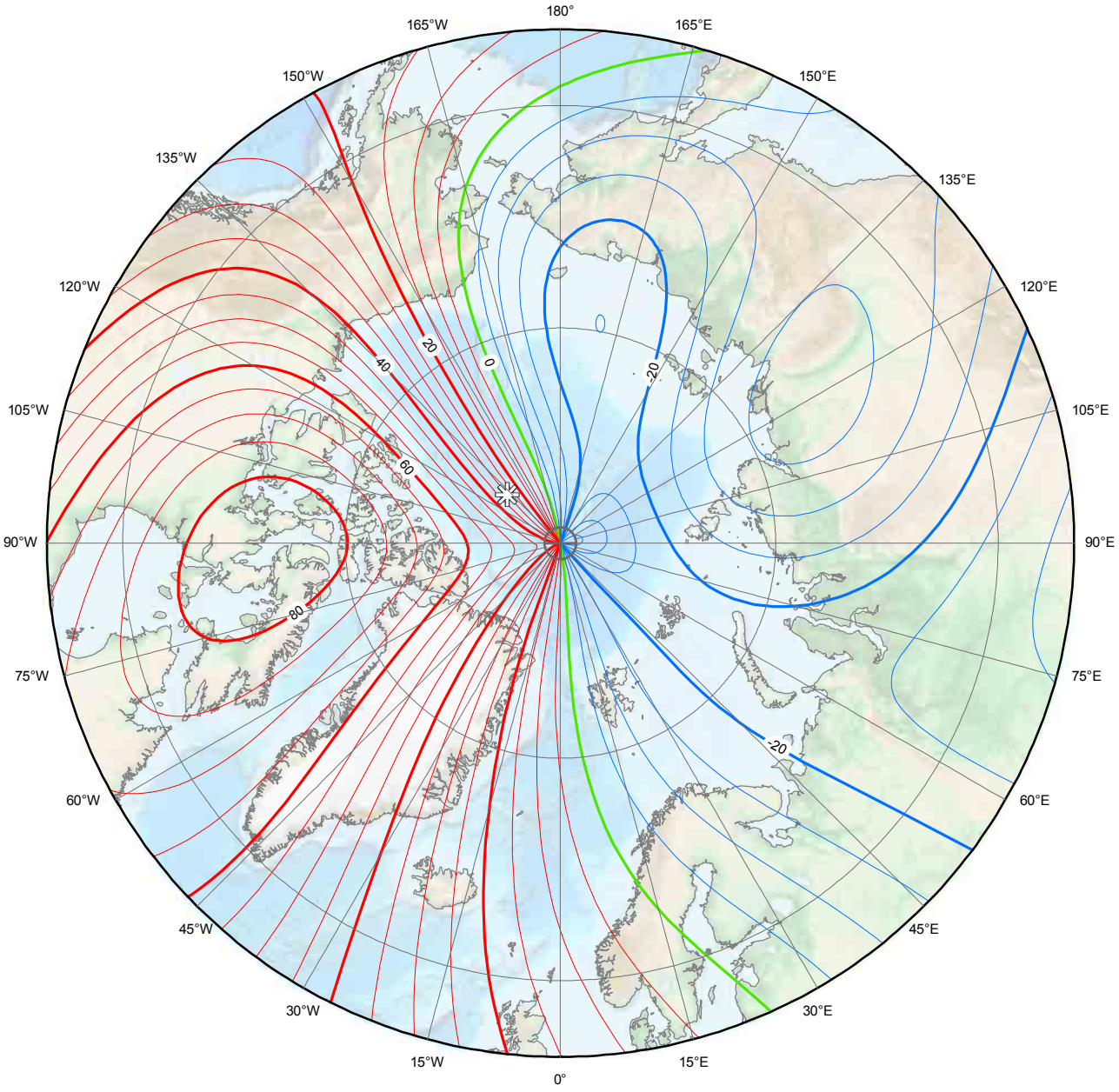

Annual change north component (X). Contour interval is 5 nT / year, red contours positive (north) change; blue negative (south) change; green zero change. North Polar Region. Polar Stereographic Projection.

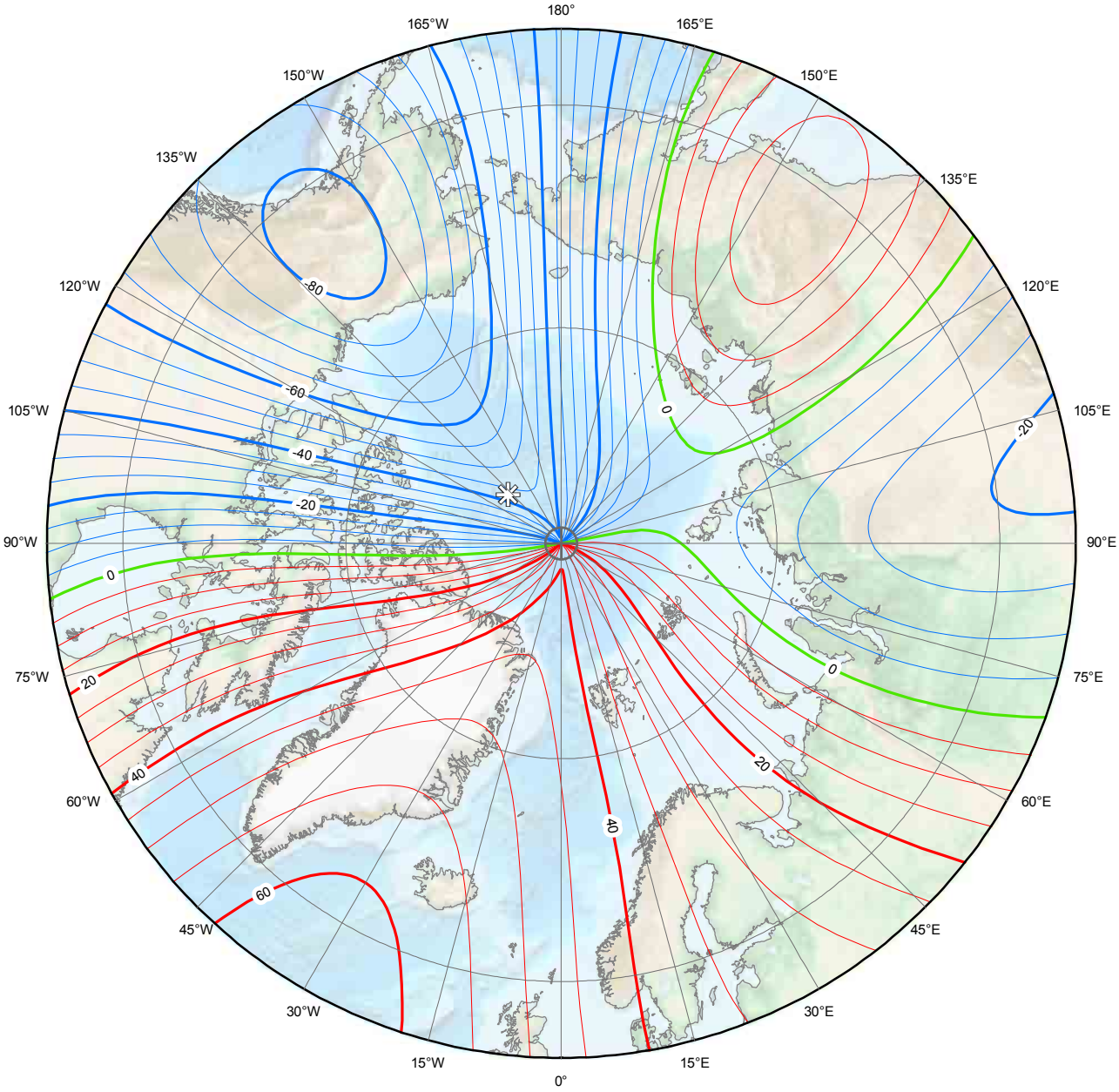

Annual change east component (Y). Contour interval is 5 nT / year, red contours positive (east) change; blue negative (west) change; green zero change. North Polar Region. Polar Stereographic Projection.

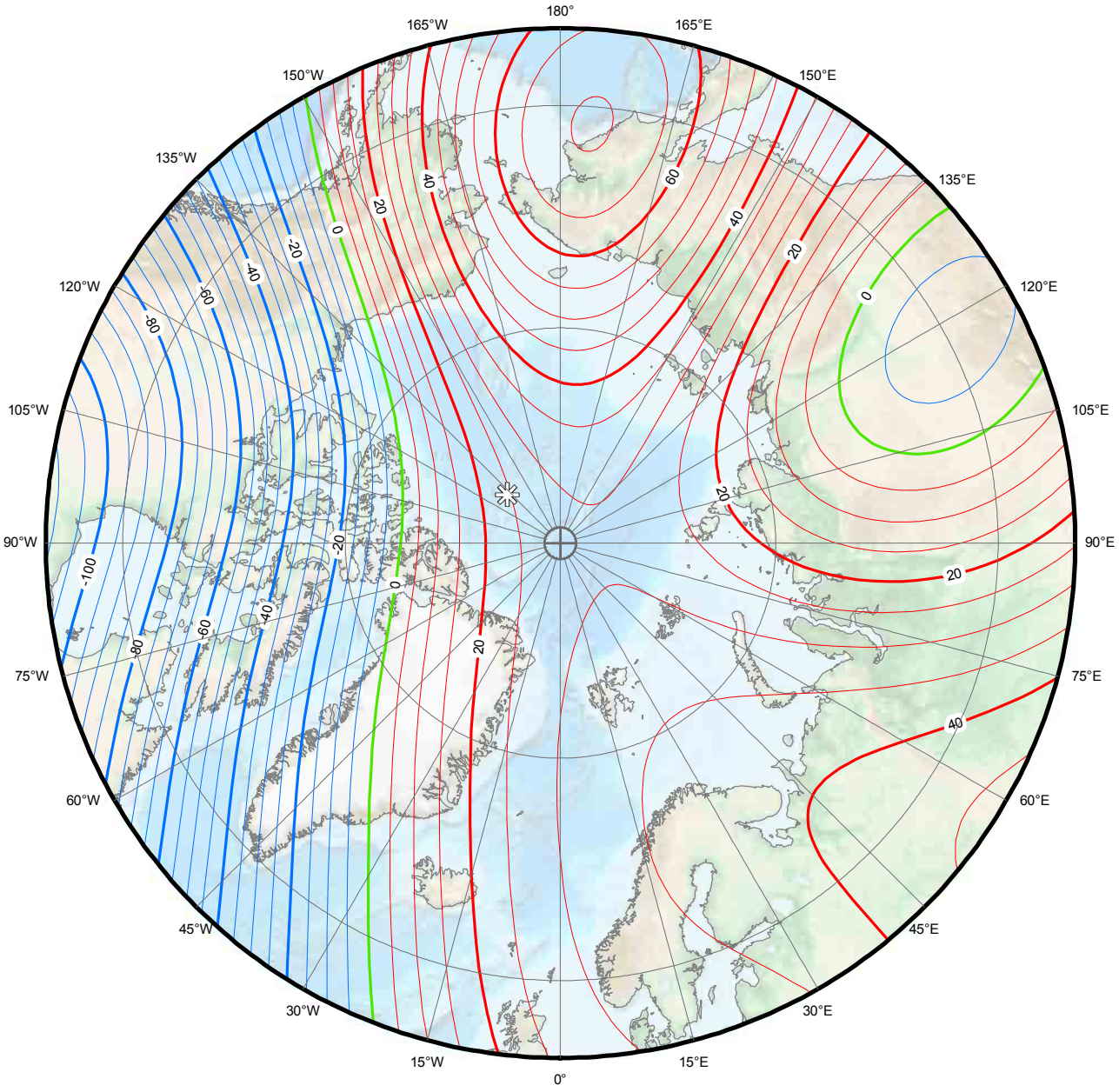

Annual change down component (Z). Contour interval is 5 nT / year, red contours positive (down) change; blue negative (up) change; green zero change. Polar Stereographic Projection.

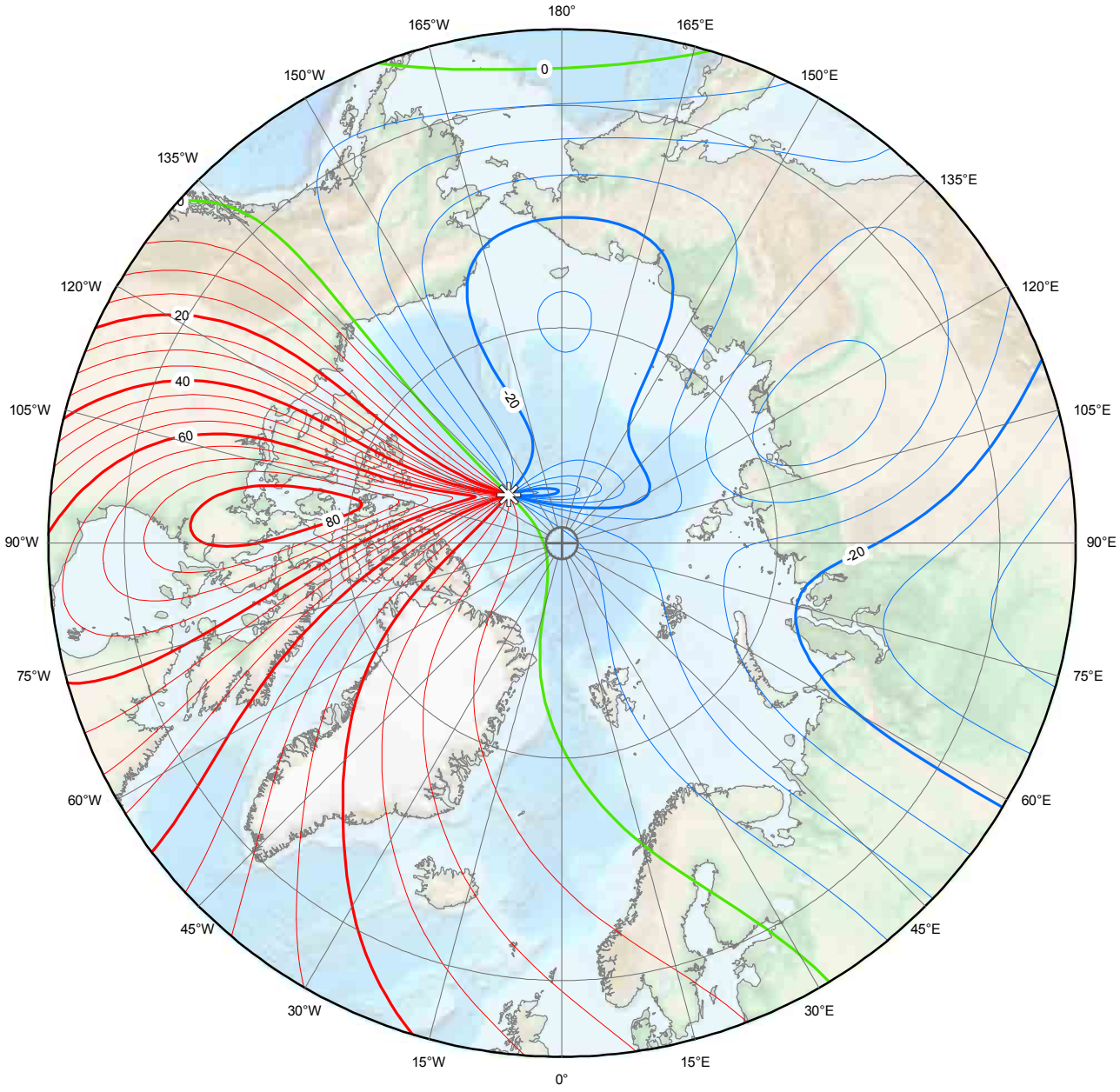

Annual change horizontal intensity (H). Contour interval is 5 nT / year, red contours positive change; blue negative change; green zero change. North Polar Region. Polar Stereographic Projection.

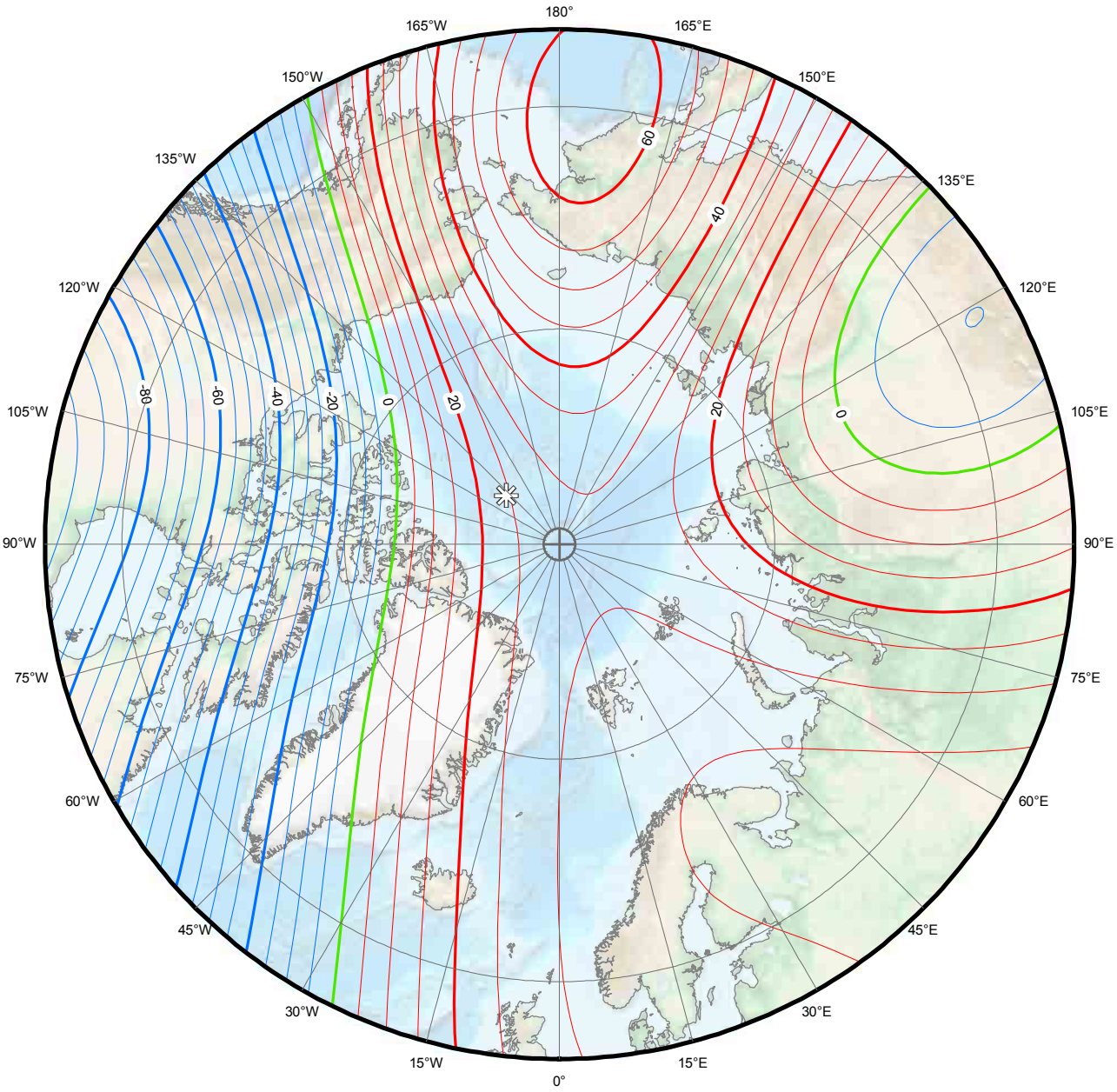

Annual change total intensity (F). Contour interval is 5 nT / year, red contours positive change; blue negative change; green zero change. North Polar Region. Polar Stereographic Projection.

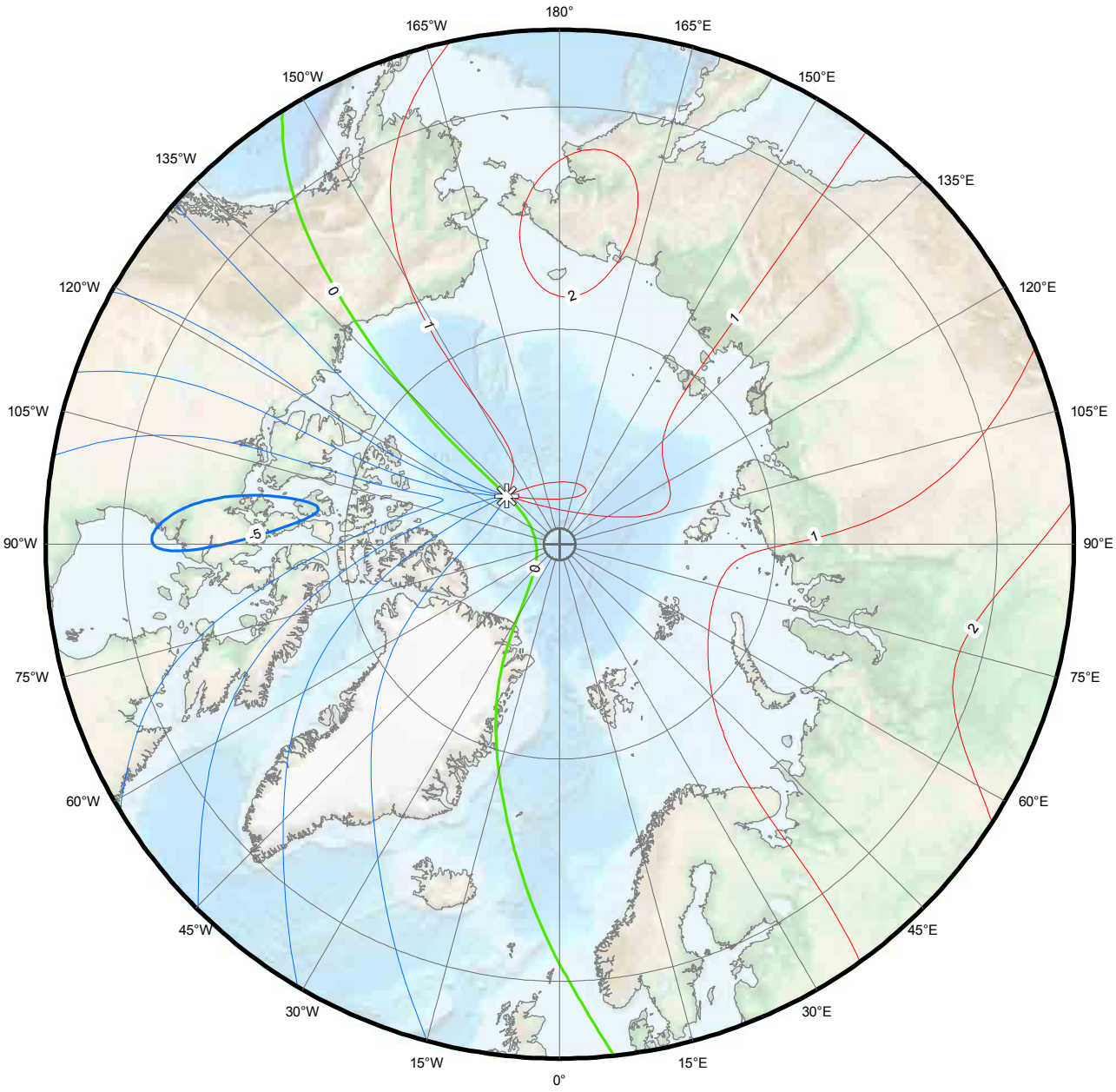

Annual change inclination (I). Contour interval is 1 arc-minute / year, red contours positive (downward) change; blue negative (upward) change; green zero change. North Polar Region. Polar Stereographic Projection.

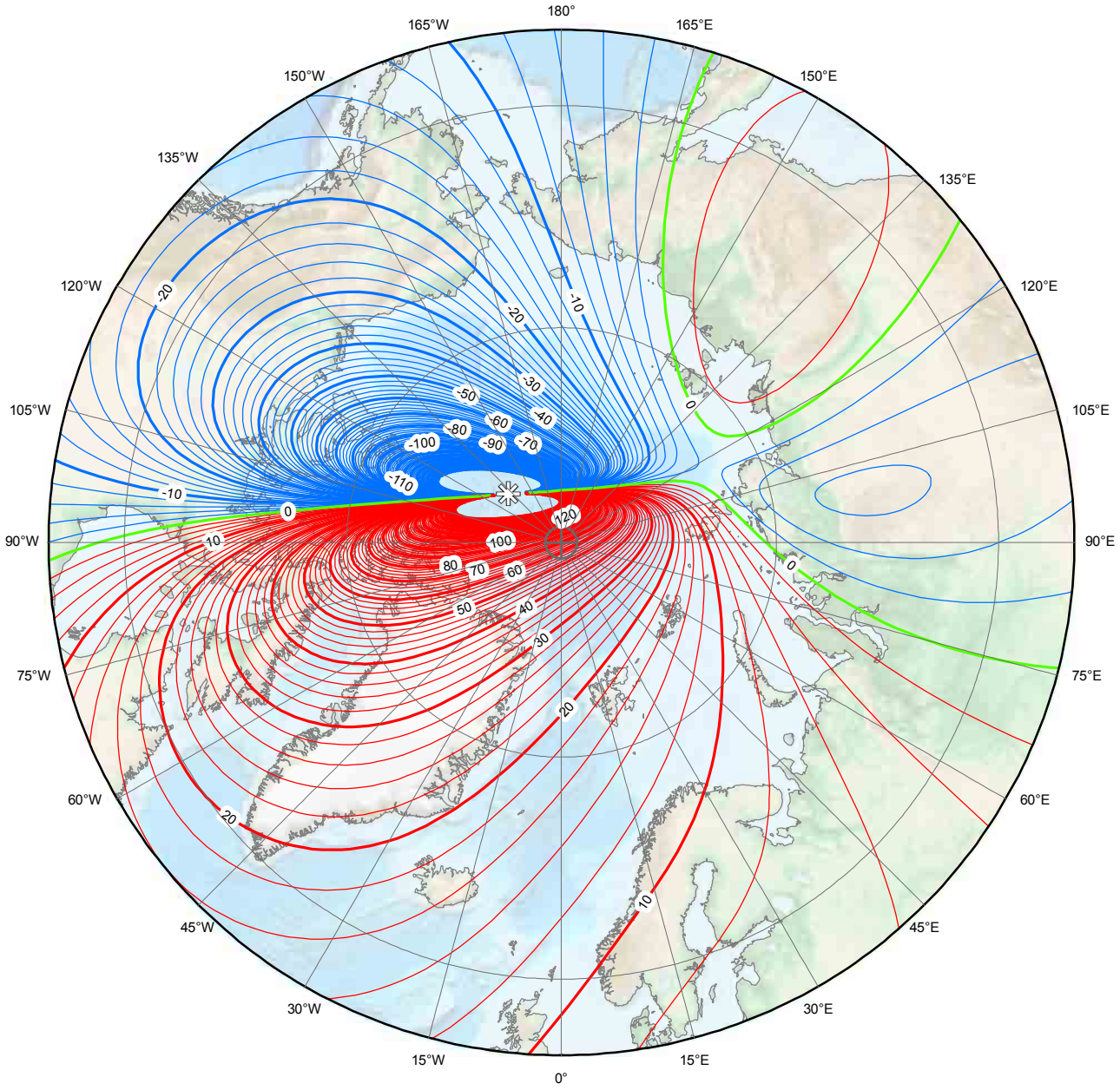

Annual change declination (D). Contour interval is 2 arc-minutes / year, red contours positive (clockwise) change; blue negative (counter- clockwise) change; green zero change. North Polar Region. Polar Stereographic Projection.

SECULAR VARIATION MAPS: SOUTH POLAR STEREOGRAPHIC PROJECTION

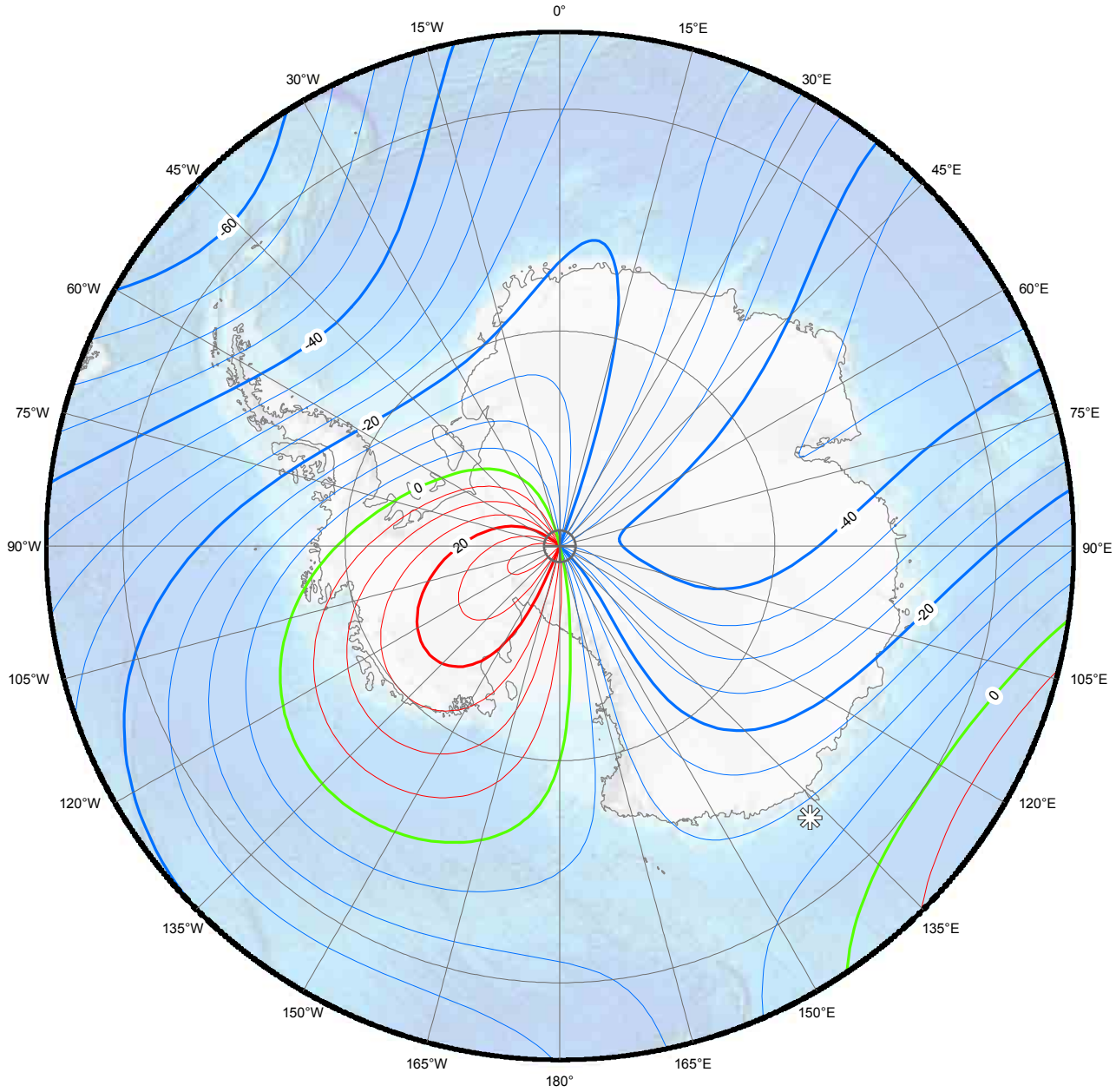

Annual change north component (X). Contour interval is 5 nT / year, red contours positive (north) change; blue negative (south) change; green zero change. South Polar Region. Polar Stereographic Projection.

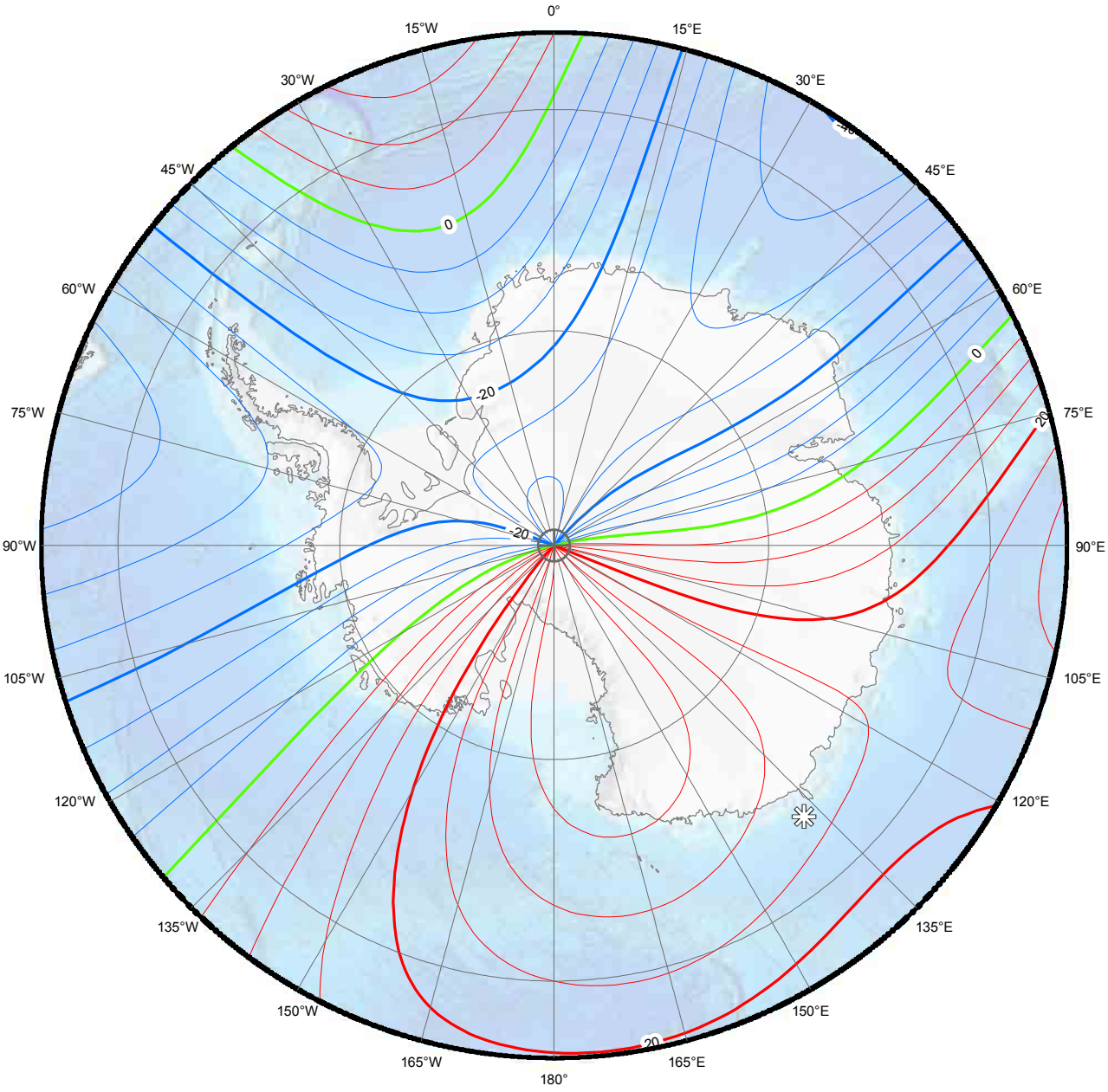

Annual change east component (Y). Contour interval is 5 nT / year, red contours positive (east) change; blue negative (west) change; green zero change. South Polar Region. Polar Stereographic Projection.

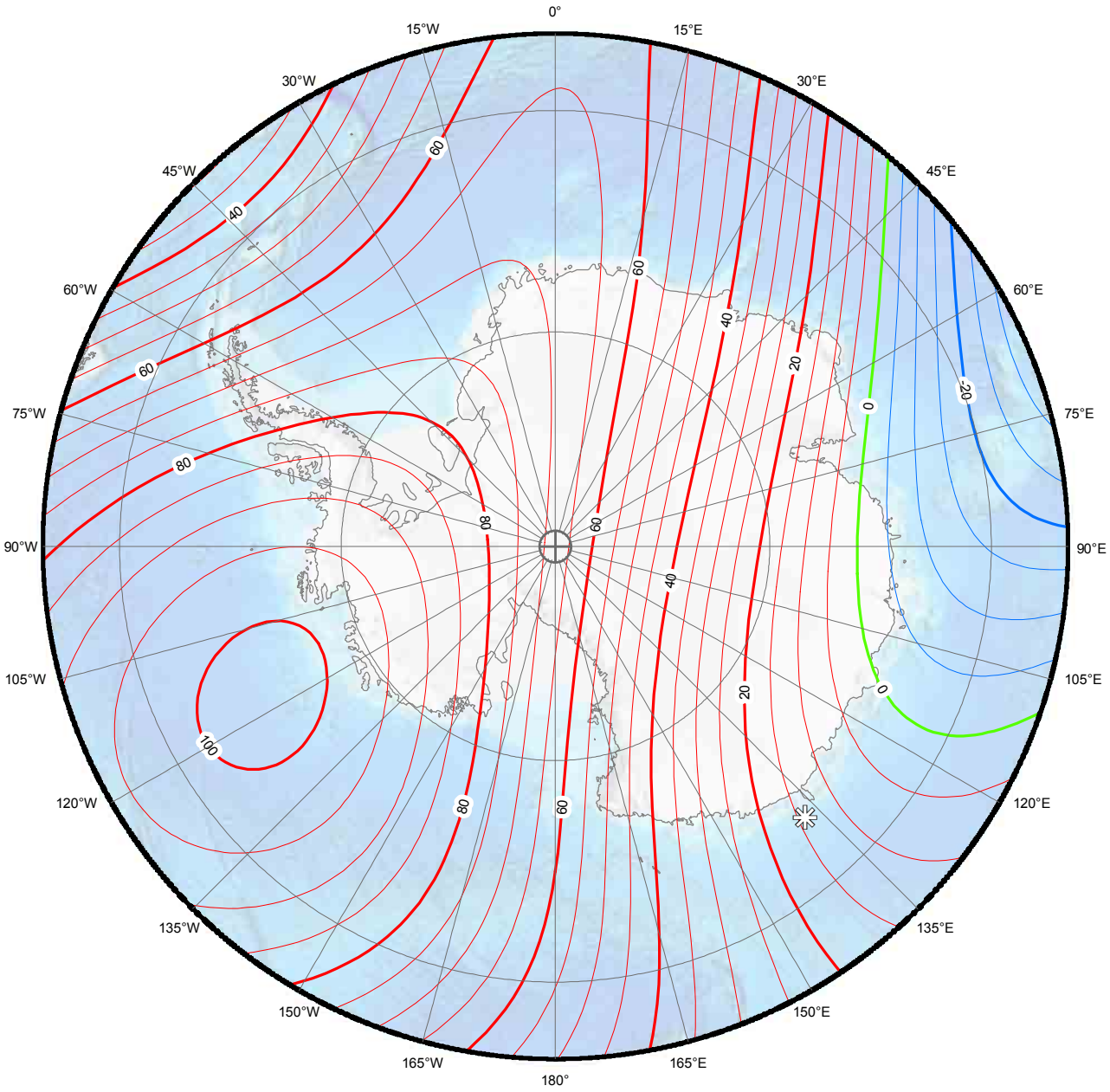

Annual change down component (Z). Contour interval is 5 nT / year, red contours positive (down) change; blue negative (up) change; green zero change. South Polar Region. Polar Stereographic Projection.

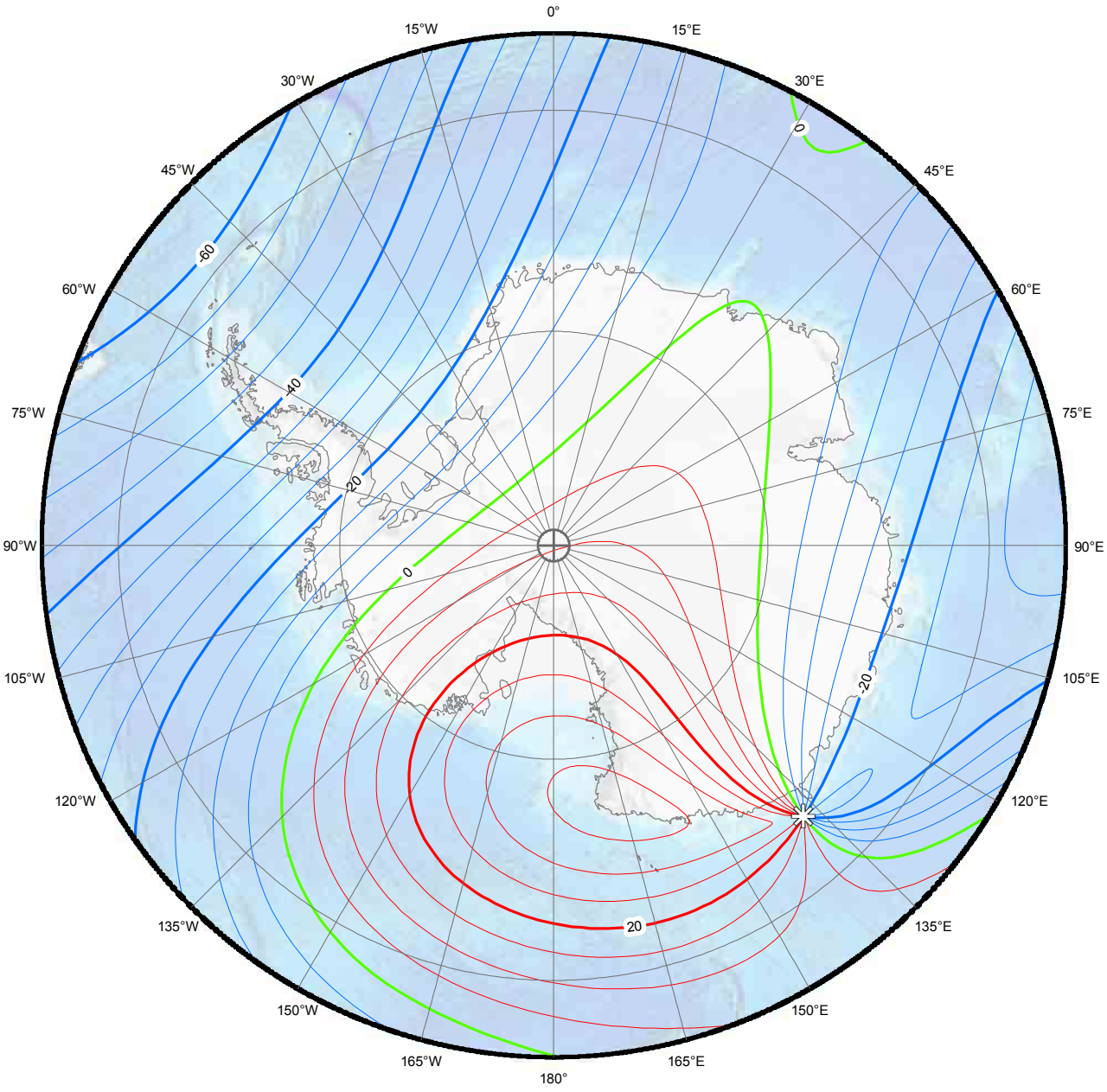

Annual change horizontal intensity (H). Contour interval is 5 nT / year, red contours positive change; blue negative change; green zero change. South Polar Region. Polar Stereographic Projection.

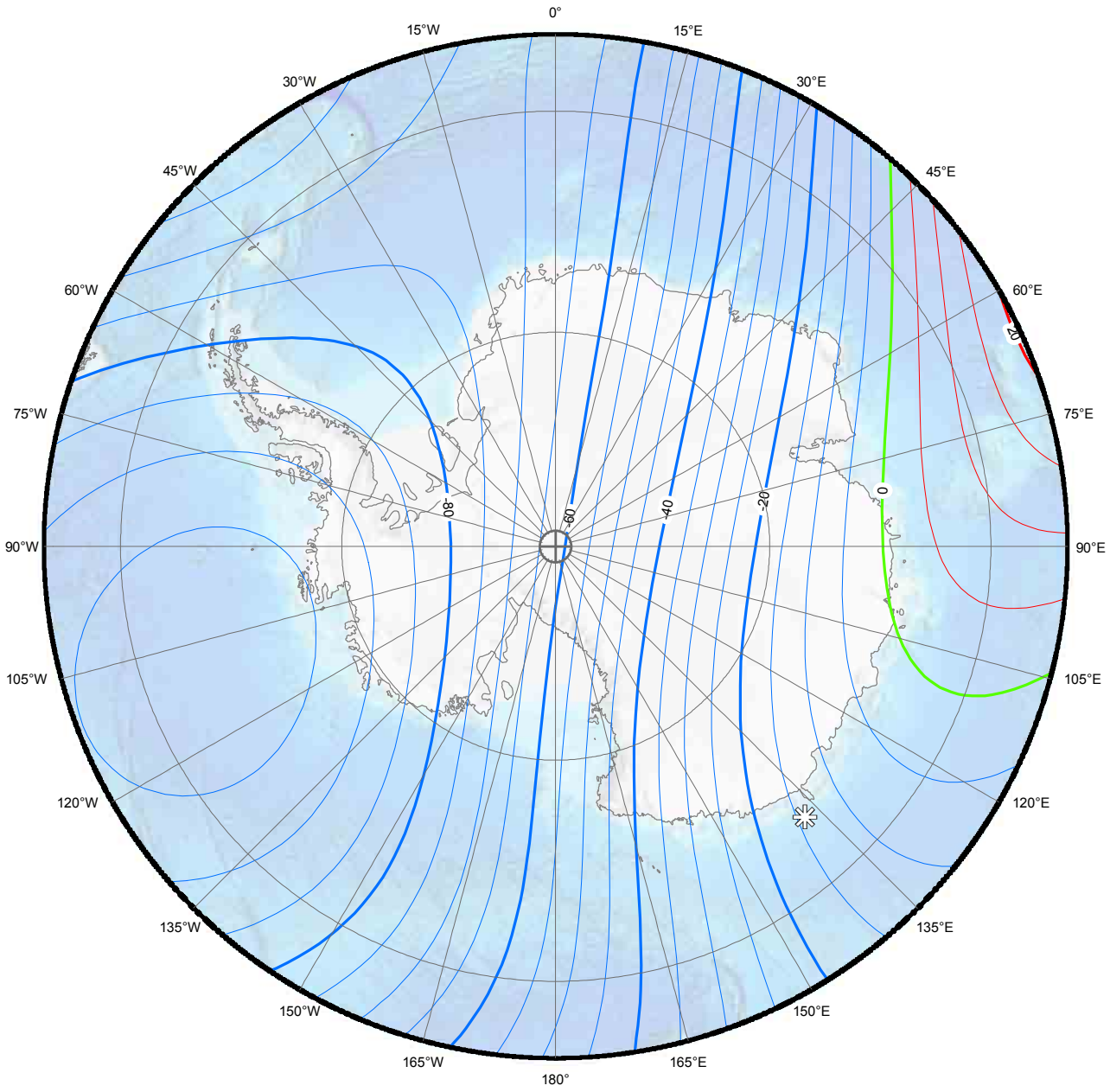

Annual change total intensity (F). Contour interval is 5 nT / year, red contours positive change; blue negative change; green zero change. South Polar Region. Polar Stereographic Projection.

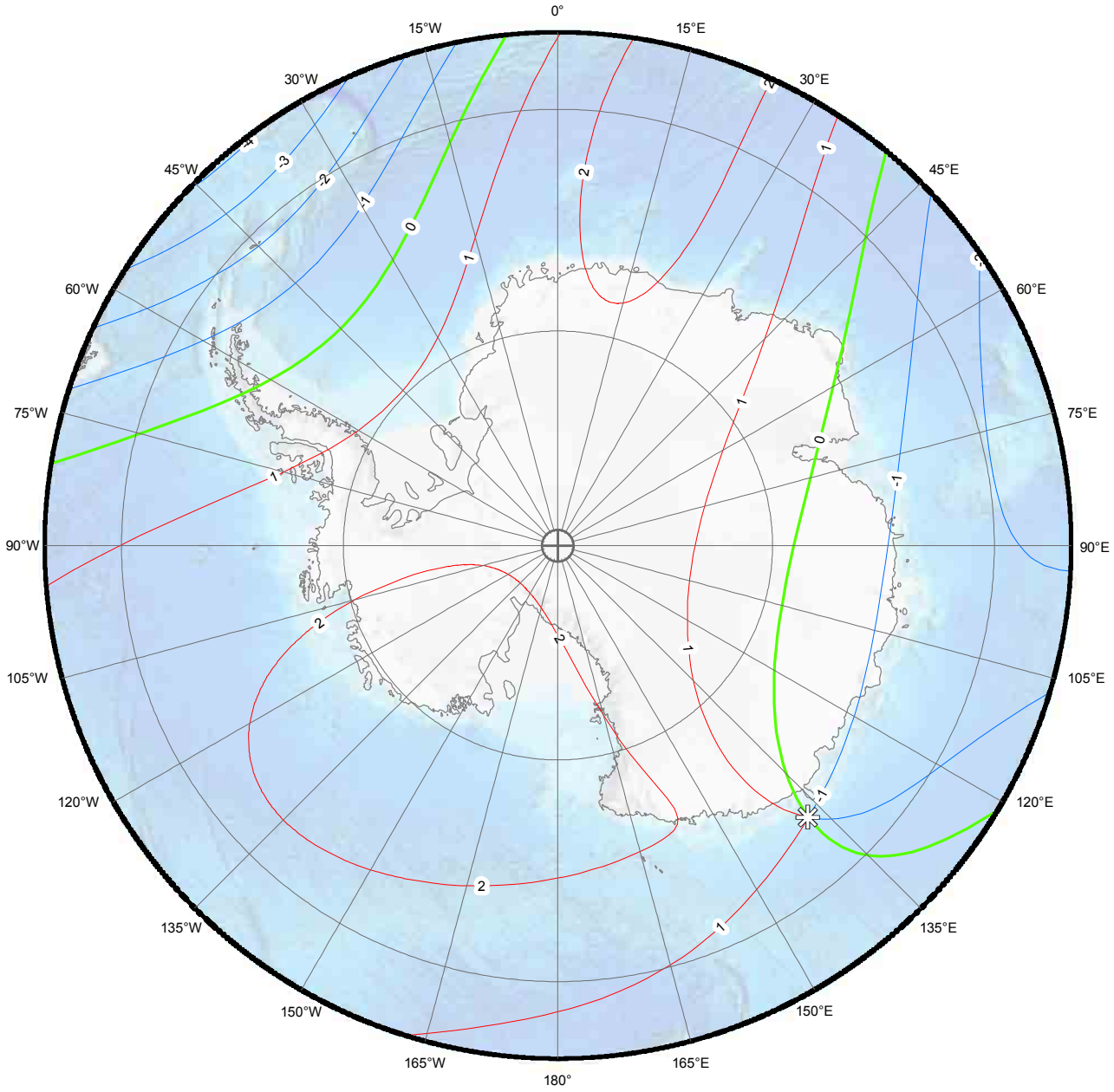

Annual change inclination (I). Contour interval is 1 arc-minute / year, red contours positive (downward) change; blue negative (upward) change; green zero change. South Polar Region. Polar Stereographic Projection.

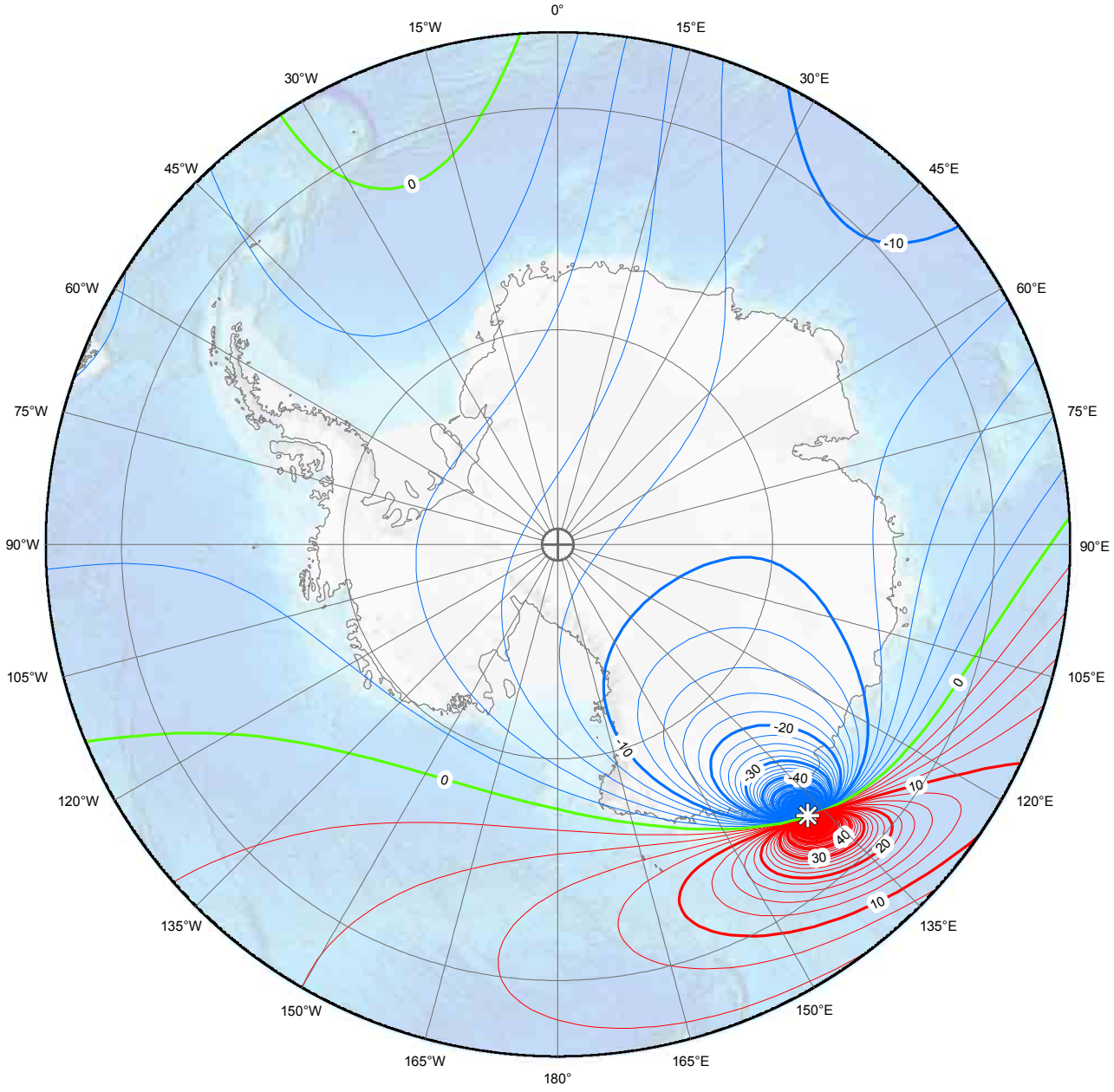

Annual change declination (D). Contour interval is 2 arc-minutes / year, red contours positive (clockwise) change; blue negative (counter-clockwise) change; green zero change. South Polar Region. Polar Stereographic Projection.

GRID VARIATION MAPS: POLAR STEREOGRAPHIC PROJECTION

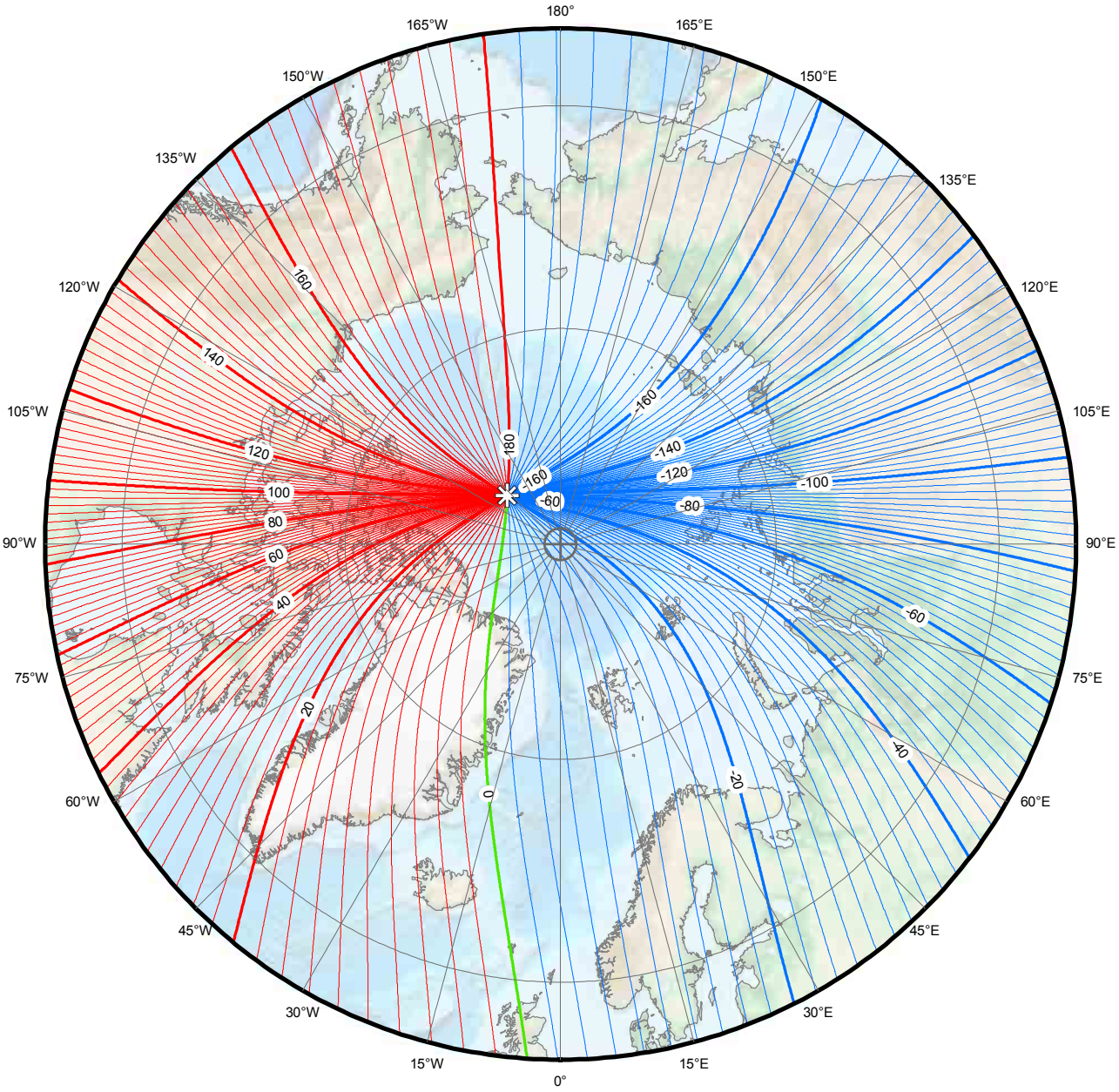

Main field grid variation (GV). Contour interval is 2 degrees, red contours positive; blue negative; green zero line. North Polar Region. Polar Stereographic Projection.

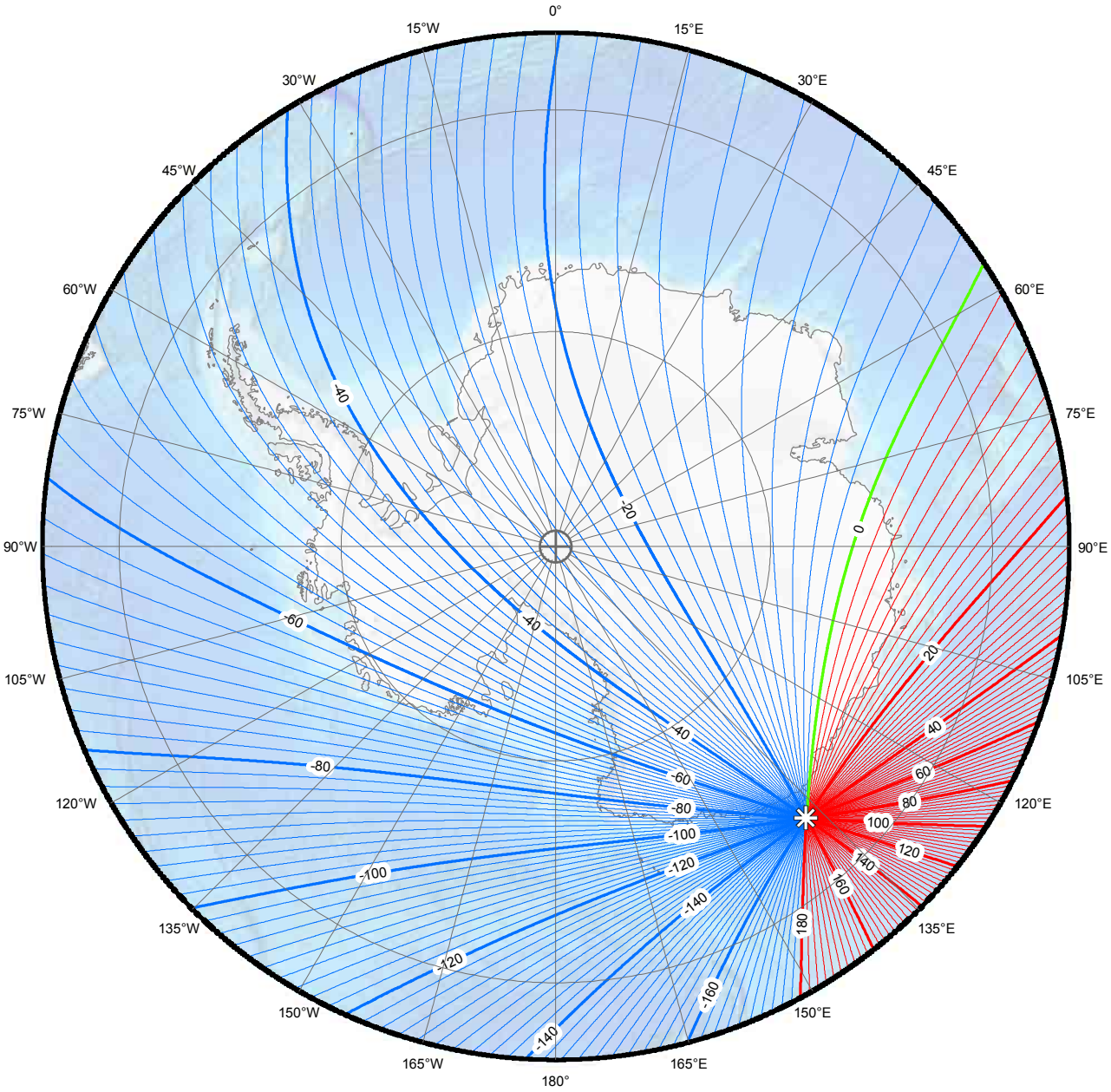

Main field grid variation (GV). Contour interval is 2 degrees, red contours positive; blue negative; green zero line. South Polar Region. Polar Stereographic Projection.

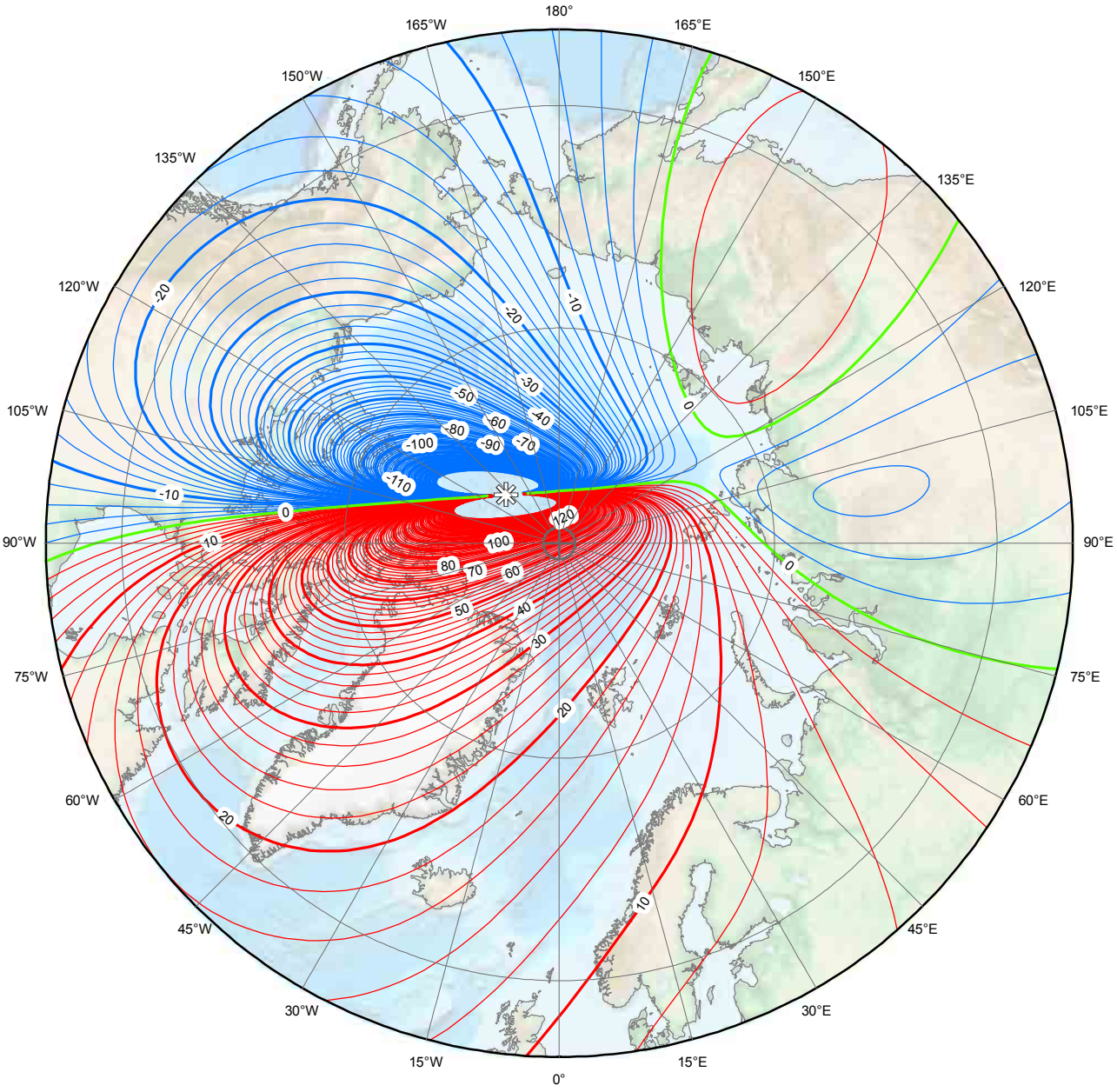

Annual change grid variation (GV). Contour interval is 2 arc-minutes / year, red contours positive (clockwise); blue negative (counter-clockwise); green zero line. North Polar Region. Polar Stereographic Projection.

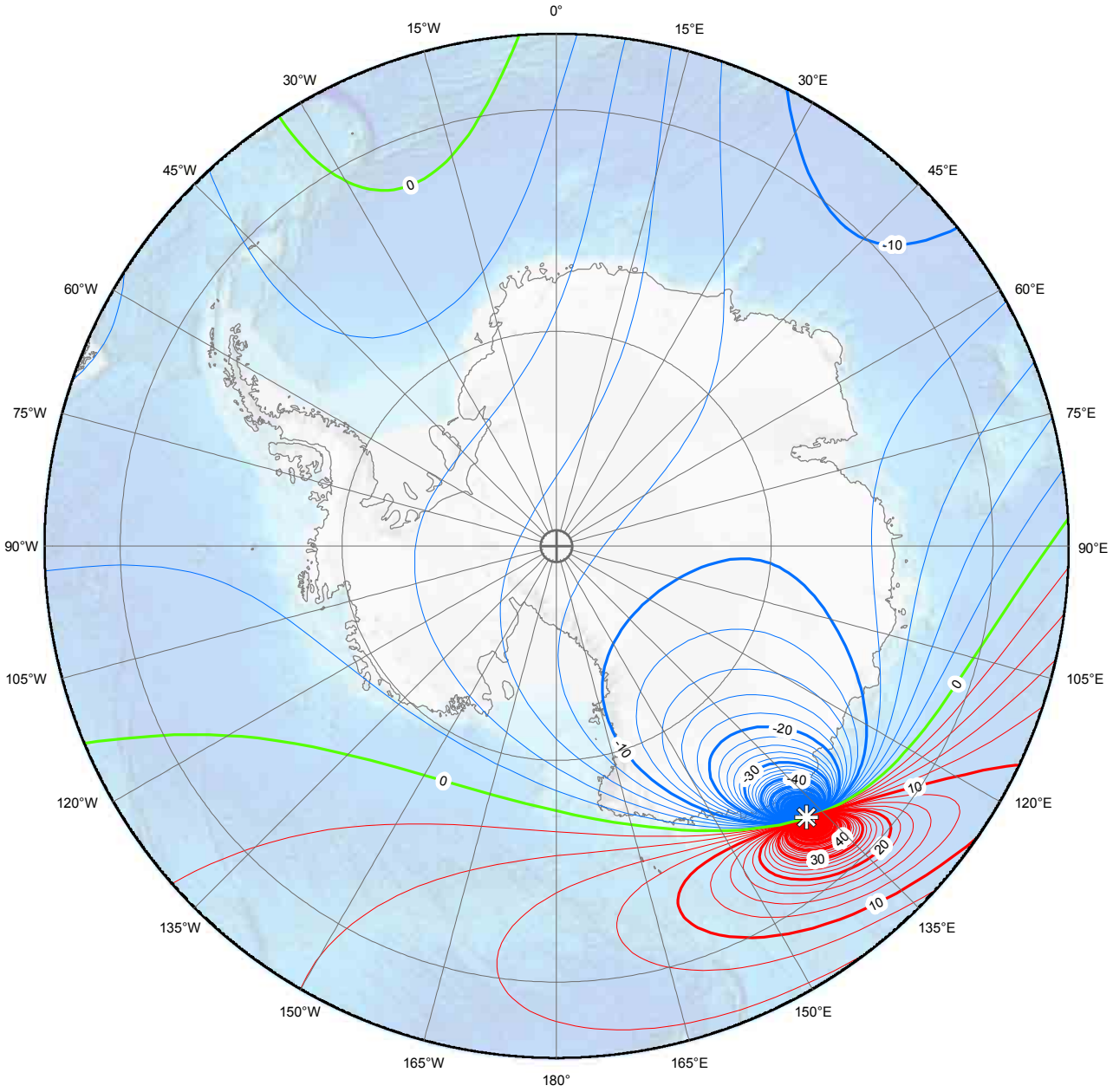

Annual change grid variation (GV). Contour interval is 2 arc-minutes / year, red contours positive (clockwise); blue negative (counter-clockwise); green zero line. South Polar Region. Polar Stereographic Projection.

GEOMAGNETIC LONGITUDE AND LATITUDE

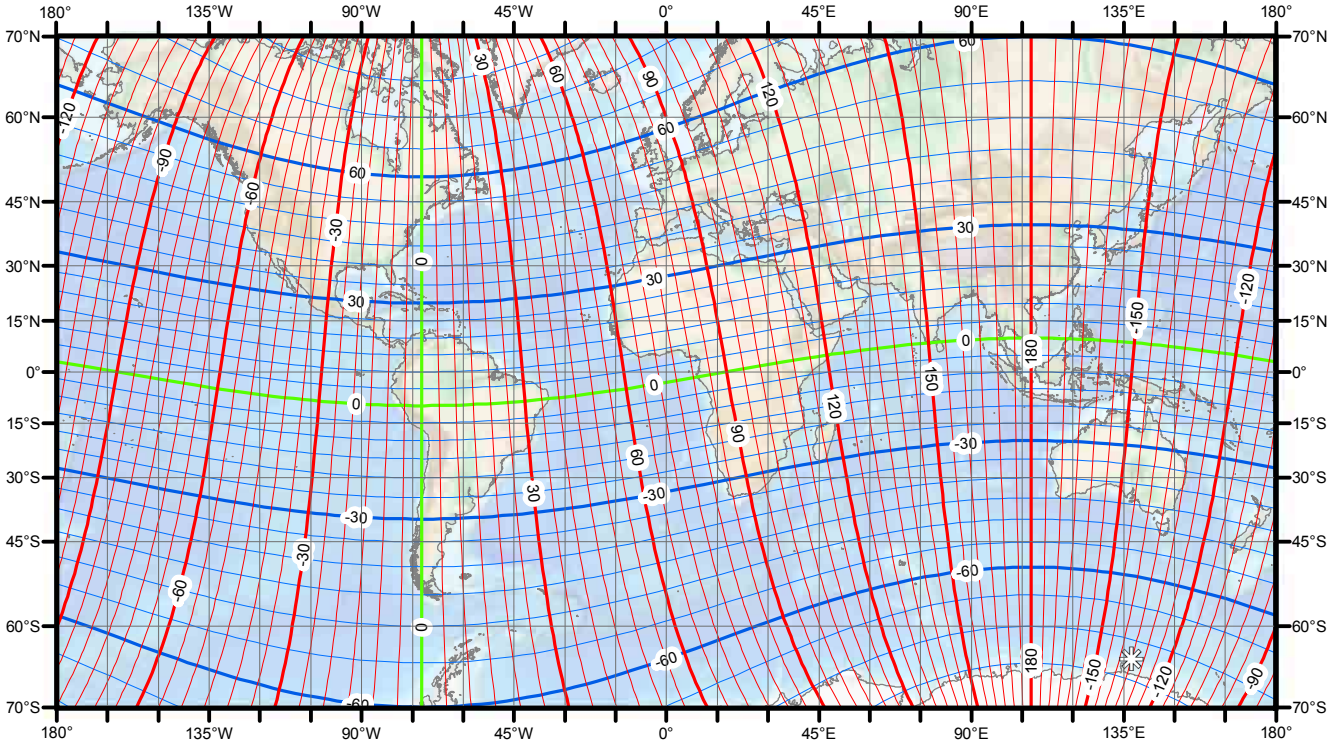

Geomagnetic longitude and latitude. Mercator projection.

5. REFERENCES AND BIBLIOGRAPHY

Abramowitz, M. and I.A. Stegun, 1972. *Handbook of mathematical functions with formulas, graphs, and mathematical tables*. Washington, D.C. : U.S. Dept. of Commerce, National Bureau of Standards.

Backus, G., R.L. Parker, and C. Constable, 1996. *Foundations of geomagnetism*. Cambridge University Press.

Defense Mapping Agency, 1993. *Military specification for World Magnetic Model (WMM).* Document MIL-W-89500. Retrieved from http://www.tpub.com/content/MIL-SPEC/MIL-W/MIL-W-89500/

Gradshteyn, I.S. and I.M. Ryzhik, 1994. *Table of integrals, series and products* (5th ed). Academic Press.

Heiskanen, W. and H. Moritz, 1967. *Physical geodesy*. San Francisco: W.H. Freeman and Company.

Holme, R., N. Olsen, M. Rother and H. Lühr, 2003. CO2 – A CHAMP magnetic field model. In *First CHAMP mission results for gravity, magnetic and atmospheric studies*, edited by C. Reigber, H. Lühr, and P. Schwintzer, Springer, 220-225.

Jankowski, J. and C. Sucksdorff, 1996. *Guide for magnetic measurements and observatory practice.* Boulder: International Association of Geomagnetism and Aeronomy. Retrieved from http://www.iugg.org/IAGA/iaga_pages/pdf/IAGA-Guide-Observatories.pdf

Kan, J.R. and L.C. Lee, 1979. Energy coupling function and solar wind magnetosphere dynamo. *Geophys. Res. Lett.*, 6 (7), 577–580. doi:10.1029/GL006i007p00577

Kuvshinov, A. and N. Olsen, 2005. 3-D modelling of the magnetic fields due to ocean tidal flow. In *Earth observation with CHAMP: results from three years in orbit*, Springer, 359-365. doi:10.1007/3-540-26800-6_57

Langel, R.A., 1987. The main field. In *Geomagnetism*, edited by J.A. Jacobs, Academic Press, 249-512.

Langel, R.A. and W.J. Hinze, 1998. *The magnetic field of the earth's lithosphere: The satellite perspective.* Cambridge University Press.

Lemoine, F.G., S.C. Kenyon, J.K. Factor, R.G. Trimmer, N.K. Pavlis, D.S. Chinn, C.M. Cox, S.M. Klosko, S.B. Luthcke, M.H. Torrence, Y.M. Wang, R.G. Williamson, E.C. Pavlis, R.H. Rapp and T.R. Olson, 1998.*The development of the joint NASA GSFC and NIMA Geopotential Model EGM96*. Technical Report NASA/TP-1998-206861, NASA Goddard Space Flight Center, Greenbelt, Maryland.

Lühr, H. and S. Maus, 2010. Solar cycle dependence of magnetospheric currents and a model of their near-Earth magnetic field. Submitted to *Geophys. Res. Lett*.

Lühr H., M. Rother, S. Maus, W. Mai and D. Cooke, 2003. The diamagnetic effect of the equatorial Appleton anomaly: Its characteristics and impact on geomagnetic field modeling. *Geophys. Res. Lett.,* 30 (17), 1906. doi:10.1029/2003GL017407

Macmillan, S., 2007. Observatories, Overview. In *Encyclopedia of geomagnetism and paleomagnetism,* edited by D. Gubbins and E. Herrero-Bervera, Springer, 708-711.

Maus, S., 2007. Ocean, electromagnetic effects. In *Encyclopedia of geomagnetism and paleomagnetism*, edited by D. Gubbins and E. Herrero-Bervera, Springer, 740-742.

Maus, S. and P. Weidelt, 2004. Separating magnetospheric disturbance magnetic field into external and transient internal contributions using 1D conductivity model of the Earth. *Geophys. Res. Lett.,* 31 (12), L12614. doi:10.1029/2004GL020232

Maus, S. and H. Lühr, 2005. Signature of the quiet-time magnetospheric magnetic field and its electromagnetic induction in the rotating Earth. *Geophys. J. Int.,*162, 755-763. doi: 10.1111/j.1365-246X.2005.02691.x

Maus, S., M. Rother, C. Stolle, W. Mai, S. Choi, H. Lühr, D. Cooke and C. Roth, 2006. Third generation of the Potsdam Magnetic Model of the Earth (POMME). *Geochem. Geophys. Geosyst.*, 7, Q07008. doi:10.1029/2006GC001269

McLean, S., S. Macmillan, S. Maus, V. Lesur, A. Thomson and D. Dater, 2004. *The US/UK World Magnetic Model for 2005-2010.* NOAA Technical Report NESDIS/NGDC-1. Retrieved from http://www.ngdc.noaa.gov/geomag/WMM/data/TRWMM_2005.pdf

Merrill, R.T., M.W. McElhinny and P.L. McFadden, 1996. *The magnetic field of the earth: paleomagnetism, the core and the deep mantle*. Elsevier Science & Technology.

Military Specification for World Magnetic Model (WMM), 1996. McElhinny and P.L. McFadden, *The magnetic field of the earth.* Document MIL-W, Academic Press.

NATO Standardization Agency, 2006. *STANAG 7172 Use of Geomagnetic Models* (1st ed).

Olsen, N., L. Tøffner-Clausen, T.J. Sabaka, P. Brauer, J.M.G. Merayo, J.L. Jörgensen, J.-M. Léger, O.V. Nielsen, F. Primdahl and T. Risbo, 2003. Calibration of the Ørsted vector magnetometer. *Earth, Planets and Space*, 55, 11-18.

Olsen, N., H. Lühr, T.J. Sabaka, M. Mandea, M. Rother, L. Tøffner-Clausen and S. Choi, 2006. CHAOS - A Model of Earth's Magnetic Field derived from CHAMP, Ørsted, and SAC-C magnetic satellite data. *Geophys. J. Int.,* 166, 67-75. doi:10.1111/j.1365-246X.2006.02959.x

Parkinson, W.D., 1983. *Introduction to geomagnetism.* Scottish Academic Press.

Reigber, C., H. Lühr and P. Schwintzer, 2002. CHAMP mission status. *Adv. Space Res.,* 30**,** 129-134.

Sugiura, M., 1964. Hourly values of the equatorial Dst for the IGY. *Ann. IGY*, 35, 9-45.

Thomson, A.W.P. and V. Lesur, 2007. An improved geomagnetic data selection algorithm for global geomagnetic field modeling. *Geophys. J. Int.,* 169, 951-963. doi:10.1111/j.1365-246X.2007.03354.x

Thomson, A.W.P., B. Hamilton, S. Macmillan and S.J. Reay, 2010. A novel weighting method for satellite magnetic data and a new global magnetic field model. *Geophys. J. Int*., in print.

Viljanen, A. and L. Hakkinen, 1997. IMAGE magnetometer network. In *Satellite-ground based coordination sourcebook*, edited by M. Lockwood, M.N. Wild, and H.J. Opgennoorth, ESA publications, Noordwijk, SP-1198, p. 111.